Appraisal of Friction Coefficients Between TBM and Conditioned Soil

A Laboratory Investigation Adopting a Direct Shear Apparatus

By

Matteo Ambrosi

in partial fulfilment of the requirements for the degree of

Master of Science
in Civil Engineering

at the Delft University of Technology,
to be defended publicly on Wednesday August 28, 2019 at 3:00 PM.

Supervisor:	Dipl. Ing. Kathrin Glab, TU Delft
Thesis committee:	Dr. Ir. Dominique Ngan-Tillard, TU Delft
	Ir. Kristina Reinders, TU Delft
	Dr. Ir. Wout Broere, TU Delft

Abstract

During the advance of a tunnel boring machine (TBM), the torque applied to rotate the cutterhead must overcome the resisting moments acting on it. Hence, one of the major concerns of TBM design is to determine the torque and power requirements of the excavation machine.
The first empirical approach for torque estimation was developed in the 80's by JSCE. This estimation fits the recorded mean torque for 5-8m diameter projects, but overestimates torque as TBM diameter increases. Newer approaches estimate TBM torque and thrust requirements as sum of multiple components, focusing on the friction between ground and cutterhead. However, the recommended or selected friction coefficients range between a wide interval (typically 0.05-0.75), depending on soil and operational conditions. Consequently, the torque and thrust estimations relying on the above-mentioned friction coefficients can be considerably imprecise, as well.

Previous research regarding soil-machine/steel friction coefficients has been collected and studied. Successively, interface shear tests have been performed at TU Delft, to study whether and how friction coefficients could be determined consistently in the laboratory. Three soil types have been examined, ranging from coarse sand to kaolin clay. A metal plate cut out from a worn TBM cutterhead has been added to a direct shear apparatus to test the abovementioned soils. The latter are either water saturated or treaded with bentonite or foam, to assess the influence of conditioners on soil interface friction. Bentonite slurries and foam suspensions have been prepared in the laboratory using common industry products. Overall, in excess of 60 interface shear tests have been performed, considering various permutations of soil, load and conditioning. Results show that lubricated friction coefficients (i.e. when soil samples are conditioned) are up to 25% and 50% lower than for water-saturated conditions, for sand and clay respectively.

A direct shear apparatus proves to be useful to study and select friction coefficients for TBM preliminary design, as it provides satisfactory results for non-conditioned and bentonite-conditioned soils. The same apparatus, however, cannot fully capture the lubricating effect of foam on sand. Improved estimation of friction coefficients requires more advanced equipment, or substantial modifications to the direct shear apparatus.

Sommario

Durante l'avanzamento di una fresa meccanica a piena sezione (TBM), la coppia necessaria per ruotare la fresa deve superare i momenti resistenti agenti su di essa. Di conseguenza, uno dei principali aspetti riguardo la progettazione di TBM è di determinare i requisiti di coppia e potenza della macchina.
Il primo approccio empirico per valutare la coppia richiesta da una TBM fu sviluppato negli anni '80 dalla JSCE. Questo approccio fornisce risultati accurati per progetti fra 5-8m di diametro, ma sovrastima la coppia nel caso di tunnel di dimensioni superiori. Approcci più moderni computano la coppia e la spinta richiesta da un a TBM come somma di più componenti, concentrandosi sull' attrito sviluppato fra terreno e fresa. Tuttavia, i coefficienti d' attrito adottati o suggeriti variano lungo un intervallo ampio (tipicamente 0.05-0.75), in base alle condizioni di terreno e scavo. Di conseguenza, la relativa stima di coppia e spinta richiesta dalla macchina può essere altrettanto imprecisa.

Ricerche precedenti riguardo i coefficienti d'attrito fra terreno e macchina/metallo sono state raccolte e studiate. Successivamente, prove di taglio sono state eseguite presso l'Università di Delft, per studiare se e come i coefficienti d'attrito possano essere determinati coerentemente in laboratorio. Tre tipi di terreno sono stati esaminati, da sabbia grossolana ad argilla kaolinitica. Una placca di acciaio ritagliata dalla fresa di una TBM usata è stata aggiunta ad un apparato di taglio diretto per testare i terreni sopracitati. Questi ultimi erano saturi d'acqua, oppure trattati con bentonite o schiuma, per valutare l'effetto degli additivi sull' attrito superficiale dei terreni. Le miscele di bentonite e schiuma sono state preparate in laboratorio da prodotti comunemente usati nell'industria. Complessivamente, sono state eseguite più di 60 prove di taglio superficiali, considerando varie permutazioni di terreno, carico e addittivi. I risultati mostrano che i coefficienti d'attrito riscontrati per terreni trattati con bentonite o schiuma sono fino al 25 e 50% più bassi che in acqua, rispettivamente per sabbia e argilla.

Un apparato di taglio diretto si dimostra utile nella selezione preliminare dei coefficienti d'attrito fra terreno e TBM, fornendo risulati soddisfacenti per terreni non trattati o trattati con bentonite. Il medesimo apparato, tuttavia, non può replicare fedelmente l'effetto lubrificante della schiuma sulla sabbia. Per prevedere coefficienti d'attrito più precisi sono necessari dispositivi più avanzati, o modifiche sostanziali ad un apparato di taglio diretto.

Preface

As far as my memory can trace back in time, I have always been fascinated by excavations, tunnels, working sites and digging machines. The best way to keep me busy as a small child was to hand me a toy excavator and a handful of breadcrumbs to play with. It is not surprising, then, that I ended up at TU Delft to study Geo-Engineering.

Here, during the first year of studies, I became particularly interested in the subject of tunnel excavation. The lectures on this topic were my favourites and visiting some tunnel working sites was inspiring! Just after finishing my exams, I met Kathrin Glab, who was looking for MS students to embark on a thesis on TBM excavation. I accepted the challenge, and after eight months of work my thesis is finally completed.

Never had I worked on such a large task, focusing on all the details and planning each step from the ground up. It has been a memorable experience, as I have had the opportunity of experiencing both the experimental and the analytical side of such an investigation.

Many people have helped and supported me during the past months. I particularly want to thank Kathrin Glab, my daily supervisor, and Wout Broere, the head of my committee, for presenting me this challenge and encouraging me along the way. My gratitude also goes to all the laboratory technicians: the numerous hours I have worked in the laboratory would have been vain without the help of Wim Verwaal, Han de Visser, Marc Friebel and Karel Heller. Finally, I want to thank my family and friends from Italy and the Netherlands for their support and confidence in me.

Matteo Ambrosi
Delft, July 2019

Nomenclature

Abbreviations

CEC	Cation Exchange Capacity
EPB	Earth Pressure Balance
FER	Foam Expansion Ratio
FIR	Foam Injection Ratio
GSI	Geological Strength Index
OCR	Over Consolidation Ratio
SR	Shear Rate
TBM	Tunnel Boring Machine
TOC	Total Organic Content

Parameters

C_c	Coefficient of uniformity	[-]
C_u	Coefficient of curvature	[-]
D_{10}	Grain diameter at 10% passing	[mm]
D_{30}	Grain diameter at 30% passing	[mm]
D_{50}	Grain diameter at 50% passing	[mm]
D_{60}	Grain diameter at 60% passing	[mm]
D_r	Relative density	[-]
F_f	Friction force	[N]
F_w	TBM weight	[kN]
G_s	Specific gravity	[-]
K_0	Coefficient of lateral earth pressure at rest	[-]
P_v	TBM thrust	[kN]
Q_F	Foam volume	[m^3]
Q_L	Surfactant solution volume	[m^3]
Q_S	Soil volume to be excavated	[m^3]
Q_f	Surfactant mass	[gr]
Q_l	Surfactant solution mass	[gr]
R_a	Average surface roughness	[µm]
R_i	Soil conditioning reduction factor	[-]
R_{max}	Maximum surface roughness	[µm]
c_f	Surfactant concentration	[%]
f_i	TBM shape reduction factor	[-]
q_c	CPT cone penetration resistance	[MPa]
CI	Consistency index	[-]
D	TBM diameter	[m]
E	Elastic modulus	[MPa]
F	TBM thrust	[kN]
FER	Foam expansion ratio	[-]
FIR	Foam injection ratio	[%]
GSI	Geological strength index	[MPa]
H	Soil depth	[m]
L	TBM shield length	[m]
LL	Liquid limit	[-]
OCR	Over consolidation ratio	[-]
PL	Plastic Limit	[-]
R	TBM radius	[m]

SR	Shear rate	[mm/min]
T	TBM torque	[Ton·m]
TOC	Total organic content	[-]
w	Water content	[-]
a	Adhesion	[kPa]
c	Cohesion	[kPa]
e	Void ratio	[-]
f	Friction coefficient	[-]
α	Torque empirical factor	[Ton/m^2]
β	Thrust empirical factor	[kN/m^2]
γ	Volumetric weight	[kN/m^3]
δ	Interface friction angle	[°]
η	Cutterhead opening ratio	[-]
μ	Interface friction coefficient	[-]
ρ	Density	[g/cm^3]
σ	Normal stress	[kPa]
τ	Tangential stress	[kPa]
φ	Internal friction angle	[°]

Subscripts

$\perp$	Perpendicular
0	At zero (initial) time
avg	Average
$dense$	State of high soil compaction
dry	Dry conditions
k	Kinetic condition
$loose$	State of low soil compaction
p	Peak value
r	Residual value
s	Static condition
sat	Water-saturated conditions

List of Figures

Figure 1.1: Structure and main components of a double-shield TBM (www.herrenknecht.com). 1
Figure 1.2: TBM cutterhead (in blue) and shield (in white) assembled prior to excavation (tunnellingjournal.com)..... 2
Figure 1.3: Structure of an EPB shield TBM. The screw conveyer (pictured in red) goes through the bulkhead and into the excavation chamber (www.herrenknecht.com). 2
Figure 1.4: Structure of a slurry shield TBM. A pressurized air cushion allows fine tuning of slurry pressure. The pipe system is displayed in light blue, the suction pipe is displayed in green (www.herrenknecht.com). 3
Figure 1.5: Prediction of TBM thrust according to Equation 1, depending on cutterhead diameter (Zhang, Qu, Cai, Kang, & Huang, 2014). 4
Figure 1.6: Prediction of TBM torque according to Equation 2, depending on cutterhead diameter (Zhou & Zhai, 2018). 4
Figure 2.1: Soil failure envelope. The intercept of the failure envelope represents cohesion (McCarthy, T. Direct Shear Test, Slide Player). 8
Figure 3.1: Comparison between predicted (dotted) and measured (bold) torque, for three soil types and two opening ratios (Shi et al., 2011). 10
Figure 3.2: Comparison between calculated longitudinal drag force (in blue) and measured resistance to shield advance (in red) (Festa, 2015). 10
Figure 3.3: Comparison between installed and predicted cutterhead torque, for slurry TBM's (Ates et al., 2014). 12
Figure 3.4: Comparison between installed and predicted cutterhead torque, for EPB TBM's (Ates et al., 2014). 12
Figure 3.5: Comparison between installed and predicted cutterhead thrust (Ates et al., 2014). 13
Figure 3.6: Comparison between recorded (red) and predicted (blue) torque values (Godinez et al.). 13
Figure 3.7: Soil-machine friction coefficients from tunneling literature. **Square** datapoints: non-lubricated conditions; **circular** datapoints: lubricated conditions. **Green** datapoints: values measured/back-figured; **Blue** datapoints: values as generic guideline. Note: positioning of datapoints along horizontal axis is generic. 16
Figure 4.1: Static (δs) and kinetic (δk) interface friction angles between loose (left) and dense (right) sand and mild steel (Butterfield & Andrawes, 1972). 17
Figure 4.2: Comparison of shear strength development between interface and internal shear tests (Littleton, 1976). 18
Figure 4.3: Effect of shear speed on interface frictional stress between clay and steel (Stafford & Tanner, 1982b). ... 19
Figure 4.4: Typical domain of shear failure modes, according to soil type and steel surface roughness (Tsubakihara et al., 1993). 20
Figure 4.5: Dependency of cohesion (light purple) and adhesion (blue) between clay and steel on water content (Kooistra et al., 1998). 21
Figure 4.6: Interface friction envelopes for sand shearing on smooth and rough steel plates (Al-Mhaidib, 2006). 22

Figure 4.7: Plots from interface shear tests between clay and smooth steel (blue) and clay and rough steel (red), for various normal loads. Note that normal load is displayed in Pounds per square inch (Tokarz, 2014). 23
Figure 4.8: Friction ratio (δ / φ), function of average plate roughness. K1, CG and K1G refer to kaolinite, clay of Guelma and mixture of the previous two, respectively (Feligha et al., 2015). 24
Figure 4.9: Fitting of Equation 11 for sand data from Table 4.3. Note: datapoints in red are measurements for which plate roughness is not available from literature (for which Ra is nominally taken as 5μm). 29
Figure 4.10: Fitting of Equation 12 for clay data from Table 4.3 29
Figure 5.1: Structure of laboratory studies. 34
Figure 6.1: Application ranges of EPB machines (Thewes, 2007). 35
Figure 6.2: Application ranges of shield machines with slurry supported tunnel face (Thewes, 2007). 36
Figure 6.3: Granulometric profile of soil A. 36
Figure 6.4: Internal shear failure envelope of soil A. 37
Figure 6.5: Granulometric profile of soil B. 38
Figure 6.6: Internal shear failure envelope of soil B. 38
Figure 6.7: Granulometric profile of soil C. Note that the right-most side of the profile has been cut-out to exclude soil particles larger than 10% the size of the shear box. 39
Figure 6.8: Internal shear failure envelopes of soil C. Green envelope refers to peak strength, orange envelope refers to residual strength. 40
Figure 6.9: Shear box and its accessories [www.ele.com]. 41
Figure 6.10: Shear machine 41
Figure 6.11: Metal plate insert (light surface damage from its previous use can be seen). 42
Figure 6.12: Custom-made rubber gasket fitted to the loading cap. 44
Figure 6.13: Bentonite-conditioned sample of soil C, prior to fitting porous stone and loading cap. 45
Figure 6.14: Bentonite slurry placed on the underside of clay specimens. 46
Figure 6.15: Foam-conditioned sample of soil C; prior to fitting porous stone and loading cap. 46
Figure 6.16: Foam suspension (2% surfactant concentration, FER = 11.5-12). 49
Figure 7.1: In green are the measurements within 10% from the max. shear registered in the test. These values are averaged to obtain a representative τ value. 50
Figure 7.2: Comparison between data from literature (blue) and results from water-saturated interface shear tests of soil A (yellow). 51
Figure 7.3: Comparison between data from literature (blue) and results from water-saturated interface shear tests of soil B (yellow). 52
Figure 7.4: Comparison between data from literature (blue) and results from water-saturated interface shear tests of soil C (yellow). 53
Figure 8.1: Leakage of tinted bentonite highlights the serviceability limit of the shear box gasket (approx. 200-300 kPa). 56

Figure 8.2: Comparison of interface shear tests (soil B). Water-saturated tests in solid lines, bentonite-conditioned tests in dashed lines. Normal loads are of 50.0, 99.7 and 193.4 kPa. Note: additional tests at normal loads of 400.7 and 327.3 kPa are not shown (mutual comparison of shear not possible). 57
Figure 8.3: Comparison of interface shear tests (soil C). Water-saturated tests in solid lines, bentonite-conditioned tests in dashed lines. Normal loads are of 50.0, 99.7 and 193.4 kPa. Note: additional tests at normal loads of 400.7 and 327.3 kPa are not shown (mutual comparison of shear not possible). 58
Figure 8.4: Equal amounts of sand (100 gr of soil C) mixed with bentonite (left) and water (right). 59
Figure 8.5: Schematization of equal amounts of sand, conditioned with bentonite (left) and saturated with water (right). 59
Figure 8.6: Comparison of interface shear tests (soil C). Water-saturated tests in solid lines, mild bentonite-conditioned tests in dashed lines. Normal loads are of 50.0, 99.7 and 193.4 kPa. 60
Figure 8.7: Comparison of interface shear tests (soil A). Water-saturated tests in solid lines, bentonite-conditioned tests in dashed lines. Normal loads are of 50.0, 99.7 and 193.4 kPa. Note: additional tests at normal loads of 400.7 and 327.3 kPa are not shown (mutual comparison of shear not possible). 61
Figure 9.1: Foam leaking out of shear box assembly. 63
Figure 9.2: Comparison of interface shear tests (soil B). Water-saturated tests in solid lines, foam-conditioned tests in dashed lines. Normal loads are of 50.0, 99.7 and 193.4 kPa. Note: additional tests at normal loads of 400.7 and 327.3 kPa are not shown (mutual comparison of shear not possible). 64
Figure 9.3: Comparison of interface shear tests (soil C). Water-saturated tests in solid lines, foam-conditioned tests in dashed lines. Normal loads are of 50.0, 99.7 and 193.4 kPa. The foam-conditioned test at 50.0 kPa is an outlier but is reported anyway. Note: additional tests at normal loads of 400.7 and 327.3 kPa are not shown (mutual comparison of shear not possible). 65
Figure 9.4: Comparison of interface shear tests (soil C). Water-saturated tests in solid lines, foam-conditioned tests in dashed lines (thick foam). Normal loads are of 50.0, 99.7 and 193.4 kPa 66
Figure 10.1: Soil-machine friction coefficients from tunneling literature. **Square** datapoints: non-lubricated conditions; **circular** datapoints: lubricated conditions. **Green** datapoints: values measured/back-figured; **Blue** datapoints: values as generic guideline. Note: positioning of datapoints along the horizontal axis is arbitrary (but within the correct soil type), due to lack of information. Thesis results depicted in **red**. 70
Figure 10.2: Sand-steel friction coefficients from laboratory studies (Table 4.3). Thesis results depicted in **red**. 71
Figure 10.3: Clay-steel friction coefficients from laboratory studies (Table 4.3). Thesis results depicted in **red**. 71
Figure 10.4: Shear envelopes of soil A (kaolin). **Yellow** depicts soil inner shear strength. **Orange**, **Green** and **Blue** depict respectively water-saturated, foam-conditioned and bentonite-conditioned interface shear strength. 72
Figure 10.5: Shear envelopes of soil B (fine sand). **Yellow** depicts soil inner shear strength. **Orange**, **Green** and **Blue** depict respectively water-saturated, foam-conditioned and bentonite-conditioned interface shear strength. 73

Figure 10.6: Shear envelopes of soil C (coarse sand). **Yellow** depicts soil inner shear strength. **Orange**, **Green**, **Blue** and **Red** depict respectively water-saturated, foam-conditioned, bentonite-conditioned and thick foam-conditioned interface shear strength. 73
Figure 0.1: Fall cone test 1. 80
Figure 0.2: Fall cone test 2. 81
Figure 0.3: Fall cone test 3. 82
Figure 0.4: Plots from internal shear tests of soil A (water-saturated), conducted at normal loads of 50.0, 99.7, 193.4 and 400.7 kPa. Shear resistance is shown function of horizontal displacement. 83
Figure 0.5: Plots from internal shear tests of soil A (water-saturated), conducted at normal loads of 50.0, 99.7, 193.4 and 400.7 kPa. Shear resistance is shown function of vertical displacement. 83
Figure 0.6: Plots from internal shear tests of soil B (water-saturated), conducted at normal loads of 50.0, 99.7, 193.4 and 400.7 kPa. Shear resistance is shown function of horizontal displacement. 85
Figure 0.7: Plots from internal shear tests of soil B (water-saturated), conducted at normal loads of 50.0, 99.7, 193.4 and 400.7 kPa. Shear resistance is shown function of vertical displacement. 85
Figure 0.8: Plots from internal shear tests of soil C (water-saturated), conducted at normal loads of 50.0, 99.7, 193.4 and 400.7 kPa. Shear resistance is shown function of horizontal displacement. 89
Figure 0.9: Plots from internal shear tests of soil C (water-saturated), conducted at normal loads of 50.0, 99.7, 193.4 and 400.7 kPa. Shear resistance is shown function of vertical displacement. 89
Figure 0.10: Metal plate from TBM cutterhead. 90
Figure 0.11: Results of roughness measurement tests. Ra: arithmetical mean height of surface asperities; Ry/Rz: maximum height/width of the surface asperities; Rq: root mean square deviation of the surface asperities. 91
Figure 0.12: Plots from interface shear tests of soil A (water-saturated), conducted at normal loads of 50.0, 99.7, 193.4 and 400.7 kPa. Shear resistance is shown function of horizontal displacement. 92
Figure 0.13: Plots from interface shear tests of soil A (water-saturated), conducted at normal loads of 50.0, 99.7, 193.4 and 400.7 kPa. Vertical displacement is shown function of horizontal displacement (starting point is at end of consolidation). 92
Figure 0.14: Plots from interface shear tests of soil A (bentonite-conditioned), conducted at normal loads of 50.0, 99.7, 193.4 and 327.3 kPa. Shear resistance is shown function of horizontal displacement. 94
Figure 0.15: Plots from interface shear tests of soil A (bentonite-conditioned), conducted at normal loads of 50.0, 99.7, 193.4 and 400.7 kPa. Vertical displacement is shown function of horizontal displacement. 94
Figure 0.16: Plots from interface shear tests of soil A (foam-conditioned), conducted at normal loads of 50.0, 99.7, 193.4 and 327.3 kPa. Shear resistance is shown function of horizontal displacement. 96
Figure 0.17: Plots from interface shear tests of soil A (foam-conditioned), conducted at normal loads of 50.0, 99.7, 193.4 and 400.7 kPa. Vertical displacement is shown function of horizontal displacement. 96
Figure 0.18: Plots from interface shear tests of soil B (water-saturated), conducted at normal loads of 50.0, 99.7, 193.4 and 400.7 kPa. Shear resistance is shown function of horizontal displacement. 98

Figure 0.19: Plots from interface shear tests of soil B (water-saturated), conducted at normal loads of 50.0, 99.7, 193.4 and 400.7 kPa. Vertical displacement is shown function of horizontal displacement. 98
Figure 0.20: Plots from interface shear tests of soil B (bentonite-conditioned), conducted at normal loads of 50.0, 99.7, 193.4 and 327.3 kPa. Shear resistance is shown function of horizontal displacement. 100
Figure 0.21: Plots from interface shear tests of soil B (bentonite-conditioned), conducted at normal loads of 50.0, 99.7, 193.4 and 327.3 kPa. Vertical displacement is shown function of horizontal displacement. 100
Figure 0.22: Plots from interface shear tests of soil B (foam-conditioned), conducted at normal loads of 50.0, 99.7, 193.4 and 327.3 kPa. Shear resistance is shown function of horizontal displacement. 102
Figure 0.23: Plots from interface shear tests of soil B (foam-conditioned), conducted at normal loads of 50.0, 99.7, 193.4 and 327.3 kPa. Vertical displacement is shown function of horizontal displacement. 102
Figure 0.24: Plots from interface shear tests of soil C (water-saturated), conducted at normal loads of 50.0, 99.7, 193.4 and 400.7 kPa. Shear resistance is shown function of horizontal displacement. 104
Figure 0.25: Plots from interface shear tests of soil C (water-saturated), conducted at normal loads of 50.0, 99.7, 193.4 and 400.7 kPa. Vertical displacement is shown function of horizontal displacement. 104
Figure 0.26: Plots from interface shear tests of soil C (bentonite-conditioned), conducted at normal loads of 50.0, 99.7, 193.4 and 327.3 kPa. Shear resistance is shown function of horizontal displacement. 106
Figure 0.27: Plots from interface shear tests of soil C (bentonite-conditioned), conducted at normal loads of 50.0, 99.7, 193.4 and 327.3 kPa. Vertical displacement is shown function of horizontal displacement. 106
Figure 0.28: Plots from interface shear tests of soil C (“mild” bentonite-conditioned), conducted at normal loads of 50.0, 99.7 and 193.4 kPa. Shear resistance is shown function of horizontal displacement. 108
Figure 0.29: Plots from interface shear tests of soil C (“mild” bentonite-conditioned), conducted at normal loads of 50.0, 99.7 and 193.4 kPa. Vertical displacement is shown function of horizontal displacement. 108
Figure 0.30: Plots from interface shear tests of soil C (foam-conditioned), conducted at normal loads of 50.0, 99.7, 193.4 and 327.3 kPa. Shear resistance is shown function of horizontal displacement. 110
Figure 0.31: Plots from interface shear tests of soil C (foam-conditioned), conducted at normal loads of 50.0, 99.7, 193.4 and 327.3 kPa. Vertical displacement is shown function of horizontal displacement. 110
Figure 0.32: Plots from interface shear tests of soil C (foam-conditioned), conducted at normal loads of 50.0, 99.7 and 193.4. Shear resistance is shown function of horizontal displacement. 112
Figure 0.33: Plots from interface shear tests of soil C (foam-conditioned), conducted at normal loads of 50.0, 99.7 and 193.4 kPa. Vertical displacement is shown function of horizontal displacement. 112

List of Tables

Table 3.1 9
Table 3.2 (Song et al., 2010) 11
Table 3.3: Summary of soil-machine friction coefficients from tunneling literature. 14
Table 4.1: $f\varphi$ values for different test scenarios (upper line refers to smooth steel, lower line refers to rough steel) (Potyondy, 1982). 18
Table 4.2 (Stafford & Tanner, 1982b): 20
Table 4.3: Summary of friction angles and coefficients from literature of laboratory studies. 25
Table 6.1: Grain properties of soil B. 38
Table 6.2: Grain properties of soil C. 39
Table 6.3: Properties of Ibeco B1 (provided by Imerys). 40
Table 6.4: 48
Table 8.1: Interface friction angle reduction due to bentonite conditioning (soil B). The last line shows values averaged over all tests (including those at 327.3 and 400.7 kPa). 57
Table 8.2: Interface friction angle reduction due to bentonite conditioning (soil C). The last line shows values averaged over all tests (including those at 327.3 and 400.7 kPa). 58
Table 8.3: Interface friction angle difference between mild bentonite-conditioned and water-saturated specimens (soil C). The last line shows values averaged over all tests. 60
Table 8.4: Residual interface friction angle difference between bentonite-conditioned and ordinary specimens (soil A). The last line shows values averaged over all tests. 61
Table 9.1: Interface friction angle difference between foam-conditioned and water-saturated specimens (soil B). The last line shows values averaged over all tests (including those at 327.3 and 400.7 kPa). 64
Table 9.2: Interface friction angle difference between foam-conditioned and water-saturated specimens (soil C). The last line shows values averaged over all tests (including those at 327.3 and 400.7 kPa). 65
Table 9.3: Interface friction angle difference between thick foam-conditioned and water-saturated specimens (soil C). The last line shows values averaged over all tests. 66
Table 0.1: Results of interface shear tests of soil A (water-saturated). 93
Table 0.2: Results of interface shear tests of soil A (bentonite-conditioned). 95
Table 0.3: Results of interface shear tests of soil A (foam-conditioned). 97
Table 0.4: Results of interface shear tests of soil B (water-saturated). 99
Table 0.5: Results of interface shear tests of soil B (bentonite-conditioned). 101
Table 0.6: Results of interface shear tests of soil B (foam-conditioned). 103
Table 0.7: Results of interface shear tests of soil C (water-saturated). 105
Table 0.8: Results of interface shear tests of soil C (bentonite-conditioned). 107
Table 0.9: Results of interface shear tests of soil C (“mild” bentonite-conditioned). 109

Table 0.10: Results of interface shear tests of soil C (foam-conditioned)..... 111

Table of Contents

Abstract ii

Sommario iii

Preface iv

Nomenclature vi

List of Figures ix

List of Tables xiv

Table of Contents xvii

1 Introduction 1

1.1 TBM excavation 1
1.2 TBM performance predictive models 3
1.3 Problem Statement and Objectives 4
1.4 Scope 5
1.5 Approach 5

Part 1: Background 6

2 Theory on friction 7

3 Friction coefficients from tunnelling literature 9

4 Friction coefficients from laboratory literature 17

Part 2: Laboratory Studies 32

5 Introduction to laboratory studies 33

6 Materials and Methods 35

6.1 Materials 35
6.1.1 Soils 35
6.1.1.1 Soil A 36
6.1.1.2 Soil B 37
6.1.1.3 Soil C 39
6.1.2 Bentonite 40
6.1.3 Foaming Agent 40
6.1.4 Shear Apparatus 41

6.1.5 Bentonite Apparatus 42
6.1.6 Foam Apparatus 42
6.2 Methods 43
6.2.1 Shear box set-up 43
6.2.1.1 Internal Strength 43
6.2.1.2 Interface Friction 43
6.2.2 Preparation Techniques 44
6.2.2.1 Water-saturated Specimens 44
6.2.2.2 Conditioned Specimens (Bentonite Slurry) 44
6.2.2.3 Conditioned Specimens (Foam Suspension) 46
6.2.2.4 Bentonite Slurry 47
6.2.2.5 Foam Suspension 47
7 Experiment Results 50
7.1 Soil A 51
7.1.1 Water-saturated 51
7.1.2 Bentonite-conditioned 51
7.1.2 Foam-conditioned 52
7.2 Soil B 52
7.2.1 Water-saturated 52
7.2.2 Bentonite-conditioned 52
7.2.3 Foam-conditioned 53
7.3 Soil C 53
7.3.1 Water-saturated 53
7.3.2 Bentonite-conditioned 54
7.3.3 Foam-conditioned 54
Part 3: Analysis and Discussion 55
8 Bentonite Conditioning 56
8.1 Sand 56
8.2 Clay 61
9 Foam Conditioning 63
9.1 Sand 64
9.2 Clay 68
Part 4: Conclusions and Recommendations 69
10 Conclusions 70
11 Recommendations 75
Bibliography 76
Part 5: Appendices 79

A. Soil A Classification Tests 79
I. Density (Pycnometer): 79
II. Plastic Limit: 79
III. Liquid Limit: 80
IV. Internal Shear Strength 83
B. Soil B Classification Tests 84
I. Density (Pycnometer): 84
II. Internal Shear Strength 85
C. Soil C Classification Tests 86
I. Density (Pycnometer): 86
II. Max/Min Void Ratio and Density 86
III. Internal Shear Strength 89
D. Surface Roughness Measurements 90
E. Interface Shear Tests, soil A 92
I. Water-saturated 92
II. Bentonite-conditioned 94
III. Foam-conditioned 96
F. Interface Shear Tests, soil B 98
I. Water-saturated 98
II. Bentonite-conditioned 100
III. Foam-conditioned 102
G. Interface Shear Tests, soil C 104
I. Water-saturated 104
II. Bentonite-conditioned (high bentonite/soil ratio) 106
III. Bentonite-conditioned (low bentonite/soil ratio) 108
IV. Foam-conditioned 110
V. Foam-conditioned (thicker foam) 112

1 Introduction

The present chapter introduces tunnel boring machines (TMB's), illustrating their typical design and functioning principles. Additionally, it is described how the main TBM driving parameters (torque and thrust) are estimated in practice. The current shortcomings of this estimation, as well as possible improvements are discussed, underlying the relevance of friction on the subject. Further along the text, the objective and scope of the thesis are announced. Finally, the approach of the thesis is discussed at the end of the chapter.

1.1 TBM excavation

TBM's are devices which allow a full mechanization of the tunnel building process: from the actual excavation and removal of the ground, to the instalment of the lining segments. These machines come in various sizes and designs and have evolved to adapt to a wide spectrum of excavation conditions.
From a technical perspective, a TBM is made of multiple modules, each performing a different task within the whole machine. These work in contemporaneous as a chain line, allowing seamless tunnelling progress. Figure 1.1 below depicts a schematization of a typical TBM, showing its main constitutive parts:

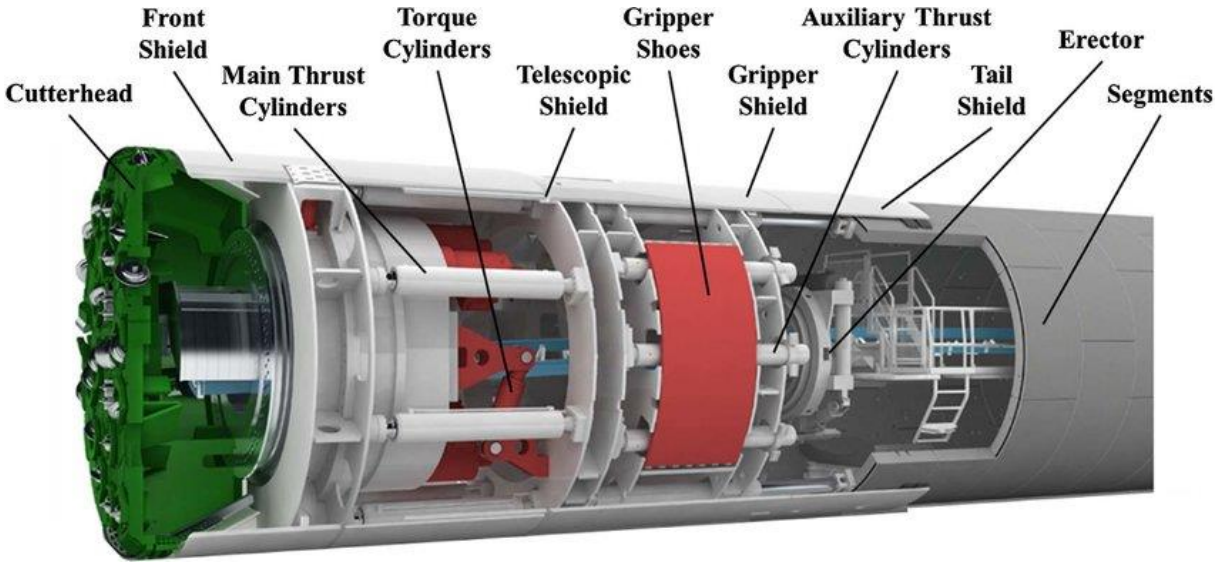

Figure 1.1: Structure and main components of a double-shield TBM (www.herrenknecht.com).

The outer "skin" of a TBM, known as shield, consists of a cylindrical hollow structure. Its function is to support the surrounding ground while this is being excavated, protecting the inner TBM components and the workers. Ground protection facing the excavation head comes from a frontal barrier known as bulkhead. The shield is sometimes divided in multiple sections, depending on the complexity of the machine. The shield is intermittently pushed forward by a jacking system, contemporaneously allowing excavation advance and lining instalment. The last completed lining ring acts as a loading frame for the hydraulic jacks.
A circular cutterhead equipped with cutting tools is located at the front of the machine, matching the leading end of the shield. Electric motors provide thrust and torque to the cutterhead, allowing it to rotate and excavate the soil in front of it. Figure 1.2 below depicts the front shield and cutterhead of a TBM assembled together.

Figure 1.2: TBM cutterhead (in blue) and shield (in white) assembled prior to excavation (tunnellingjournal.com).

Inside the TBM, the volume located between the cutterhead rear face and the bulkhead is known as excavation chamber. In this section, excavated soil is collected and gradually transported to the tail of the machine and out of the tunnel. Accurate pressure calibration of the soil mass in the excavation chamber is paramount. Insufficient pressure could result in un-acceptable ground settlements at the surface, as well as groundwater possibly entering the machine. On the other hand, excessive pressure could result in a so-called blow-out (ground heave and disaggregation).
The optimal technical design of the supporting system depends on type and condition of the soil to be excavated. Two kinds are most commonly used and define the two main varieties of TBM: EPB and slurry machines.

In EPB machines, a screw conveyer transports the excavated material from the excavation chamber to the tail of the TBM. The material collected in the excavation chamber is used as a supporting mean: the rate at which it is withdrawn by the screw conveyer regulates the pressure at the excavation face. Faster actuation of the screw results in a pressure reduction at the face (and vice-versa). This design implies that the machine advance rate is subordinated to the capacity of the screw conveyer. Prior to its removal, the excavated soil is often combined with foam and/or additives. These create a homogeneous soil “paste” which has improved mechanical characteristics. Moreover, soil conditioners are also used to reduce machine wear and to make the excavation face watertight. Figure 1.3 below shows a schematization of an EPB TBM:

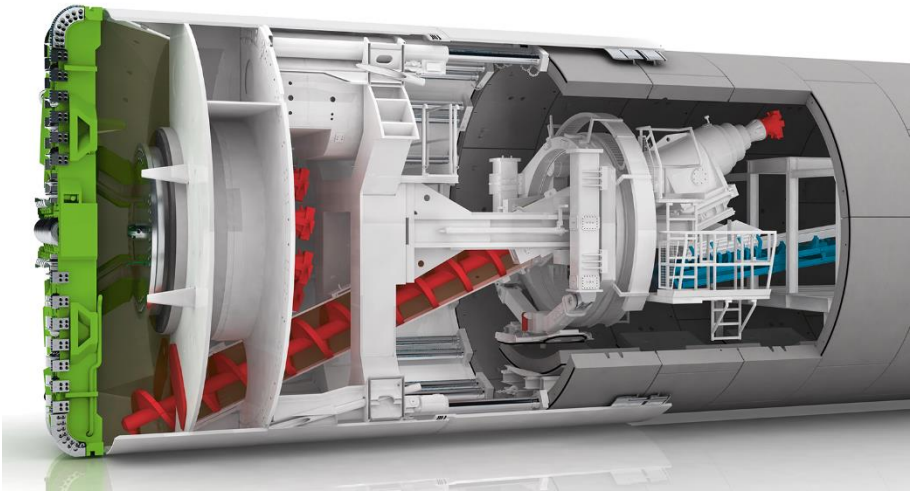

Figure 1.3: Structure of an EPB shield TBM. The screw conveyer (pictured in red) goes through the bulkhead and into the excavation chamber (www.herrenknecht.com).

In slurry machines, support pressure at the excavation face is provided by a liquid bentonite suspension, also known as slurry. This suspension is prepared in a dedicated plant outside the TBM and is fed to the excavation chamber via a pipe system. Bentonite pressure is adjusted so it balances the soil and water pressure profiles acting on the working face. Unlike for EPB machines, therefore, the excavation rate is not subordinated by the face pressure requirements.

The excavated soil is mixed by the cutterhead with the bentonite. A suction pipe carries the soil-loaded slurry to the separation plant. Here the excavated material is filtered out of the bentonite, before the latter is re-circulated into the system. Figure 1.4 below shows a schematization of a slurry shield TBM:

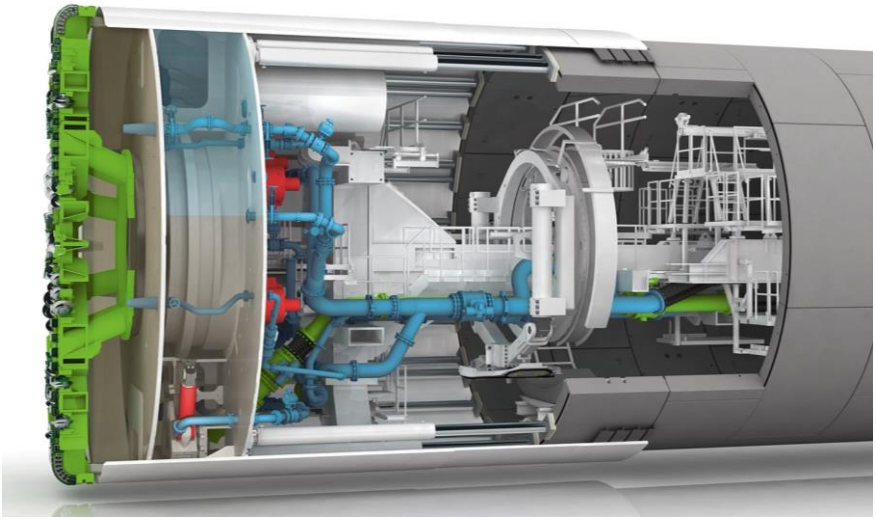

Figure 1.4: Structure of a slurry shield TBM. A pressurized air cushion allows fine tuning of slurry pressure. The pipe system is displayed in light blue, the suction pipe is displayed in green (www.herrenknecht.com).

EPB machines are ideally suited to excavate through fine-grained soils, or in general through materials which contain a high-enough proportion of fine particles. These are, in fact, necessary to form a "workable" soil paste which is capable of withstanding ground pressure. Nonetheless, development of soil additives and foams have made possible to extend the applicability range of EPB shields to coarser soils.
As for slurry shields, their use is preferably limited to coarse-grained soils, or in general materials which contain a low-enough proportion of fine particles. These, in fact, tend to "bond" to the slurry and require considerable effort to be filtered in the bentonite treatment plant. Additionally, the technical design of slurry shields is comparatively more intricate than that of EPB machines, meaning their use is more complex.

1.2 TBM performance predictive models

In TBM practice, the preliminary evaluation of thrust and torque requirements of excavating machines is commonly performed using Equation 1 (Krause, 1987) and Equation 2 (Japan Society of Civil Engineers, 2007), respectively:

Equation 1:

$$P_V = \beta \cdot D^2$$

Equation 2:

$$T = \alpha \cdot D^3$$

Where:

- P_V is the TBM thrust force [kN];
- T is the TBM torque [Ton·m];
- D is the TBM diameter [m];
- β is an empirical factor = 500 to 1200;
- α is an empirical factor = 1 to 2.5.

These equations have been developed empirically, by evaluating monitoring data from numerous excavation projects. These expressions relate thrust and torque exclusively to cutterhead diameter, while all the other crucial variables (site geology, soil conditioning, TBM design, etc.) are simply conveyed by the empirical coefficients β and α. As a result, as shown in Figure 1.5 and Figure 1.6 below, Equation 1 and Equation 2 provide only a rough estimation of TBM thrust and torque requirements. This inaccuracy has become increasingly problematic, as the average diameter of TBM's has grown considerably over the years.

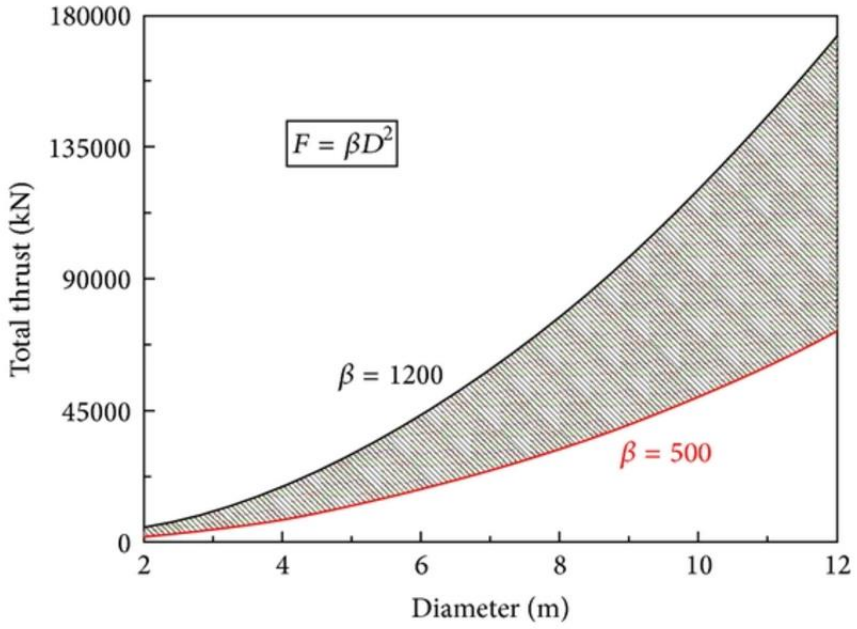

Figure 1.5: Prediction of TBM thrust according to Equation 1, depending on cutterhead diameter (Zhang, Qu, Cai, Kang, & Huang, 2014).

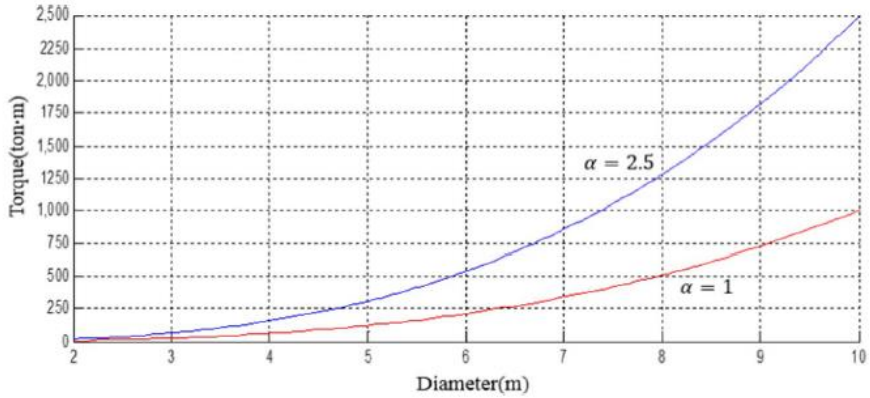

Figure 1.6: Prediction of TBM torque according to Equation 2, depending on cutterhead diameter (Zhou & Zhai, 2018).

To improve TBM preliminary design, researchers have developed more comprehensive models to predict thrust and torque parameters, among which (Japan Society of Civil Engineers, 2007) and (Shi, Yang, Gong, & Wang, 2011). In these studies, the overall TBM thrust and torque are modelled as sum of multiple components. Each of these terms relates to specific mechanisms and dynamics which influence the overall thrust and/or torque of the excavating machine.
For both above-mentioned models, the most influential components (i.e. those which have the highest influence over the total TBM thrust and torque) have been shown to depend on the friction between soil and excavation machine. Accordingly, to make effective use of these predictive models, as well as to help to develop new ones, friction coefficients need to be determined precisely. Consequently, improved knowledge of friction coefficients is an important step towards more accurate TBM design.

1.3 Problem Statement and Objectives

Soil-machine friction coefficients selected in mechanized excavation practice are usually back-figured empirically from data of previous tunneling projects. They are generalized based on soil and operational conditions and used as inputs for the preliminary design of future TBM projects. The effect of soil conditioning, if taken into account, is considered simply by reducing friction coefficients by a certain factor, according to qualitative practical experience.
By following this approach, friction coefficients lack a physical connection to the excavation mechanisms and to the soil characteristics. Moreover, the databases from which friction coefficients are generalized are compiled with data from hundreds of tunneling projects. These have distinct characteristics and might adopt different assumptions and

models to back-figure excavation data. Consequently, resulting friction coefficients are inevitably generic and convey wide tolerances. This uncertainty hinders the design of excavation machines, which must be built to excessively high margins, compared to the capacity required in the field.

The objectives of this thesis are:

- To classify and examine the available sources reporting:
  - Theoretical or empirical friction coefficients between excavating machine and ground;
  - Empirical friction coefficients between soil and steel obtained from laboratory studies

  and to investigate a relation between friction coefficients belonging to these two groups;
- To perform interface shear tests between various soils and steel and to determine soil-steel friction coefficients from the outcome of these tests;
- To quantify the influence of soil additives on the friction coefficients determined from the above-mentioned interface shear tests between soil and steel;
- To assess whether a direct shear apparatus, along with ordinary geotechnical investigations, can provide results which are satisfactory and useful for TBM design and use.

1.4 Scope

The scope of this thesis is to extend the results of an ordinary geotechnical laboratory analysis to the evaluation and selection of soil-machine friction mechanisms found in TBM excavation. This study is intended to improve the estimation of friction coefficients of TBM excavation and to provide a measure of the lubricating effects of soil conditioners.
This thesis could provide valuable information for the preliminary design of excavation machines and projects. The quantitative results of the study could be implemented in the recently developed TBM predictive models, making them more effective. Overall, the outcome of the thesis could result in more accurate knowledge of machine requirements and parameters, yielding a more economical usage of TBM.'s

1.5 Approach

The focus of the study is primarily on soil type and state, as well as on the use of soil additives. Values obtained from the laboratory investigation are also supplemented and compared with a summary of those available from literature.
First a selection of soil types relevant to typical TBM ground conditions is made. Laboratory classification tests are, then, performed on the abovementioned soils, to obtain detailed quantitative information on their properties and characteristics. Afterwards, soil-steel interface shear tests are conducted to measure the interface friction angle of the chosen soil types, when shearing against steel. These tests are performed varying soil properties and for multiple boundary conditions of shear rate, normal stress, etc. The effects of foam and slurry to soil-steel friction is analyzed during the interface shear tests, by treating the specimens before testing.
Finally, the results obtained from the laboratory investigation are compared and assessed with values reported from literature. This allows to establish whether the thesis has produced meaningful results which are applicable in practice.

Part 1: Background

2 Theory on friction

The present paragraph consists of a general dissertation on the notion of friction. Relevant concepts such as friction coefficient, friction angle and failure envelope are introduced. The theory presented in this paragraph is the foundation upon which the next parts of the thesis build on.

In general terms, friction is the force opposing to the sliding and/or rolling motion of a body against another one. Friction manifesting between bodies at rest is defined as static. Friction manifesting between bodies in motion relative to each other is defined as kinematic.
The friction developing between two undeformable bodies is expressed by Equation 3:

Equation 3:

$$F_f = \mu \cdot F_\perp$$

Where:

- F_f is the friction force;
- $F_\perp$ is the force perpendicular to the contact surface between the two bodies;
- μ is the friction coefficient;

The latter is function of surface material and geometry, and for static conditions is always greater or equal than for kinematic conditions.
The relation between friction and normal force (or stress) can also be expressed in terms of the friction angle φ, defined by Equation 4 as:

Equation 4:

$$\varphi = tan^{-1}\,\mu$$

The shear resistance of a soil is mainly determined by the friction acting between its grains (for internal strength) or its grains and an outer surface (for interface strength). The higher is the friction, the more force is required to shear the soil, whether "internally" or along a surface.
Some soils, more specifically those with fine particles, show a noticeable shear resistance even for null normal loads. This property is defined as cohesion (c) and is the soil particle-to-particle strength independent of normal load. Similarly, the soil-to-external surface strength independent of normal load is defined as adhesion, a. Cohesion and adhesion are not a result of friction mechanisms. They are, rather, a consequence of the attraction forces acting between differently charged molecules.

The strength profile, or envelope, of soils depends on their cohesion/adhesion and frictional properties and is often expressed with the Mohr-Coulomb criterion. This relates shear strength τ to normal load σ through the friction angle φ, as shown in Equation 5:

Equation 5:

$$\tau = tan\,\varphi \cdot \sigma + c$$

Figure 2.1 below shows an example of Mohr-Coulomb shear envelope:

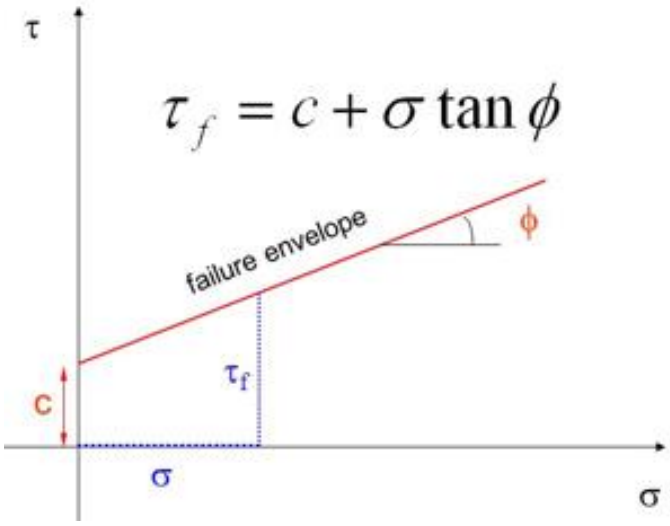

Figure 2.1: Soil failure envelope. The intercept of the failure envelope represents cohesion (McCarthy, T. Direct Shear Test, Slide Player).

Failure envelopes analogous to the one in Figure 2.1 are obtainable by measuring the shear resistance of a specimen subjected to at least two different normal loads. Each pair of τ-σ values corresponds to a point in the homonymous plane. The line intersecting these two points is the soil shear envelope. Soil shear envelopes can be convex, meaning that friction angle decreases with increasing normal load. This feature cannot be recognized, if relying on only two points in the τ-σ plane. Consequently, it is advised to derive strength envelopes from as many τ-σ points as possible. Failure envelopes can be drawn for both internal and external shear tests. In the first case, internal friction angle and cohesion (φ, c) are be the measured parameters. In the second case, interface friction angle and adhesion (δ, a) are the measured parameters.

3 Friction coefficients from tunnelling literature

The present paragraph summarizes the friction coefficients between ground and TBM reported by literature on mechanized tunnel excavation. The publications listed have either a theoretical or empirical background. In the first case, the studies deal with general conditions, without referring to any specific excavation project. Therefore, these publications are to be seen as guidelines. In the second case, the reported ground-machine friction coefficients are back-figured from actual excavation project data.
At the end of the chapter, Table 3.3 summarizes friction coefficients based on influential parameters. This information is later used as a reference to assess and possibly validate the results obtained from the thesis laboratory investigation.

(Lunardi, Gatti, & Cassani, 2011) describe the geological and geotechnical assessments performed to select the optimal EPB TBM for the "Sparvo" tunnel, Italy. This project consists of two parallel bores with a cutting diameter of 15.62 m and a length of 2600m. The tunnel alignment initially goes through a thin stratum of clayey-silty deposits, followed by a highly-deformed clay formation. A tectonic contact, then, marks the passage from the clays to sandstones, with intervening siltite and argillite strata. Before breaking through the opposite side, the abovementioned clay formation is found again. Properties and characteristics of these strata can be found in Table 3.3.
The thrust required by the TBM is estimated by (Lunardi et al., 2011) as sum of multiple contributions, similarly to (Japan Society of Civil Engineers, 2007) and (Shi et al., 2011). The soil-machine shield friction coefficient is estimated by (Lunardi et al., 2011) to be 0.25-0.35, without reference to any of the specific soils mentioned above. The use of bentonite lubricant is reported to be able to lower this coefficient down to 0.15.

(Ramoni, 2010) summarizes the information of the previous works of (Gehring, 1995), (Herzog, 1985) and (POHL) and provides a table illustrating typical friction coefficients between TBM shield and ground. Various, generic soil types are considered, as well as the effect of bentonite lubrication. Shield-soil friction coefficients analogous to those of (Ramoni, 2010) are also provided by (Maidl, Thewes, & Maidl, 2013).

(Shi et al., 2011) developed a model to predict cutterhead torque requirements, based on TBM specifications and its interaction with the surrounding soil. The authors suggest modelling torque as sum of eight, independent components, the most influential of which have been found to depend on the friction between soil and machine. A simulation test rig, consisting of a 1.8m diameter TBM and a soil excavation chamber, is used to validate the model. Three kinds of soil are tested, namely clay, sandy soil and sandy gravel.
All the eight expressions for torque prediction include f, the coefficient of dynamic friction between soil and machine (equivalent to μ). This is reported by (Shi et al., 2011) to be 0.2, 0.3 and 0.35 for clay, sandy soil and sandy gravel, respectively.
The first three of the eight torque components reported by (Shi et al., 2011) (T_1, T_2, T_3) are analyzed to back-figure the actual f value used within the same expressions. It is to be noted that a discrepancy is found between the f values reported by the authors (0.2, 0.3, 0.35) and the back-figured ones. There appears to be considerable scatter in the latter ones, instead of a single value per each soil, as can be seen in Table 3.1:

Table 3.1

η	T_1 [kNm]	f_{T_1}	T_2 [kNm]	f_{T_2}	T_3 [kNm]	f_{T_3}
			Clay			
0.3	21.63	**0.2605**	27.56	**0.1107**	10.38	**0.125**
0.7	12.13	**0.3408**	27.56	**0.1107**	5.83	**0.1635**
			Sandy Soil			
0.3	31.57	**0.3482**	40.21	**0.3796**	15.16	**0.1672**
0.7	17.07	**0.4555**	40.21	**0.3796**	8.49	**0.2185**
			Sandy Gravel			
0.3	35.09	**0.387**	48.79	**0.4708**	18.76	**0.2069**
0.7	21.90	**0.5635**	48.79	**0.4708**	10.52	**0.2707**

Compared with the data obtained from the experimental test rig, torque figures calculated by the predictive model of (Shi et al., 2011) agree on clay, but are lower for the other soils tested (up to 30 kNm of difference), as can be seen in Figure 3.1 below:

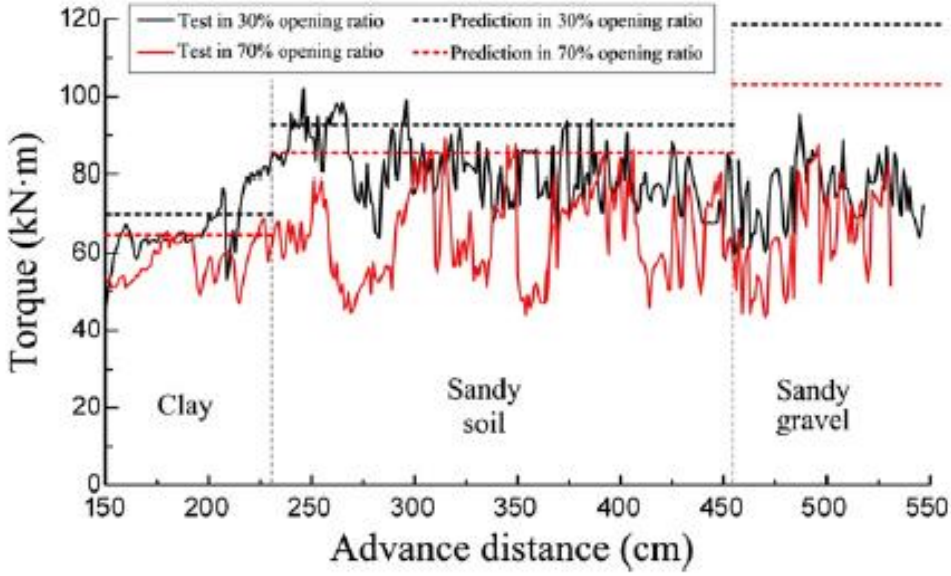

Figure 3.1: Comparison between predicted (dotted) and measured (bold) torque, for three soil types and two opening ratios (Shi et al., 2011).

This discrepancy in torque between predictions and test data is attributed to soil additives. Foam and Bentonite injection, in fact, are said to reduce soil-machine friction, leading to lower measured torque, compared to the model predictions. The authors themselves suggest soil conditioning should be taken into consideration to acquire improved results.

(Festa, 2015) investigated the mechanical equilibrium of a TBM operating in soft soil, based on monitoring data recorded during the construction of the Hubertus tunnel, The Hague. The two parallel tubes were bored using a 10.5 m diameter machine, mainly through sand with varying degree of density. Machine data was processed and later used to verify multiple physical processes occurring during mechanized excavation.
To calculate the resistance to the machine advance, the author adopts an average constant friction coefficient of μ = 0.05, initially applied along the whole tunnel alignment. This value yields an overall average longitudinal equilibrium between calculated drag force and measured resistance to shield advance. According to (Festa, 2015), such a low value is selected because friction coefficient is regarded as a calibration factor to best fit the data, rather than an actual soil parameter. Figure 3.2 below shows the calculated longitudinal drag force (with μ = 0.05), compared with the measured resistance to shield advance.

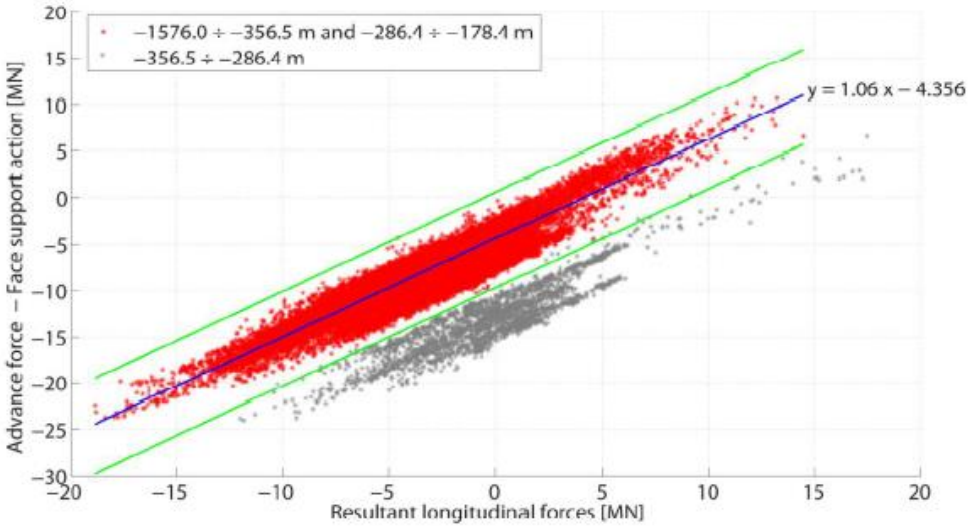

Figure 3.2: Comparison between calculated longitudinal drag force (in blue) and measured resistance to shield advance (in red) (Festa, 2015).

A variable friction coefficient is believed to have been capable of yielding longitudinal equilibrium at any "local" advance. A maximum friction coefficient of 0.25 is proven to be high enough to make longitudinal balance possible, even in the most unfavorable sections of the tunnel.
Finally, (Festa, 2015) highlights a discrepancy between the average friction coefficient assumed in the model (0.05) and the typical values from literature (> 0.3). This mis-match is believed to result from the fact that the TBM shield is usually not in direct contact with the surrounding soil, because an interface bentonite layer exists between soil and shield wall. Such layer produces a lubricating effect that would justify the adoption of average friction coefficients as low as 0.05.

(Song, Liu, & Guo, 2010) analyzed the effect of geology, driving parameters and cutterhead design in TBM excavation and formulated a cutterhead torque forecast model. TBM torque is modelled as sum of seven distinct components, each referring to a specific mechanism occurring during excavation. Similarly to other publications, (Song et al., 2010) highlights how the above-mentioned torque components are mainly dependent on friction between excavation machine and surrounding soil.
Authors address, then, to additional engineering data recorded from different tunnel projects, to assess the capability of their forecast model to predict torque. Table 3.2 below depicts, for each of these projects, the parameters used. The error range of the model predictions proves to be within 10% of the data recorded on field.

Table 3.2 (Song et al., 2010)

Project ID	D (m)	η	k	μ	γ (KN/m³)	H_c (m)	P (Kpa)	c (KN/m²)	w/ω (m)	Forecast value (KN·m)	T (KN·m)	Error
Shanghai subway No.2(West Extension I)	6.34	0.3	0.86	0.14	16.00	14.95	205.91	22.0	0.03	1157.56	1108.0	-4.47%
Shanghai subway No.2(West Extension II)	6.34	0.4	0.74	0.27	16.00	17.49	207.41	25.0	0.09	1902.65	2062.0	7.73%
Shanghai subway No.6	6.34	0.3	0.78	0.22	14.00	14.00	153.58	6.0	0.07	1311.54	1212.0	-8.21%
Tianjin subway (Contract part)	6.39	0.3	0.65	0.38	19.06	11.81	145.90	17.2	0.03	2121.45	1981.6	-7.06%
Guangzhou subway No.2	6.30	0.28	0.41	0.73	19.60	14.70	118.77	52.4	0.09	4020.57	4038.0	0.43%
Japanese subway	7.95	0.45	0.79	0.21	19.00	25.50	383.77	70.0	0.05	5151.82	5000.0	-3.04%
Tianjin subway No.9	6.34	0.36	0.65	0.38	19.06	11.80	250.00	15.0	0.10	1715.01	1709.6	-0.32%
Chengdu subway No. 1	6.25	0.35	0.46	0.65	23.00	12.78	54.60	0.0	0.09	3787.80	3970.0	4.59%

It is worth noting that friction coefficients reported in Table 3.2 spread over a wide range of values (i.e. from 0.14 to 0.73), which is considerably broader than what is typically reported by other literature. Additional information possibly explaining this scatter is often missing (whenever available, further information can be seen in Table 3.3).
Moreover, it is not clear whether friction coefficients of Table 3.2 are derived prior to excavation, or if they are back-figured according to the driving parameters recorded during excavation.

(Ates, Bilgin, & Copur, 2014) compiled a database of operational and design parameters of 262 TBM's used worldwide after 1985. Torque values obtained from the predictive models of (Shi et al., 2011) and (Japan Society of Civil Engineers, 2007) are compared with empirical data from each project of the above-mentioned database. Within the predictive models, soil-machine friction coefficients μ are taken as 0.25, regardless of soil type. Whenever soil conditioning was used during excavation, friction coefficients μ used in the models lower to 0.10-0.15 for slurry machines and 0.1-0.2 for EPB machines. As can be seen in Figure 3.3 and Figure 3.4 below, installed values from the database are found to be between the boundaries of torque predicted by the models.

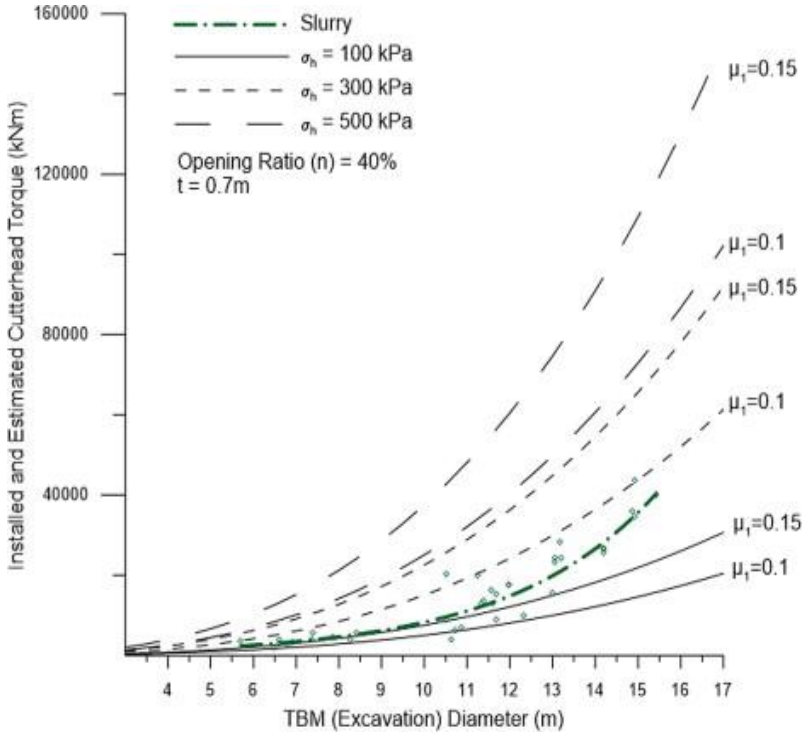

Figure 3.3: Comparison between installed and predicted cutterhead torque, for slurry TBM's (Ates et al., 2014).

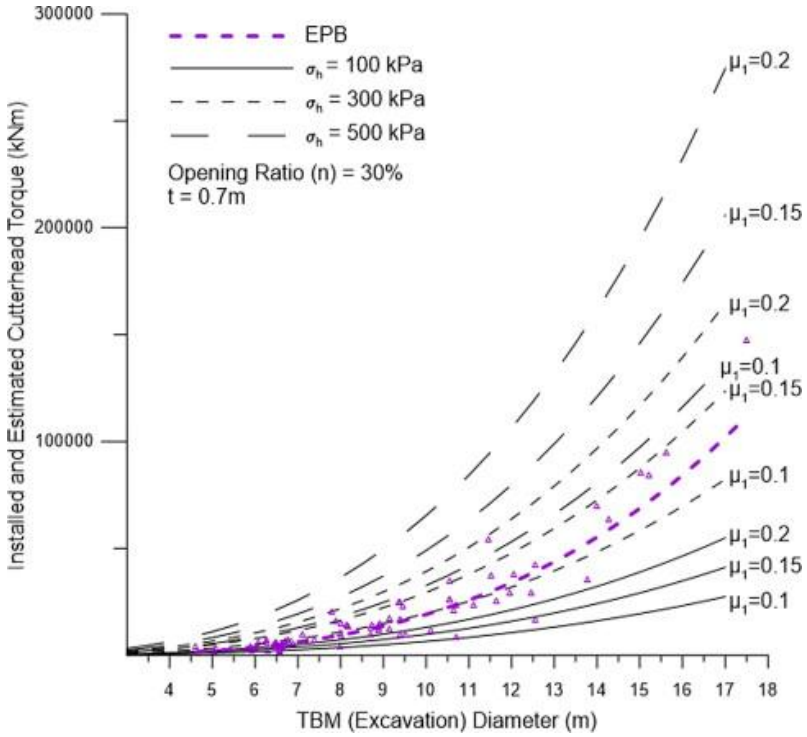

Figure 3.4: Comparison between installed and predicted cutterhead torque, for EPB TBM's (Ates et al., 2014).

Thrust values obtained from the predictive model of (Japan Society of Civil Engineers, 2007) concerning cutterhead side friction and cutting thrust are compared with empirical data from each project of the above-mentioned database. Within the predictive model, soil-machine friction coefficients μ are taken as 0.12 (for lubricated dynamic cases), 0.25 (for non-lubricated dynamic cases) and 0.45 (for static friction cases). It is possible for the authors to state that installed thrust values from the database are generally between estimated values for all types of TBM's, as can be seen in Figure 3.5 below:

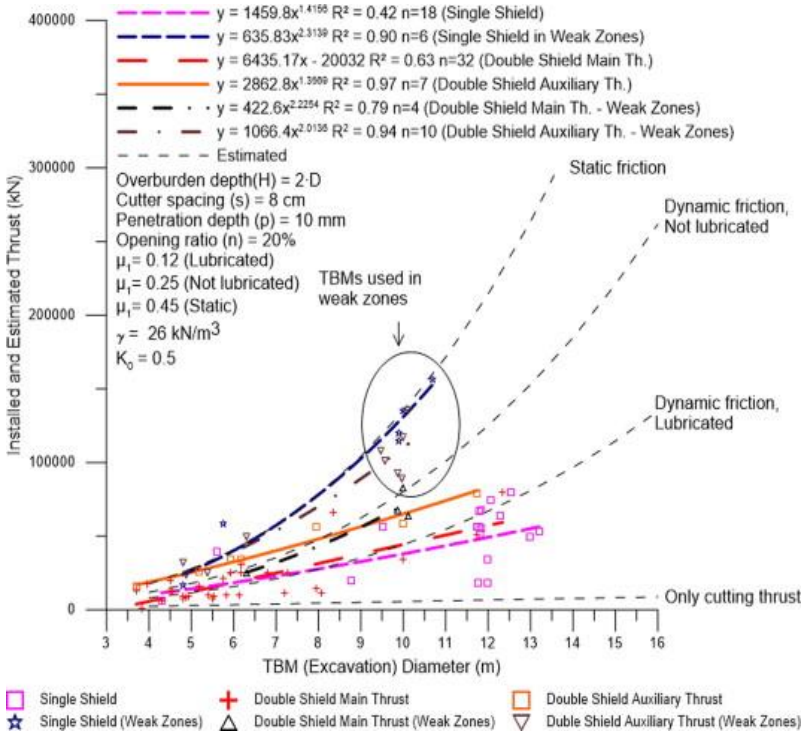

Figure 3.5: Comparison between installed and predicted cutterhead thrust (Ates et al., 2014).

(Godinez, Yu, & Mooney) investigate the ability of a modified version of the model proposed by (Shi et al., 2011) to predict the torque requirements of a 6.44m diameter TBM. Influence of parameters such as geology, soil conditioning, face pressure, etc. on torque is considered. The results from the model are compared with data obtained from a metro project in Seattle, where the above-mentioned TBM had been used.

The coefficient of friction between cutterhead and sheared conditioned soil is calculated according to Equation 6:

Equation 6:

$$\mu_i = \tan(f_i R_i \varphi)$$

where the angle of internal friction of the soil φ is reduced, accounting for soil conditioning (R_i) and irregular shape of the TBM surface (f_i). f_i is assumed = 1 for all cases, while R_i values are investigated for each soil scenario. As can be seen in Figure 3.6 below, for sand and gravel the best fitting R_i coefficients are found to be 0.35 and 0.37, respectively. As for clay, the best fitting R_i decreases to 0.15 (additional details are available in Table 3.3). These values lead authors to quantify the soil shear strength reduction due to soil conditioning as 65-67% for sand and gravel and 80% for clay.

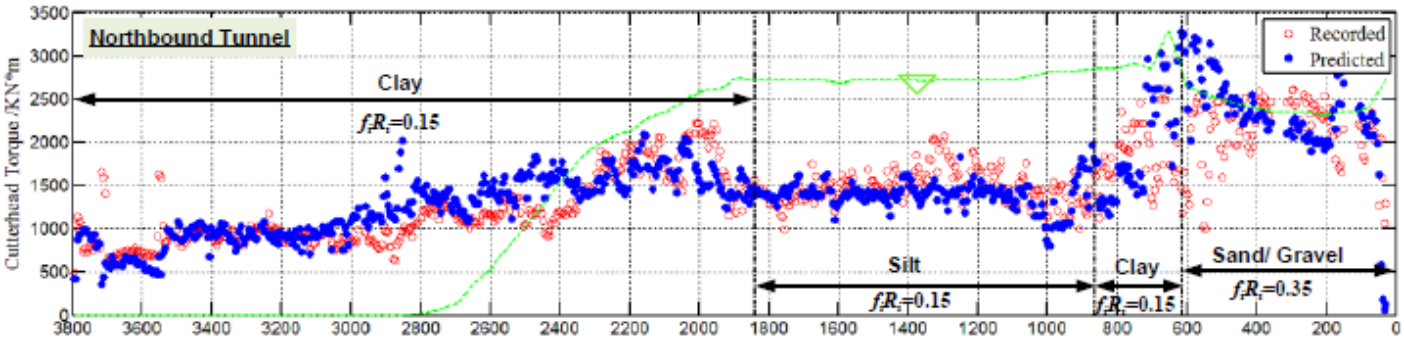

Figure 3.6: Comparison between recorded (red) and predicted (blue) torque values (Godinez et al.).

It is to be mentioned, as the authors of the present publication did themselves, that fitting of model parameters relying on measured torque is an underdetermined problem. In fact, the equations assumed to predict torque components are not necessarily correct. In other words, there are more unknowns than knowns. This creates uncertainty in the findings reported by (Godinez et al.) that require further research.

Table 3.3: Summary of soil-machine friction coefficients from tunneling literature.

Soil Type	Soil Description	Soil Properties	μ (-)		Remarks; Publication/s
			Non-Lubricated	Lubricated	
Rock	Sandstone with intervening siltite and argillite strata	γ=25 kN/m^3; *GSI*=40 MPa; *E*=2000 MPa φ=30°	**0.25-0.35**	**0.15** (Bentonite lubricants)	(Lunardi et al., 2011)
	Not specified	-	**0.25-0.30**	**0.10-0.15** (Bentonite lubricants)	(Ramoni, 2010), (Gehring, 1995), (Herzog, 1985)
Gravel	Not specified	-	**0.55**	**0.35-0.45** (Bentonite lubricants)	(Maidl et al., 2013)
	Not specified	-	**0.25-0.30**	**0.15** (Bentonite lubricants)	(Ramoni, 2010), (Gehring, 1995), (Herzog, 1985)
	Not specified	γ=20.2 kN/m^3; φ=37.8°; *c*=0.1 kPa; *W*=0.18	**0.35**	-	Discrepancy found between reportedly adopted and back-figured μ's (Shi et al., 2011)
	Water-rich sandy cobble	γ=20-23 kN/m^3; φ=38-48°; *c*=0 kPa; *E*=20-38 MPa	-	**0.65** (Foam lubricants)	(Cui & Lin, 2016), (Song et al., 2010)
Sand	Moderately compact sand	γ_{sat}=17.8-20.1 kN/m^3; φ=31-38.9°; q_c=6.9-15.6 MPa	-	**0.05** * / **0.25** ** (Bentonite lubricants)	*: value returning average longitudinal equilibrium along whole tunnel alignment; **: value returning longitudinal equilibrium at unfavorable tunnel sections (Festa, 2015)
	Highly compact sand	γ_{sat}=19.2-19.6 kN/m^3; φ=35.6-43.4°; q_c=17.3-38.7 MPa			
	Very compact sand	γ_{sat}=19.3-19.9 kN/m^3; φ=32.6-41.6°; q_c=21-40.1 MPa			
	Sand with silty and clayey layers	γ_{sat}=17.7-19.9 kN/m^3; φ=25.3-38.2°; q_c=2.4-19.5 MPa			

Sand	Not specified	-	**0.45**	**0.25-0.35** (Bentonite lubricants)	(Maidl et al., 2013)
	Sand and tills	γ_{sat}=19.9 kN/m^3; φ=39°; c=0/23.9 kPa	-	**0.24** (Foam lubricants)	(Godinez et al.)
	Not specified	-	**0.35-0.40**	**0.15** (Bentonite lubricants)	(Ramoni, 2010), (Gehring, 1995), (Herzog, 1985)
	Not specified	γ=20.2 kN/m^3; φ=30°; c=0 kPa; W=0.184	**0.30**	-	Discrepancy found between reportedly adopted and back-figured μ's (Shi et al., 2011)
	Silty sand	γ=24.7 kN/m^3; φ=21.5°; c=41 kPa; E=8.9	**0.38** *	**0.38** *	*: No information regarding lubricants use/type (Zhang et al., 2014), (Song et al., 2010)
Silt	Not specified	-	**0.30**	-	(Maidl et al., 2013)
	Hard silt	γ_{sat}=19.6 kN/m^3; φ=37°; c=0 kPa	-	**0.10** (Foam lubricants)	(Godinez et al.)
	Not specified	-	**0.35-0.40**	**0.10** (Bentonite lubricants)	(Ramoni, 2010), (Gehring, 1995), (Herzog, 1985)
	Not specified	γ=21.1 kN/m^3; φ=25.1°; c=24.8 kPa; E=7.6 MPa	**0.38** *	**0.38** *	*: No information regarding lubricants use/type (Zhang et al., 2014), (Song et al., 2010)
Clay	Clay with silt and sand	γ_{sat}=18.1-20.5 kN/m^3; φ=28-35.2°; c=0 kPa; q_c=3.1-7.8 MPa	-	**0.05** * / **0.25** ** (Bentonite lubricants)	*: value returning average longitudinal equilibrium along whole tunnel alignment; **: value returning longitudinal equilibrium at unfavorable tunnel sections (Festa, 2015)
	Inorganic clay with medium to high plasticity (APA)	γ=22 kN/m^3; φ=15+0.07·z [°]; E=13+6·z [MPa]; c=5+1.95·z [kPa]; LL=0.25-0.65; PL=0.15-0.25	**0.25-0.35**	**0.15** (Bentonite lubrication)	(Lunardi et al., 2011)
	Not specified	-	**0.20**	-	(Maidl et al., 2013)
	Hard clay	γ_{sat}=20.1 kN/m^3; φ=33°; c=13 MPa	-	**0.11** (Foam lubricants)	(Godinez et al.)
	Not specified	-	**0.30-0.35**	**0.10** (Bentonite lubricants)	(Ramoni, 2010), (Gehring, 1995), (Herzog, 1985)

Clay	Not specified	γ=18.5 kN/m^3; φ=10°; c=10 kPa; W=0.472	**0.2**	-	Discrepancy found between reportedly adopted and back-figured μ's (Shi et al., 2011)
	Silty clay	γ=20.4 kN/m^3; φ=13.3°; c=30.3 kPa; E=5.6 MPa	**0.38** *	**0.38** *	*: No information regarding lubricants use/type (Zhang et al., 2014), (Song et al., 2010)
	Silty clay	γ=14 kN/m^3; c=6 kPa	**0.22** *	**0.22** *	*: No information regarding lubricants use/type (Shi et al., 2011), (Song et al., 2010)
Generic	-	-	-	**0.10** *, **0.15** * **0.10** *, **0.15** *, **0.20** *	*: No information regarding lubricants type (Ates et al., 2014)

Green: EPB machine
Blue: hydro-shield machine
Black: TBM type not specified

Figure 3.7 below summarizes the content of Table 3.3. Note that literature only provides a generic soil characterization (e.g. "silty clay"), therefore the position of datapoints along the horizontal axis in Figure 3.7 is chosen arbitrarily (within the appropriate soil type) to help visualization.

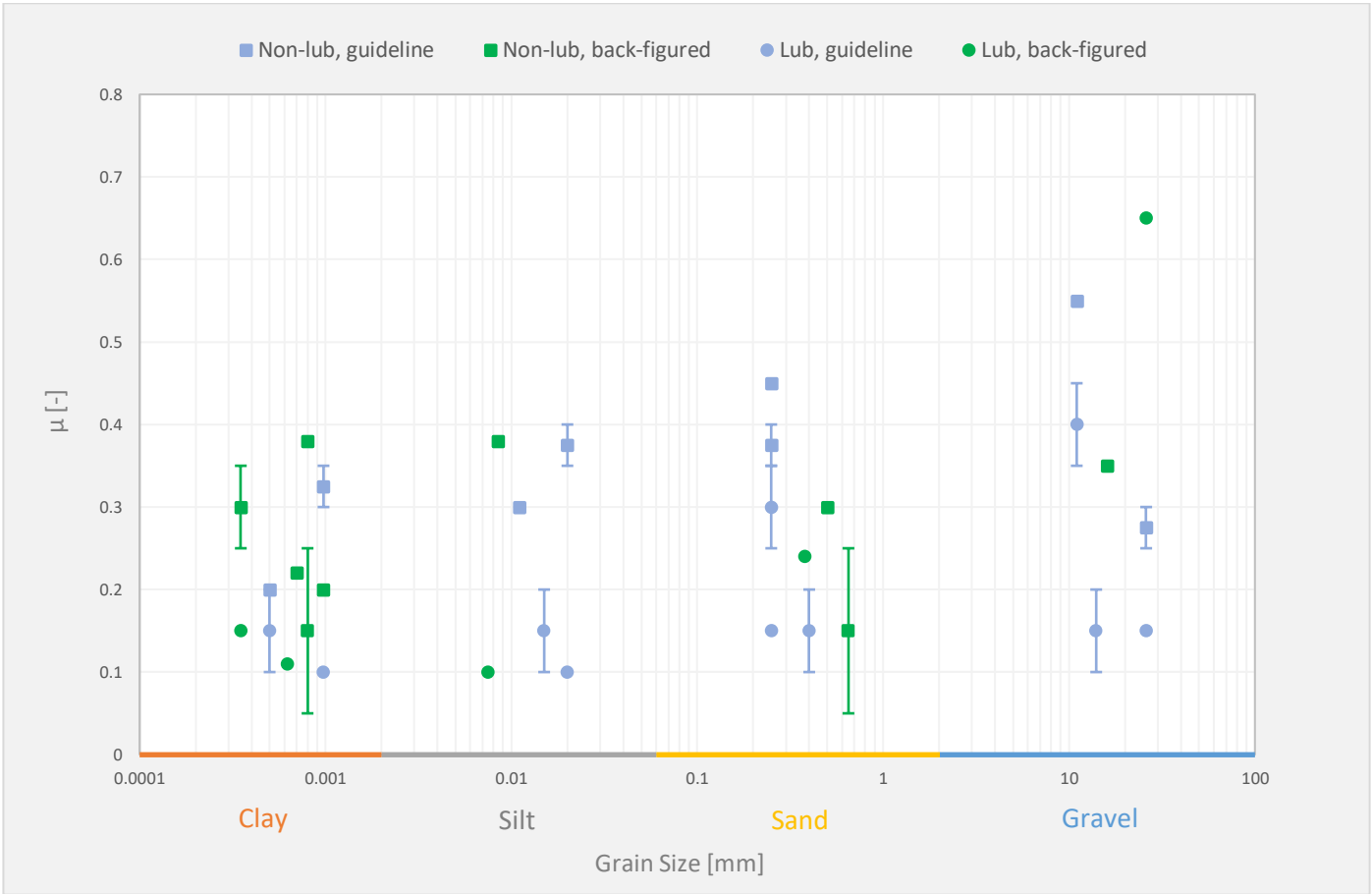

*Figure 3.7: Soil-machine friction coefficients from tunneling literature. **Square** datapoints: non-lubricated conditions; **circular** datapoints: lubricated conditions. **Green** datapoints: values measured/back-figured; **Blue** datapoints: values as generic guideline. Note: positioning of datapoints along horizontal axis is generic.*

4 Friction coefficients from laboratory literature

Friction developing along the interface between soil and various materials is a parameter of great relevance in numerous engineering fields. The design of many structures, machines and tools, in fact, depends on the resistance force developed when these are in contact with soil. Much research has been carried on this subject, studying it under multiple aspects. Some focus on soil type and its properties, while others look at how boundary conditions influence surface friction, and so on. In this chapter, the most relevant of these studies will be reviewed. The aim is to study typical soil interface friction coefficients and to understand which aspects and parameters are found to be influential. This knowledge is later used to plan accordingly the laboratory investigation of the thesis.
At the end of the chapter, a table summarizing friction coefficients based on influential parameters is provided. This information is later used as a reference to assess and possibly validate the results obtained from the thesis laboratory investigation.

(Butterfield & Andrawes, 1972) performed interface shear tests between Leighton Buzzard sand at high and low porosity and plates of various materials, including mild steel.
The relation between applied normal load and measured interface friction is found to be linear. Additionally, the static friction coefficient δ_s measured at the start of shearing reduces to a lower, constant kinetic friction angle δ_k. Both δ_s and δ_k are found to depend on the porosity/compaction of sand, increasing with decreasing porosity, as can be seen in Figure 4.1 below. The average $\delta_{loose}/\delta_{dense}$ ratio is found to be 0.64, irrespectively of plate material.

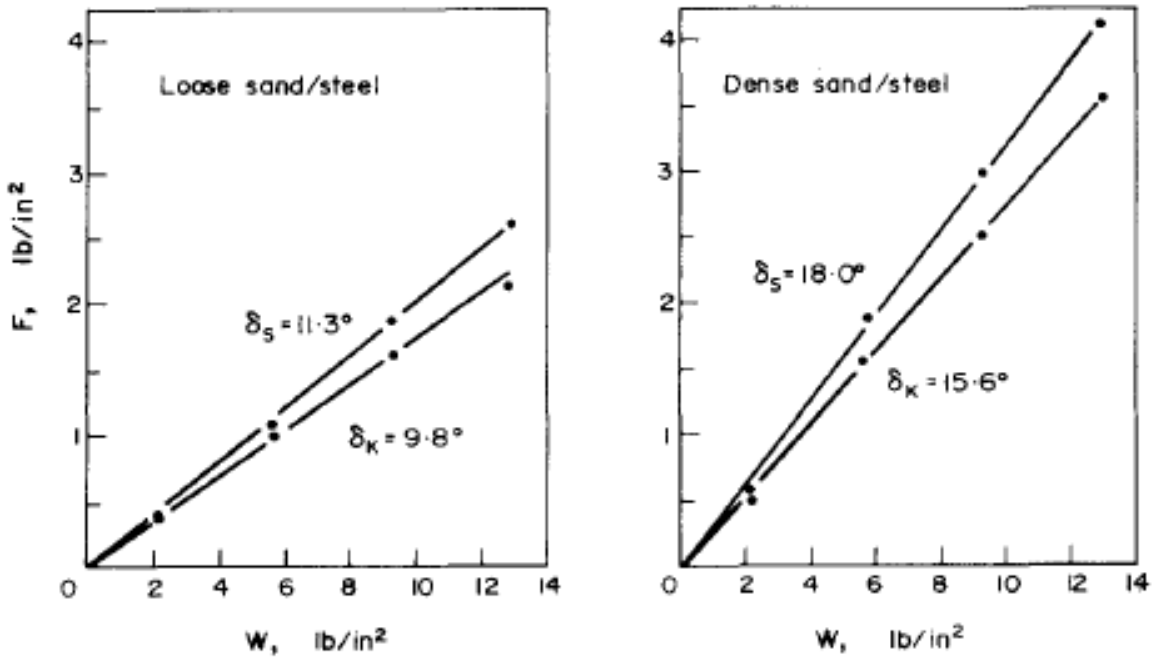

Figure 4.1: Static (δ_s) and kinetic (δ_k) interface friction angles between loose (left) and dense (right) sand and mild steel (Butterfield & Andrawes, 1972).

The purpose set by (Littleton, 1976) was to derive strength parameters for the shear resistance between clay and a smooth steel surface. The study uses a 60mm shear box to test clay samples of two varieties: kaolinite and illite. Only one metal plate is used, with an average surface roughness R_a of 0.18 μm. The two clays show average internal shear strengths of 19° 30' and 20° for kaolinite and illite, respectively. Regarding peak interface friction angles with steel, the same two clays show values of 17° 30' and 18° 15'. For clay on steel shear, failure at the interface is sudden and the peak resistance, which builds after relatively small displacement, rapidly drops to residual levels. For clay internal shear, on the other hand, shear resistance builds more slowly yet consistently with displacement, up to values slightly larger than those for interface shear. This trend can be seen in Figure 4.2 below:

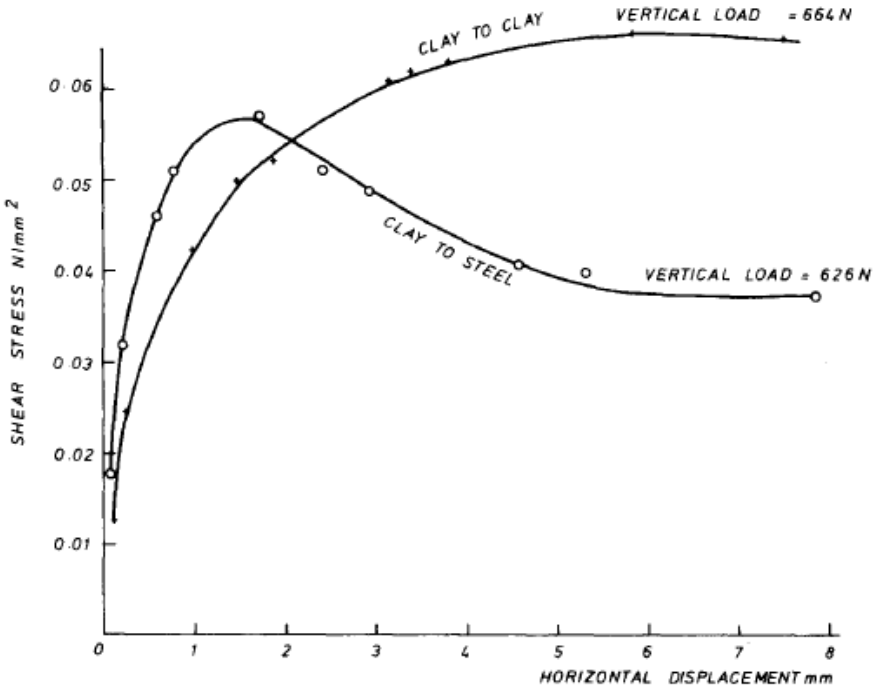

Figure 4.2: Comparison of shear strength development between interface and internal shear tests (Littleton, 1976).

(Littleton, 1976), as previously done by (Tomlison, 1969), defines the ratio between shear skin friction and undisturbed shear strength δ/φ as adhesion factor. Evidence from tests performed by (Littleton, 1976) shows adhesion factors of 0.75 and 0.6 for fast and slow shear rates, respectively. In fact, correlation of peak strengths is difficult, as they take place at un-comparable displacement levels.

(Potyondy, 1982) studies the skin friction developing between various soils and construction materials. The main parameters considered in the study are plate material type, surface roughness, soil type and moisture content and load condition.
Results are expressed using a Coulomb-type skin friction line, so that the measured interface friction of a soil is related to its internal shear strength, as shown in Equation 7:

Equation 7:

$$skin\ friction = f_c c + \sigma \cdot tan(f_\varphi \varphi)$$

Where:
f_c is the $adhesion/cohesion$ ratio
f_φ is the δ/φ ratio

Table 4.1 shows the above-mentioned coefficients measured for various test cases:

Table 4.1: f_φ values for different test scenarios (upper line refers to smooth steel, lower line refers to rough steel) (Potyondy, 1982).

Sand		Cohesionless silt			Cohesive granular soil		Clay		
0·06 < D < 2·0 mm		0·002 < D < 0·06			50% Clay + 50% Sand		D ≦ 0·06 mm		
Dry	Sat.	Dry	Sat.		Consist. I. = 1·0–0·5		Consist. Index: 1·0–0·73		
Dense		Dense	Loose	Dense					
$f\phi$	$f\phi$	$f\phi$	$f\phi$	$f\phi$	$f\phi$	fc	$f\phi$	fc	fc_{max}
0·54	0·64	0·79	0·40	0·68	0·40	—	0·50	0·25	0·50
0·76	0·80	0·95	0·48	0·75	0·65	0·35	0·50	0·50	0·80

Considering friction between sand and steel, friction angles are constant for different normal loads and are higher when shearing occurs on rough rather than smooth steel. Moisture content does not seem to have a significant effect, as sand interface and internal friction angles do not vary noticeably between dry and saturated specimens.
Considering friction between clay and steel, friction resistance may be divided into two regions: the first (for low normal loads), in which the skin resistance increases proportionally with the normal load; the second (for high normal loads), in which the skin resistance does not vary with the normal load. According to (Potyondy, 1982), in fact, once the clay density and water content stabilize, an increase in normal load does not produce any increase in skin friction. The internal shear strength of clay is found to generally reduces when increasing its water content, lowering the interface friction as well.
(Potyondy, 1982) also prepared an "intermediate" cohesive soil type (see Table 4.1). Test results regarding this soil show average frictional behavior, between that found for pure sand and pure clay.

(Stafford & Tanner, 1982b) studied how skin friction between clay and sandy clay and mild steel is influenced by the sliding speed of shear tests. A dedicated test apparatus was developed for the study, allowing rotational shear of specimens at rates between 90 and $3 \cdot 10^5$ mm/min. For both the soil types examined, friction angles are found to increase rapidly with sliding speeds up to approximately $3 \cdot 10^4$ - $6 \cdot 10^4$ mm/min. Higher shear rates do not seem to produce further increase in interface friction angles, as can be seen in Figure 4.3 below:

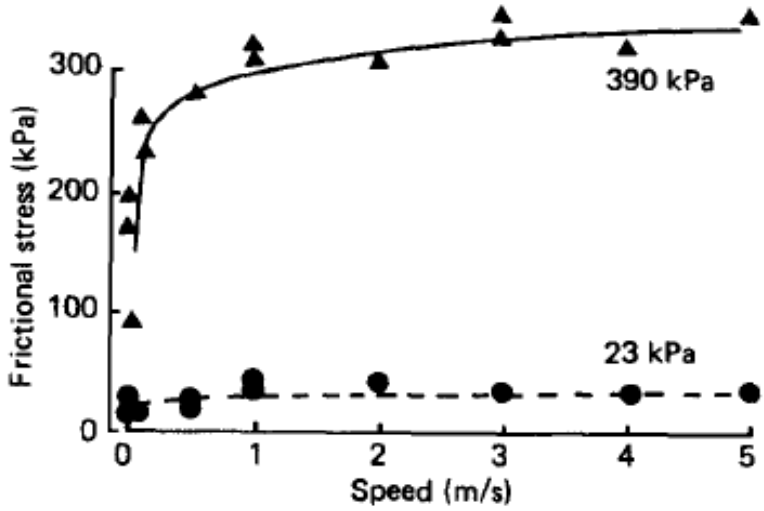

Figure 4.3: Effect of shear speed on interface frictional stress between clay and steel (Stafford & Tanner, 1982b).

It is also worth noting from Figure 4.3 how the effect of shear speed on interface frictional stress is the more noticeable, the higher the applied normal load is.
(Stafford & Tanner, 1982b) modelled test data using a logarithmic relation (Equation 8), with a significant fit for most test cases:

Equation 8:

$$\delta = a + b \cdot \log v$$

Where:
δ is the interface friction angle;
v is the sliding speed;
a, b are the regression coefficients for each test case. Their values are shown in Table 4.2:

Table 4.2 (Stafford & Tanner, 1982b):

Soil	Moisture content (%, w/w)	Dry bulk density (kg/m^3)	a	b
1	11.9	1491	20.82	1.518
	14.9	1525	28.28	2.363
	17.3	1497	27.94	2.288
	17.0	1741	24.44	3.306
2	17.9	1186	36.07	2.643
	30.1	1197	44.03	3.611
	38.6	1209	40.04	6.037

(Rinne, 1989) wrote a thesis aiming to obtain a better understanding of the factors affecting skin friction between construction materials and the surrounding soil. Two uniformly graded quartz sands are considered in the study, with equal properties, except for their different grain shapes (rounded and angular).
Prior to shear interface tests, it is noted that the internal friction angle of the angular sand is dependent on the applied normal stress, yielding a convex strength envelope, with an average friction angle of 33°. The internal friction angle of the rounded sand, on the other hand, is found to be constant at all normal stresses and equal to 29°.
Rounded sand, when sheared on smooth steel, shows peak interface friction angles independent of applied normal stress. Further shear shows noticeable post peak drop. In the same way behaves the angular sand. As can be expected, interface friction angles (both peak and residual), are higher for the angular sand sample.
When shearing both sand samples on rough steel, the same trend is observed as for the smooth steel case. The only difference is that both peak and residual friction angles result higher than those obtained for the smooth steel case.

(Tsubakihara, Kishida, & Nishiyama, 1993) make use of a simple shear test device to study the interface friction between cohesive soils (clay and sand-clay mixtures) and mild steel plates of different surface roughness. Soil specimens consist of marine clay and four artificially mixed cohesive soils, the latter being made mixing the marine clay with various amounts of sand.
A distinction is made between observed peak and residual interface coefficients, respectively μ_y and μ_r. Peak friction coefficients are found to be scarcely influenced by the sand content of specimens. However, the post-peak drop (i.e. difference between peak and residual friction coefficients) increases with increasing clay fraction of specimens.
The authors identify a so-called critical steel roughness, as the plate roughness above which shearing takes place within the soil specimen, rather than at the interface with the plate. Critical roughness proves to be higher for specimens with higher sand fraction.
Finally, three shear failure modes are observed during the tests, as can be seen in Figure 4.4 below:

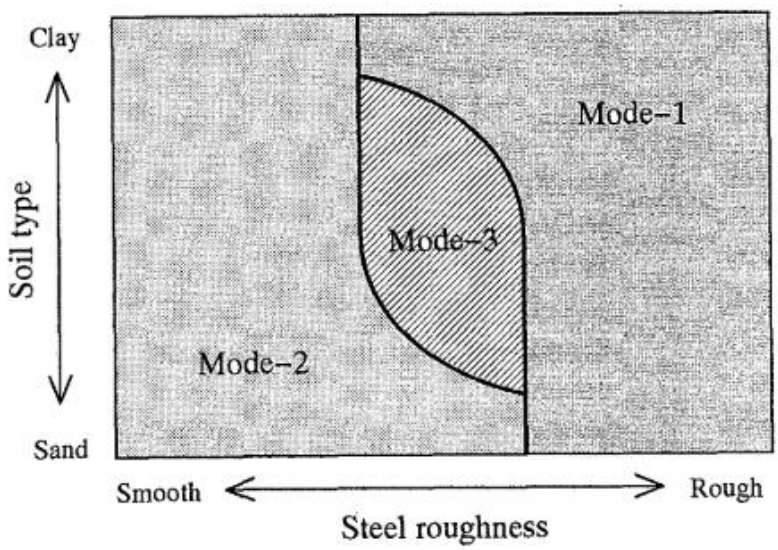

Figure 4.4: Typical domain of shear failure modes, according to soil type and steel surface roughness (Tsubakihara et al., 1993).

In Mode 1, shear failure occurs within the soil. This takes place whenever the internal shear strength of the sample is lower than the friction developed at its interface with steel. In Mode 2, failure consists in sliding at the soil-plate interface. This takes place whenever the internal shear strength of the sample is higher than the friction developed at its interface with steel. In Mode 3, shear strain and sliding displacement occur simultaneously. The abovementioned critical roughness is the value of plate roughness at which the transition from failure mode 1 to 3 (and, later, mode 2) occurs.

(Kooistra, Verhoef, Broere, Ngan-Tillard, & F., 1998) is a publication regarding the adhesion and friction between clay and steel, conducted after reported difficulties due to sticking clays during TBM tunneling. Six different clay samples are examined in a pilot study from Kooistra and classified according to specific gravity, water content, grain size and Atterberg limits.
Test results show a strong linear correlation between measured adhesive-interface friction and applied normal load, between all clay types and steel. One clay type ("Potters clay") is chosen to investigate the influence of water content on the adhesive friction between clay and steel. Analogous research ((Jancsecz, 1991) and (Spagnoli, Feinendegen, Ernst, & Weh, 2012)) shows that clay adhesion varies with water content, showing a peak value lying somewhere between liquid and plastic limit. For what concerns the "Potters clay" considered in (Kooistra et al., 1998), cohesion proves to be higher than adhesion and monotonously decreasing with increasing water content, as can be seen in Figure 4.5. Adhesion, on the other hand, shows a peak value near the clay plastic limit.

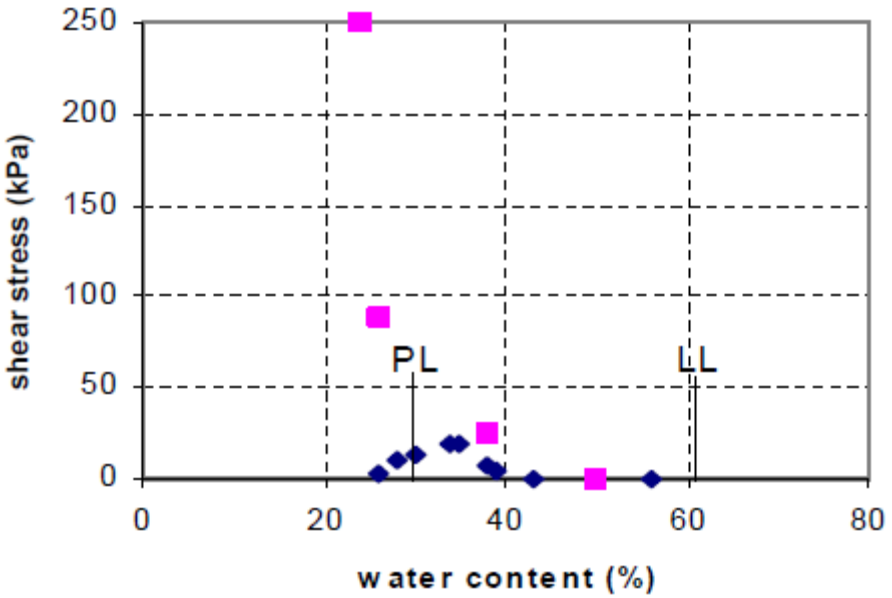

Figure 4.5: Dependency of cohesion (light purple) and adhesion (blue) between clay and steel on water content (Kooistra et al., 1998).

Such results, when compared to those from similar investigations for other clay types ((Yusu, 1990), (Jancsecz, 1991)), suggest that clay mineralogy can have a strong influence on how clay behavior varies with water content. In fact, cohesive and adhesive forces in clay originate from electrostatic and chemical properties which, in turn, depend on the clay minerals. In general, (Kooistra et al., 1998) found clays to behave more plastically and with higher cohesion and adhesion, the higher their CEC is.

A total of 45 shear tests between sand and steel are conducted by (Al-Mhaidib, 2006), investigating the influence of shear rate on interfacial friction. Soil specimens consists of poorly graded sands (SP) and their relative density is kept at 64% for all test cases. Five shear rates are adopted: 0.0048, 0.048, 0.08, 0.4 and 0.9 mm/min.
Test results show that the internal shear strength of sand specimens increases as the shear rate is increased. Similarly, interface friction between sand and steel is also found to increase with increasing shear rate, almost identically for both smooth (δ_s) and rough (δ_r) steel plates. Test data for δ_s and δ_r can be fitted to logarithmic regressions with similar slope coefficients, as shown in Equation 9 and Equation 10:

Equation 9:

$$\delta_s = 1.34 \cdot log(SR) + 23$$

Equation 10:

$$\delta_r = 1.44 \cdot log(SR) + 43.8$$

Where SR is the shear rate applied.
Figure 4.6 below depicts the interface friction envelopes for the shear tests conducted by (Al-Mhaidib, 2006):

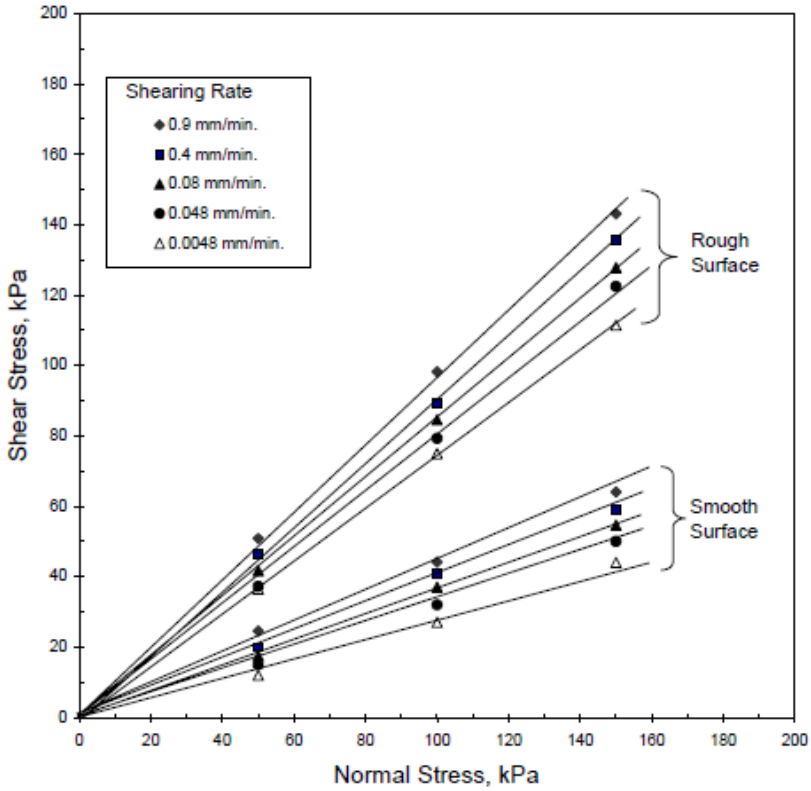

Figure 4.6: Interface friction envelopes for sand shearing on smooth and rough steel plates (Al-Mhaidib, 2006).

The δ/φ ratio is found to be independent of shear rate (i.e. interface friction and internal shear strength increase almost identically with shear rate), with average values of 0.464 and 0.951 for smooth and rough steel, respectively.

(Tiwari & Al-Adhadh, 2013) published a study where a well graded sand (SW) is sheared along steel and other materials. Four relative densities (14, 40, 68, 95 %) are adopted and specimens are tested in both dry and saturated conditions. Both internal shear strength and interface shear envelopes are found to be slightly convex, suggesting friction angles are slightly decreasing with increasing applied normal load. Internal friction angles of sand specimens prove to increase by up to 23%, between the loosest and the densest possible configuration. Such increase is not seen during sand-steel interface shear: interface friction angles are found not to vary with the compaction grade of sand. When comparing dry and saturated sand specimens, soil-steel interface friction angles slightly increase for the saturated case.

(Tokarz, 2014) is a MS thesis investigating the parameters responsible for the clay tending to stick to TBM components. The study uses a rotational ring shear apparatus to measure the interface friction between clay specimens and steel rings. The clay used in the investigation is a white kaolin.
Results for NC clay samples indicate that, when low normal load is applied (25-50 kPa), the difference between interface friction between clay and smooth steel and clay and rough steel is negligible. As the normal load is increased up to 200 kPa, however, tests reveal a much larger divergence: peak interface friction angles for the rough steel are found to be 10-20% larger than for the smooth steel, as can be seen in Figure 4.7 below:

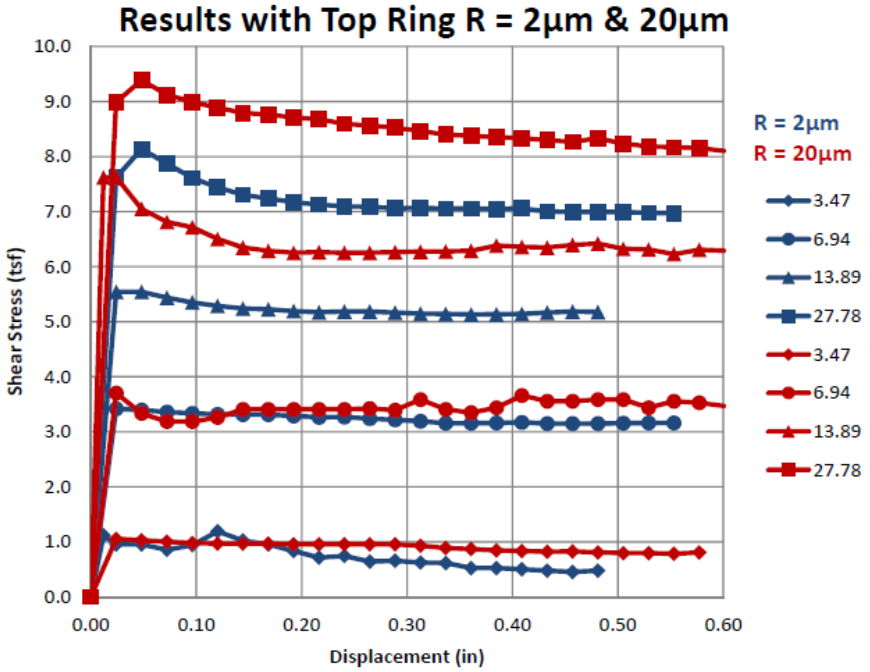

Figure 4.7: Plots from interface shear tests between clay and smooth steel (blue) and clay and rough steel (red), for various normal loads. Note that normal load is displayed in Pounds per square inch (Tokarz, 2014).

(Tokarz, 2014) also considers the effect of OCR. Tests indicate an increase of peak interface shear strength with increasing over consolidation ratio. Peak shear friction measured in the tests, in fact, increases by 10%, 19% and 28% over the NC sample for OCRs of 2, 4 and 8 respectively. This is attributed to the fact that OC specimens are found to dilate during shear, increasing suction and thus causing a rise in adhesive forces at the interface with steel. Residual interface friction, on the other hand, appears not to be affected by the OCR.

(Feligha, Hammoud, Belachia, & Nouaouria, 2015) tested four clay samples (two types of kaolin, clay of "Guelma" and a mixture of the previous types) to study the effects of interface roughness and texture on friction between cohesive soils and steel. One smooth steel plate, three grooved steel plates and four plates with abrasive paper are used during testing.
The internal shear strength of the clays is found to range between approximately 18° and 25° (for "Guelma" clay and kaolinites, respectively). The friction ratio δ/φ proves to increase with increasing average roughness R_a of the plates. In other words, as clay specimens are sheared along increasingly rougher plates, the measured interface friction angle δ becomes closer and closer to the internal shear strength of the clay. This increase of friction ratio with plate roughness follows a pattern specific to each clay type, as can be seen in Figure 4.8 below:

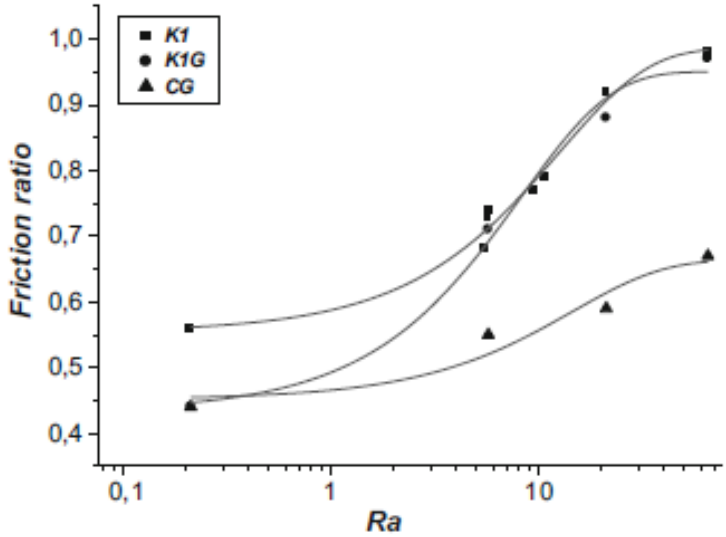

Figure 4.8: Friction ratio (δ / φ), function of average plate roughness. K1, CG and K1G refer to kaolinite, clay of Guelma and mixture of the previous two, respectively (Feligha et al., 2015).

Similarly to (Tsubakihara et al., 1993), (Feligha et al., 2015) also recognizes three possible failure modes during interface shear of clay samples. A mode in which sliding takes place and is confined to the soil-plate interface only, corresponding to the lower end of friction ratios (δ/φ = 0-0.3). A mode in which shearing takes place within the soil volume and for which the upper threshold friction ratio (δ/φ = 1) is reached. Finally, a transition mode between the previous two. The shift from the first to the second and eventually third mode occurs for increasing plate roughness.
For what concerns plate interface texture (i.e. the pattern of the surface asperities), this parameter is not found by (Feligha et al., 2015) to influence the interface shear strength of the soil tested. Plate material is also not found to influence the skin resistance between clay specimens and various plates.

To eliminate the effects of particle morphology, (Vangla & Latha, 2015) tested three sands with different grain size, but similar grain angularity, roundness, sphericity, etc.
Regarding internal shear strength, the effect of particle size on peak friction angle is found to be negligible. On the other hand, residual friction angles show to be influenced by particle size: post-peak softening increases with decreasing particle size.
As for interface shear tests, peak interface friction angles are found to be 0.4 φ_{peak}, 0.49 φ_{peak} and 0.37 φ_{peak} for coarse, medium and fine sand samples, respectively. Interface friction, therefore, shows not to depend on the particle size, at a given void ratio. A stronger dependency is rather reported by (Vangla & Latha, 2015) on the number of soil-plate contact patches per unit area. The more are the grooves left on the plate after shear, the higher is the number of contact points and, consequently, the measured interface friction.

Table 4.3: Summary of friction angles and coefficients from literature of laboratory studies.

Soil Type	Soil Properties	Test Conditions	δ [°]; μ [-]		Remarks; Publication/s
Sand	D_{50}=0.45mm; C_u=2.08; $\gamma_{min,max}$=14.55-17.85kN/m^3; G_s=2.68; φ=1.5·*ln*(*SR*)+46.08 *	Rough interface (R_a=33.4µm); D_r=0.64; *SR*=0.0048-0.9mm/min	δ_{peak}=37.0-44.5° (1.44·*ln*(*SR*)+43.80); μ_{peak}=**0.75-0.98**		(100x100)mm direct shear apparatus; (Al-Mhaidib, 2006)
		Smooth interface (R_a=1.06µm); D_r=0.64; *SR*=0.0048-0.9mm/min	δ_{peak}=16.0-23.2° (1.34·*ln*(*SR*)+23.0); μ_{peak}=**0.29-0.43**		
	D_{50}=0.94mm; C_u=2.128; $\gamma_{min,max}$=15.06-17.94kN/m^3; G_s=2.679; φ_{peak}=33/46° (Loose/Dense)	Polished mild steel (R_a:n.a.); D_r=0.0094; *SR*=1.04mm/min	δ=9.8° *; μ=**0.17**		(60x60)mm direct shear apparatus; (Butterfield & Andrawes, 1972); (Antonio Cavallaro, Michele Maugeri, & Mazzarella)
		Polished mild steel (R_a:n.a.); D_r=0.78; *SR*=1.04mm/min	δ=15.6° *; μ=**0.28**		
	D_{50}=0.73mm; C_u=3.46; $\gamma_{min,max}$=11.96-14.64kN/m^3; G_s=2.787; φ_{res}=41.18°	Stainless steel (R_a:n.a.); D_r=0.40; *SR*=0.07815mm/min;	δ_{res}=15.06°; μ_{res}=**0.27**		(60x60)mm direct shear apparatus; (Giang, Haegeman, Impe, Impe, & Menge)
	D_{50}=0.75mm; C_u=5.556; $\gamma_{min,max}$=12.51-15.58kN/m^3; G_s=2.787; φ_{res}=42.69°		δ_{res}=16.67°; μ_{res}=**0.30**		
	D_{50}=0.6mm; C_u=3.8; $\gamma_{min,\max(achieved)}$=15.6-17.61kN/m^3; G_s=2.66; φ=44.3° *	Rough interface (artificially rusted steel, R_a:n.a.); D_r=0.66; *SR*:n.a.	δ=33.70° *; μ=**0.67**		(60x60)mm direct shear apparatus; (Potyondy, 1982)
		Smooth interface (polished steel, R_a:n.a.); D_r=0.66; *SR*:n.a	δ=24.05° *; μ=**0.45**		
			δ=23.90° *; μ=**0.44**		
	D_{50}=0.40mm; C_u=1.9; $\gamma_{min,max}$=14.67-17.80kN/m^3; G_s=2.67; φ_{cv}=29°	Smooth interface (R_a=0.2-0.35µm); D_r=0.25; *SR*=5-8mm/min	δ_{peak}=16°; μ_{peak}=**0.29**	δ_{res}=12°; μ_{res}=**0.21**	UBC ring shear apparatus; (Rinne, 1989)
		Rough interface (R_a=2.5µm); D_r=0.25; *SR*=5-8mm/min	δ_{peak}=22°; μ_{peak}=**0.40**	δ_{res}=22°; μ_{res}=**0.40**	

Sand	D_{50}=0.85mm; C_u=7.5; γ=14.32-17.90kN/m^3; G_s=2.65; φ=43.84-54.54° *	R_a:n.a.; SR:n.a.	D_r=0.95	μ_{peak}= **0.7465**	μ_{peak}= **0.7255**	(100x100)mm direct shear apparatus; (Tiwari & Al-Adhadh, 2013)
			D_r=0.68	μ_{peak}= **0.7056**	μ_{peak}= **0.7120**	
			D_r=0.40	μ_{peak}= **0.5662**	μ_{peak}= **0.7490**	
			D_r=0.14	μ_{peak}= **0.6305**	μ_{peak}= **0.5688**	
Clay	"Marine clay": LL=1.29; PL=0.87; c_v=0.5m^2/year	Rough interface (R_a=80 µm); OCR=1; Drained (SR=0.001mm/s)		δ_{res}=36-45°; μ_{res}=**0.73-1**		Cyclic direct shear apparatus (low normal loads: 2-8kPa); Remolded specimens; (Boukpeti & White, 2017)
		Rough interface (R_a=80 µm); OCR=1; Un-drained (SR=0.1mm/s)		δ_{res}=19.3-24.2°; μ_{res}=**0.35-0.45**		
		Smooth interface (R_a=2 µm); OCR=1; Drained (SR=0.001mm/s)		δ_{res}=30°; μ_{res}=**0.58**		
	"Marine clay": LL=1.10; PL=0.47; c_v=0.6m^2/year	Rough interface (R_a=80 µm); OCR=1; Drained (SR=0.001mm/s)		δ_{res}=35-39°; μ_{res}=**0.7-0.8**		
		Rough interface (R_a=80 µm); OCR=1; Un-drained (SR=0.1mm/s)		δ_{res}=18.3-19.8°; μ_{res}=**0.33-0.36**		
		Smooth interface (R_a=2 µm); OCR=1; Drained (SR=0.001mm/s)		δ_{res}=20°; μ_{res}=**0.36**		
	"Clay of Guelma": LL=0.755; PL=0.342; Fraction<2μm=0.44; G_s=2.78; A_c=0.94; φ=18.6° *	SR=0.02mm/min; OCR=1	R_a=64.94μm	δ=12.43° *; μ=**0.22**		(60x60)mm direct shear apparatus; Remolded specimens; (Feligha et al., 2015)
			R_a=21.04μm	δ=10.90° *; μ=**0.19**		
			R_a=5.69μm	δ=10.21° *; μ=**0.18**		
			R_a=0.21μm	δ=8.18° *; μ=**0.14**		

Clay	"Speswhite clay": LL=0.62; PL=0.32; Fraction<2μm=0.79; W=0.80 (before consolidation)	SR=0.1 mm/ min; OCR=1	R_a=8.4 μm	δ=18.36° *; μ=**0.33**	60mm circular direct shear apparatus; Re-molded specimens; (Ngan-Tillard & Verhoef)
			R_a=4.7 μm	δ=17.89° *; μ=**0.32**	
			R_a=2.4 μm	δ=15.86° *; μ=**0.28**	
			R_a=1.2 μm	δ=15.03° *; μ=**0.27**	
	"Boom clay": LL=0.55; PL=0.24; Fraction<2μm=0.71; W=0.70 (before consolidation)		R_a=8.4 μm	δ=14.11° *; μ=**0.25**	
			R_a=4.7 μm	δ=13.70° *; μ=**0.24**	
			R_a=2.1 μm	δ=11.40° *; μ=**0.20**	
			R_a=1.2 μm	δ=11.0° *; μ=**0.19**	
	"Blue clay" (illite): LL=0.53; PL=0.20; G_s=2.72; φ_{peak}=15/20° (Un-drained/Drained)	R_a=0.18 μm; OCR=1	Drained (SR:n.a.)	$\delta_{peak,res}$=18.15, 11.3° $\mu_{peak,res}$=**0.33, 0.20**	(60x60)mm direct shear apparatus; Remolded specimens; (Littleton, 1976)
			Un-drained (SR=0.59 mm/ min)	δ_{res}=10.30° μ_{res}=**0.18**	
	kaolinite: LL=0.83; PL=0.30; G_s=2.61; φ_{peak}=14.45/19.3° (Un-drained/Drained)		Drained (SR:n.a.)	$\delta_{peak,res}$=17.30, 11.3° $\mu_{peak,res}$=**0.31, 0.20**	
			Un-drained (SR=0.59 mm/ min)	δ_{peak}=13.45° μ_{peak}=**0.24**	

Clay	"Glacial clay": LL=0.378; PL=0.218; G_s=2.71; Fraction<2μm=0.45	Rough interface (artificially rusted steel, R_a:n.a.); SR:n.a.	W=0.228; CI=0.94	δ=10.00° *; μ=**0.18**	(60x60)mm direct shear apparatus; (Potyondy, 1982)
			W=0.261; CI=0.73	δ=5.50° *; μ=**0.10**	
		Smooth interface (polished steel, R_a:n.a.); SR:n.a.	W=0.228; CI=0.94	δ=9.00° *; μ=**0.16**	
			W=0.261; CI=0.73	δ=6.30° *; μ=**0.11**	
	"Wicken clay": LL=0.78; PL=0.31-0.39; G_s=n.a.; Fraction<2μm=0.60	R_a=0.5 μm; SR=90-3·10^{5}mm/ min	W=0.179	δ=36.07+2.64·*logSR* * μ=**0.54-0.78**	Custom annular shear apparatus; Re-molded specimens; (Stafford & Tanner, 1982b)
			W=0.301	δ=44.03+3.61·*logSR* * μ=**0.67-1.05**	
			W=0.386	δ=40.04+6.04·*logSR* * μ=**0.42-0.97**	
	"Kawasaki clay": LL=0.86; PL=0.379; G_s=2.65.; Fraction<2μm=0.586	Consolidated (OCR=1); Drained (SR=0.03mm/ min)	R_a=30 μm; W=0.593	$\mu_{peak,res}$=**0.59, 0.53**	60mm simple shear apparatus; Re-molded specimens; (Tsubakihara et al., 1993)
			R_a=20 μm; W=0.585	$\mu_{peak,res}$=**0.59, 0.57**	
			R_a=10 μm; W=0.614	$\mu_{peak,res}$=**0.58, 0.46**	
			R_a=3 μm; W=0.596	$\mu_{peak,res}$=**0.56, 0.38**	

Green: dry specimens;
Blue: water-saturated specimens;
* Friction angle condition (peak, residual, average, etc.) not specified

Data in Table 4.3 above are investigated in search of a correlation linking friction coefficient to the other variables. For what concerns sand, the strongest correlation is found to be described by Equation 11 (note: R_a in mm):

Equation 11:

$$\mu = 1.012 - 0.12 \cdot ln\left[\frac{D_{50}}{R_a} \cdot (1 - D_r)\right]$$

where μ refers to residual conditions, in case more than one kind is specified in Table 4.3. Figure 4.9 below shows how Equation 11 models the data:

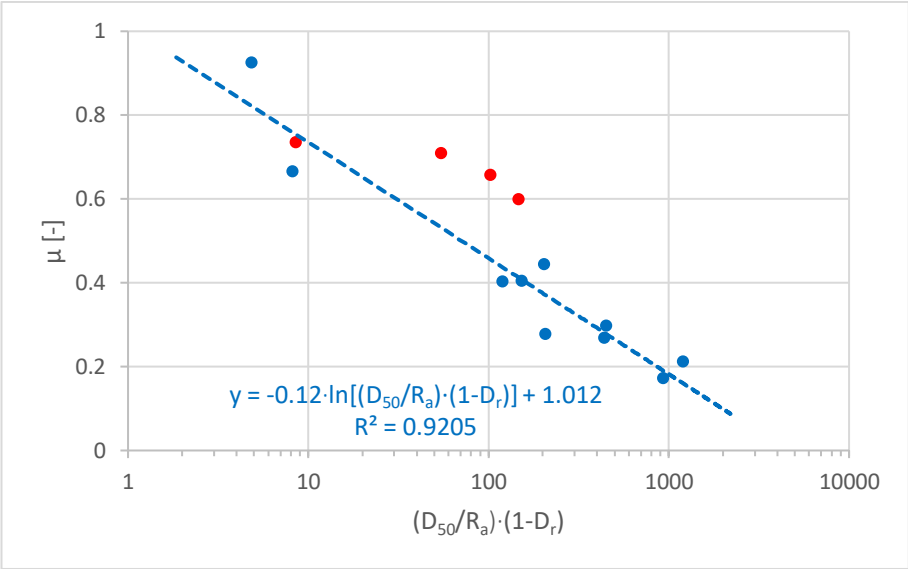

Figure 4.9: Fitting of Equation 11 for sand data from Table 4.3. Note: datapoints in red are measurements for which plate roughness is not available from literature (for which R_a is nominally taken as 5μm).

For what concerns clay, a strong correlation cannot be found. As shown in Figure 4.10 below, the only observation that can be made is that friction between clay and steel seems to be the lowest for clays with low liquid limit. Data shown in Figure 4.10 is modelled by Equation 12 (note: R_a in mm):

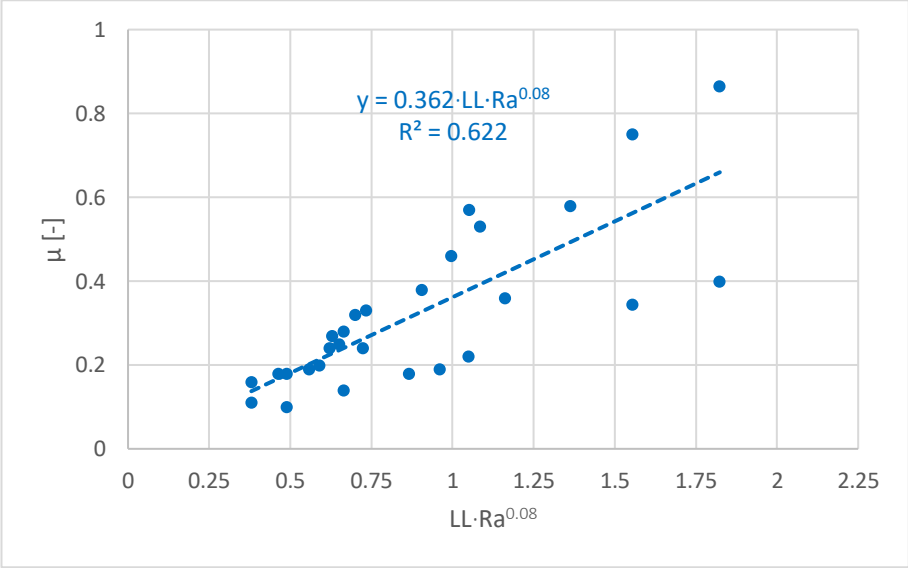

Figure 4.10: Fitting of Equation 12 for clay data from Table 4.3

Equation 12:

$$\mu = 0.362 \cdot LL \cdot (R_a)^{0.08}$$

The behavior and properties of clay are often related to its consistency index. Adhesion between clay and steel, for example, has been shown to reach a peak for intermediate consistency indexes, at around 0.4-0.6 (Kooistra et al., 1998), (Spagnoli et al., 2012), (Jancsecz, 1991). Unfortunately, most literature data collected in Table 4.3 do not include water content measurements. Consequently, an analysis of friction coefficient dependency on clay consistency index would not be informative.

The values in Table 3.3 and Table 4.3 are compared to investigate possible parallels between them. It is to be noted that friction coefficients from tunneling and laboratory literature cannot be compared rigorously, as soil characterization is often only qualitative (e.g. “Silty clay”).

For what concerns clay, tunneling literature reports friction coefficients between 0.2-0.38. This range lowers to 0.1-0.25 if soil is lubricated with additives. Clay friction coefficients reported by laboratory studies, on the other hand, are generally higher and spread over a wider range. This is especially true for high liquid limit clays: specimens with $LL \leq 0.75$ develop μ between 0.1-0.33, while specimens with $LL \geq 0.75$ develop μ between 0.25-0.9.
Accordingly, Clays with low LL tested in the laboratory and clays excavated without soil lubricants seem to develop analogous friction coefficients. On the contrary, clays with high LL tested in the laboratory show higher friction coefficients than clays excavated without soil lubricants.

For what concerns sand, tunneling literature reports friction coefficients ranging between 0.3-0.45. This range lowers to approximately 0.1-0.35 if soil is lubricated with additives. Most friction coefficients reported by laboratory studies are between 0.2-0.45, with rare exceptions at around 0.8.
Accordingly, sands tested in the laboratory and sands excavated without soil lubricants seem to develop analogous friction coefficients.

As can be expected, the use of soil lubricants during excavation is reported to lower friction coefficients by approximately 50%. On the other hand, the laboratory studies considered in paragraph 4 do not make use of soil additives. Consequently, it is not possible to establish whether the reduction in friction observed in the field due to soil conditioning could be equally measured in laboratory tests. Such interrogative is part of the thesis objective and is examined later.

Part 2: Laboratory Studies

5 Introduction to laboratory studies

In order to achieve the thesis objectives presented in paragraph 1, a comprehensive laboratory investigation is set up and carried out. The latter consists of multiple stages which are introduced in the following lines:

- First, the soils to be analysed in the laboratory investigation are selected. Sample selection is based on soil properties relevant to TBM design and excavation. To optimize sample choice, literature concerning analogous laboratory studies and TBM excavation is consulted;
- After selecting soil samples, their defining properties are measured to obtain a quantitative description of their nature. Overall, properties such as grain size distribution, soil composition, density, shear strength, etc. are examined;
- Next, the apparatus required to perform interface shear tests is selected and setup. This includes the shear test device, as well as its accessories and the metal insert. The equipment required to prepare bentonite slurries and foam suspensions is also selected and setup. Literature concerning test preparation and running is consulted, to plan how to optimally use the apparatus;
- Interface shear tests are carried out, for each of the chosen soil samples. Tests are performed for water-saturated specimens, as well as when the latter are conditioned with bentonite or foam. In case evidence shows faulty or inadequate design or use of the testing apparatus, the latter is modified and the tests are repeated;
- Finally, shear tests are examined. The results and observations extrapolated from the outcome of each shear test are furthered to later analysis and discussion.

Figure 5.1 below depicts a schematization of the laboratory studies structure:

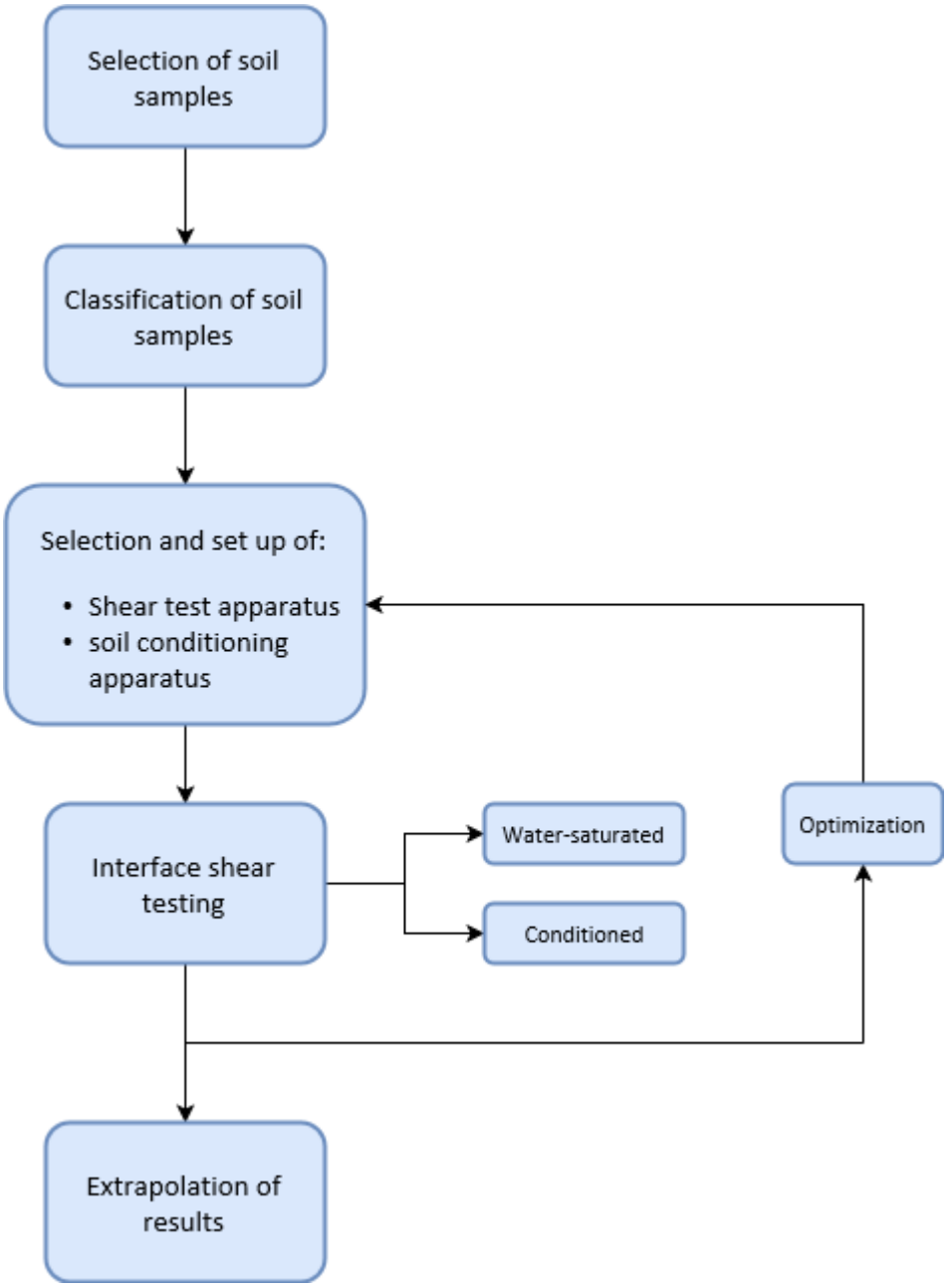

Figure 5.1: Structure of laboratory studies.

6 Materials and Methods

The present chapter starts by listing and describing the materials, tools and devices used throughout the laboratory investigation of the thesis. Further along the text, the methods and procedures adopted during the experimental analysis are also presented and discussed.

6.1 Materials

The following sub-chapter lists and describes the materials used during the laboratory investigation of the thesis. These consist of three soil samples, two types of soil conditioners and the equipment required to perform multiple tests. This includes a shear box and its accessories, steel plates from a TBM shield, mixing and measuring apparatus for the soil conditioners, as well as generic tools and devices typically found in a geotechnical laboratory (fall cone test apparatus, soil sieves, weighting scale, oven, containers, etc.).

6.1.1 Soils

As explained in the introduction (paragraph 1), the thesis is structured within the context of TBM design and operation. Consequently, to produce results relevant to such background, the soil types to be selected for laboratory investigation should replicate the ground behaviors and properties commonly found in TBM excavation.
Soil choice is based on typical soil application range of TBM face support methods. Each system (EPB, hydro-shield, mixed) has been developed for specific ground conditions. Therefore, the soils to be analyzed in the laboratory should convey the ground characteristics specific to each face support method. The focus goes, first, to EPB shields. As can be seen in Figure 6.1 below, the soil applicability field of EPB machines is wide: from fine clay, to medium-coarse sand. As average soil particle size increases, however, more additives are required to maintain good excavation performance, up to the point where hydro-shields become the preferred solution. Based on these considerations, two soils relevant to EPB shields should be considered for the laboratory investigation:

- A soil consisting of clay and silt particles, with a relatively low coefficient of uniformity. This sample covers the finer portion of the application range of EPB machines and it is labelled as soil A.
- A soil consisting of silt and fine to medium sand particles, with a relatively high coefficient of uniformity. This sample covers the average to coarse portion of the application range of EPB machines and it is labelled as soil B.

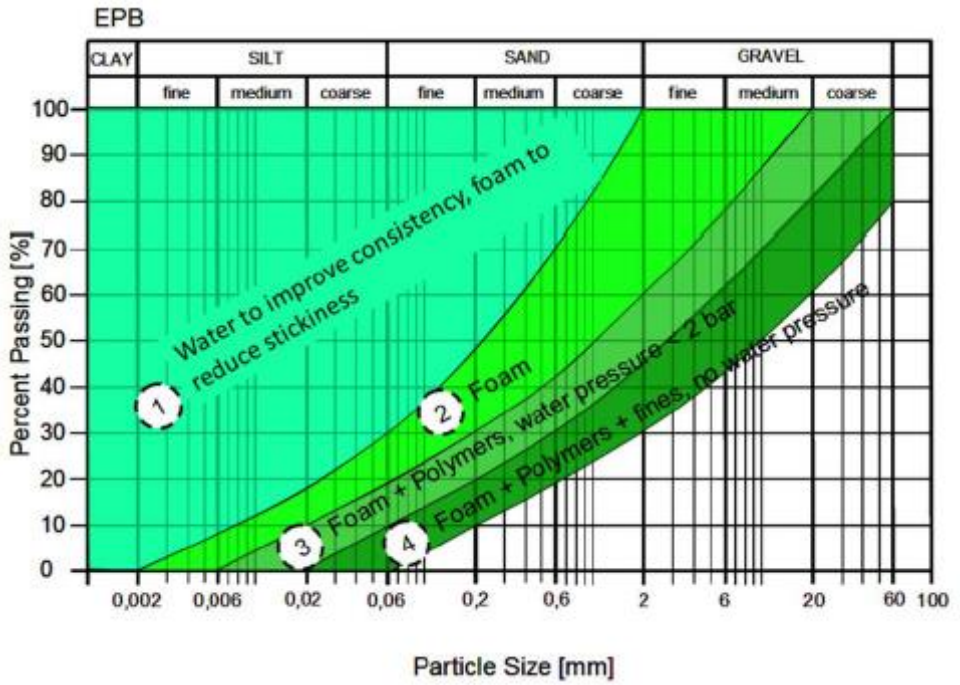

Figure 6.1: Application ranges of EPB machines (Thewes, 2007).

For what concerns hydro shields, it can be seen in Figure 6.2 below how they are generally more suited to coarser soils, compared to EPB's:

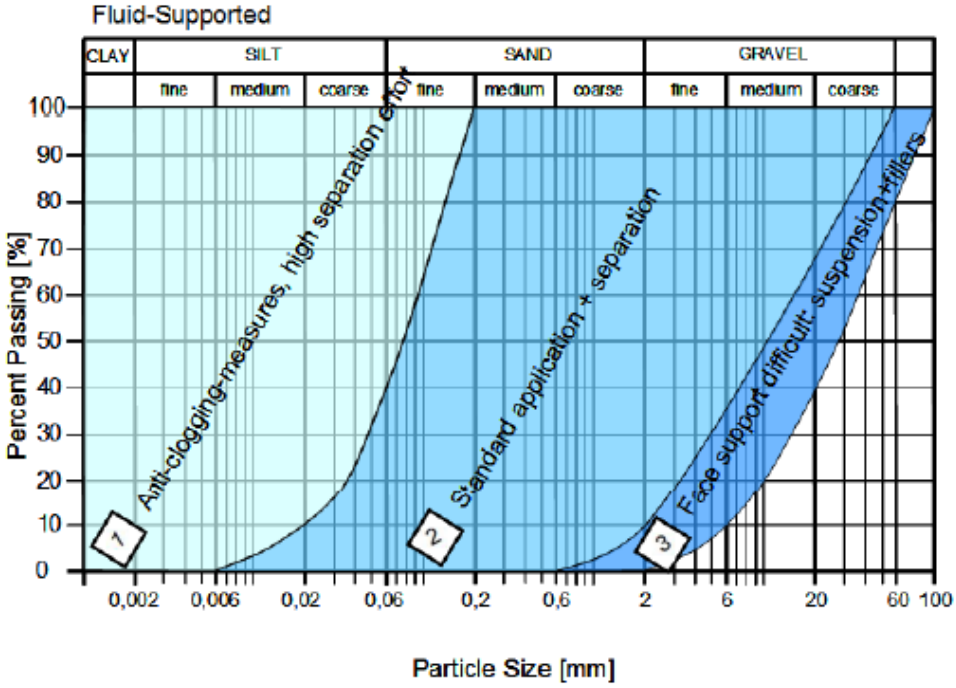

Figure 6.2: Application ranges of shield machines with slurry supported tunnel face (Thewes, 2007).

Based on this consideration, soil A is not relevant to slurry shield applications. On the other hand, soil B is relevant for slurry as well as EPB shields, as it stands on the overlapping application field of the two designs. Finally, a third soil is considered for the laboratory investigation, labelled as soil C. It consists of medium to coarse sand and fine gravel, with a relatively low coefficient of uniformity. This sample conveys the ground characteristics optimal for slurry shield use, for which EPB's are not suited.

6.1.1.1 Soil A

Soil A is a kaolin clay. According to standard *ASTM D-2487*, soil A lies between a "high and low plasticity clay", CH and CL respectively.
The particle size distribution of soil A is analyzed using a hydrometer, according to standard *ASTM 7926-17*. Figure 6.3 below shows the obtained granulometric profile of soil A:

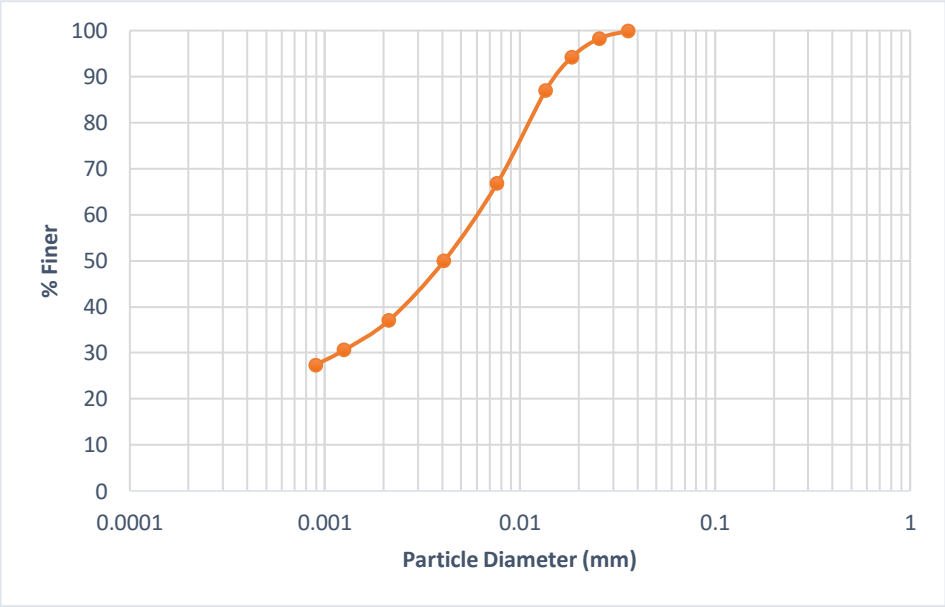

Figure 6.3: Granulometric profile of soil A.

The specific gravity of soil A is determined using a digital pycnometer and is found to be G_s **= 2.6342 +/- 0.0028**. Further details regarding this test can be found in Appendix A.
The plastic limit of soil A is obtained according to standard *ASTM D-4318*. The resulting average plastic limit is found to be to be PL **= 30.32%**. Further details regarding this test can be found in Appendix A.
The liquid limit of soil A is obtained according to standard *ASTM D-4318*, with the fall cone procedure. The resulting average liquid limit is found to be LL **= 49.72%**. Further details regarding this test can be found in Appendix A.
The internal shear strength φ of soil A is measured according to standard *ASTM D-3080*, at normal loads of 50, 100, 200 and 400 kPa. Shear rate is maintained at 0.01 mm/min and the tests are conducted in water-saturated conditions. Prior to shearing the specimens, vertical consolidation is allowed, until the vertical displacement has reached a steady state (see paragraph 6.2.1.1). Plots resulting from the shear tests can be found in Appendix A. Figure 6.4 below shows the failure envelope of soil A obtained from the shear tests:

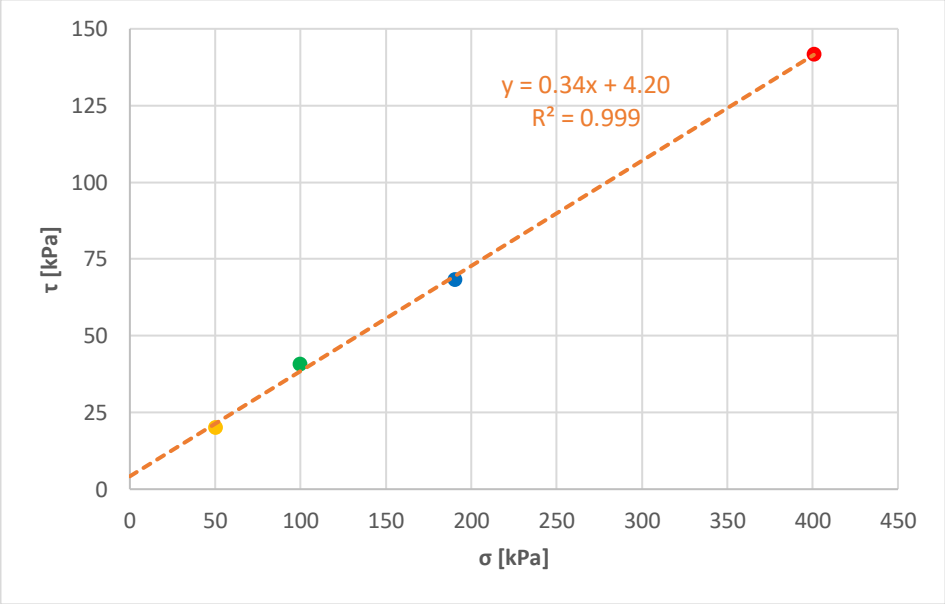

Figure 6.4: Internal shear failure envelope of soil A.

During shearing, soil A shows monotonic contractive behavior, for all four normal loads. Constant volume conditions are never reached, as all tests are stopped at lateral displacement equal to 10% of the specimens' size (6mm). Shear resistance increases up to a peak and residual average value of $\varphi_{p,r}$ **= 18.9°**. Cohesion is equal to c **= 4.2 kPa**.

6.1.1.2 Soil B

Soil B is a natural sand with appreciable fines content and a small fraction of organic matter. This material comes from a landfill property of Hamburg Port Authority. According to standard *ASTM D-2487*, soil B is classified as "silty sand", SM. The particle size distribution of soil B is analyzed with the wet-sieving procedure, according to standard *ASTM D-6913*. Figure 6.5 below shows the obtained granulometric profile of soil B. Relevant grain properties of soil B are shown in Table 6.1 below:

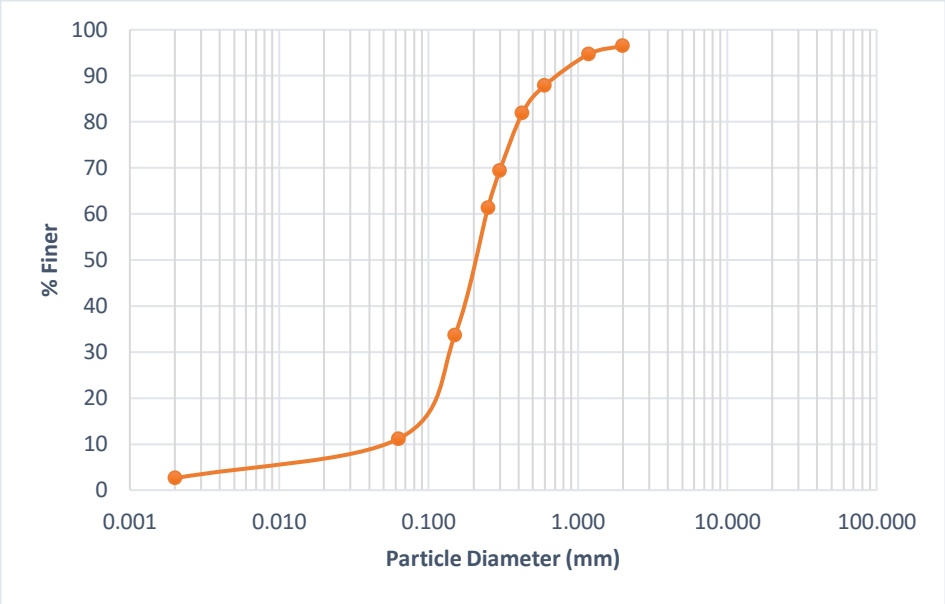

Figure 6.5: Granulometric profile of soil B.

Table 6.1: Grain properties of soil B.

D_{10} [mm]	D_{30} [mm]	D_{60} [mm]	C_u	C_c	TOC*
0.0547	0.136	0.245	4.483	1.378	1.1%

*: Value provided by Prof. Julia Gebert.

The specific gravity of soil B is determined using a digital pycnometer and is found to be $\boldsymbol{G_s}$ **= 2.6225 +/- 0.0009**. Further details regarding this test can be found in Appendix B.
Maximum and minimum void ratios of soil B cannot be determined, as the usual "Japanese method" does not yield a meaningful result in case of specimens exhibiting cohesion.
The internal shear strength φ of soil B is measured according to standard *ASTM D-3080*, at normal loads of 50, 100, 200 and 400 kPa. Shear rate is maintained at 0.1 mm/min and the tests are conducted in water-saturated conditions. Prior to shearing the specimens, vertical consolidation is allowed, until the vertical displacement reaches a steady state (see paragraph 6.2.1.1). Plots resulting from the shear tests can be found in Appendix B. Figure 6.6 below shows the failure envelope of soil B obtained from the shear tests:

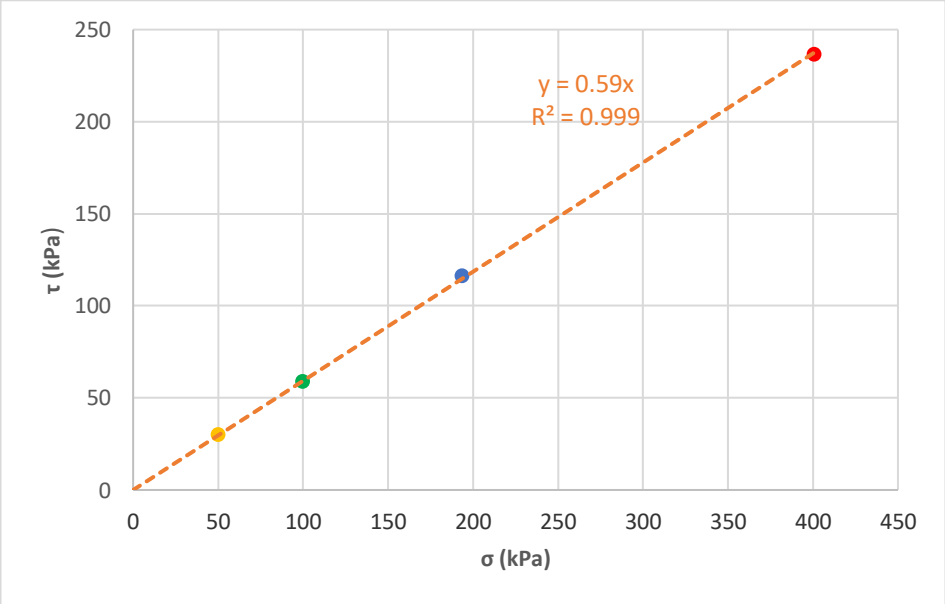

Figure 6.6: Internal shear failure envelope of soil B.

During shearing, soil B showed monotonic contractive behavior, for all four normal loads. Constant volume conditions are never reached, as all tests are stopped at lateral displacement equal to 10% of the specimens' size (6mm). Shear resistance is observed to increase up to a peak and residual average value of $\boldsymbol{\varphi_{p,r}}$ **= 30.5°.**

6.1.1.3 Soil C

Soil C is an alluvial, non-sieved "Maas" sand. According to standard *ASTM D-2487*, soil C is classified as "poorly graded sand", SP. The particle size distribution of soil C is analyzed with the dry-sieving procedure, according to standard *ASTM D-6913*. Figure 6.7 below shows the obtained granulometric profile of soil C. Relevant grain properties of soil C are shown in Table 6.2 below:

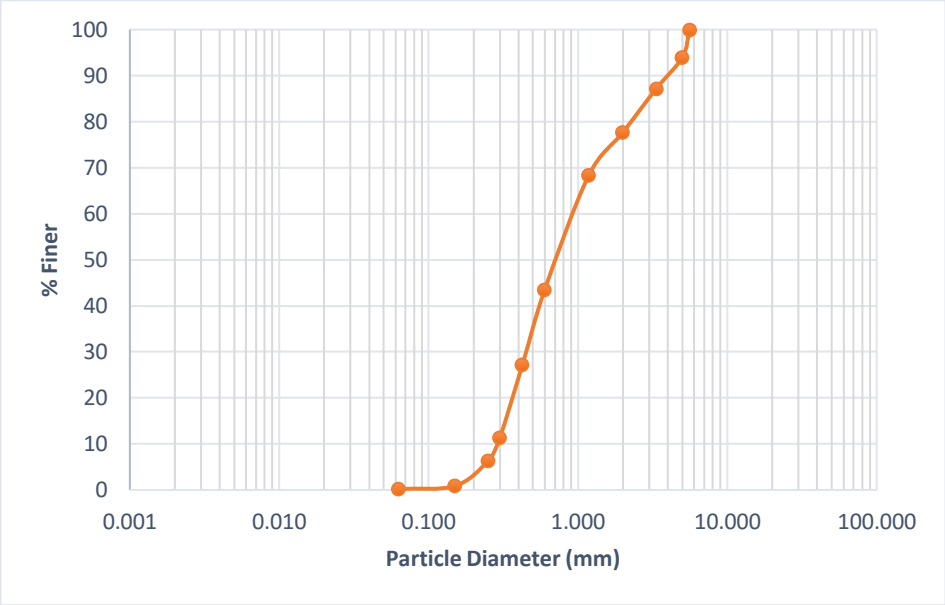

Figure 6.7: Granulometric profile of soil C. Note that the right-most side of the profile has been cut-out to exclude soil particles larger than 10% the size of the shear box.

Table 6.2: Grain properties of soil C.

D_{10} [mm]	D_{30} [mm]	D_{60} [mm]	C_u	C_c
0.286	0.455	0.985	3.440	0.733

The specific gravity of soil C is determined using a digital pycnometer and is found to be $\boldsymbol{G_s}$ **= 2.6416 +/- 0.0009**. Further details regarding this test can be found in Appendix C.
Maximum and minimum void ratios of soil C are determined according to standard *ASTM D-4254,* (so called "Japanese method") and are found to be $\boldsymbol{e_{max}}$ **= 0.624,** $\boldsymbol{e_{min}}$ **= 0.412**. The corresponding minimum and maximum dry density of soil C are found to be $\boldsymbol{\rho_{min}}$ **= 1.627** g/cm3 and $\boldsymbol{\rho_{max}}$ **= 1.871** g/cm^3. Further details regarding this test can be found in Appendix C.
The internal shear strength φ of soil C is measured according to standard *ASTM D-3080*, at normal loads of 50, 100, 200 and 400 kPa. Shear rate is maintained at 0.5 mm/min and the tests are conducted in water-saturated conditions (see paragraph 6.2.1.1). Plots resulting from the shear tests, for each of the above-mentioned normal loads, can be found in Appendix C. Figure 6.8 below shows the failure envelopes of soil C obtained from the shear tests:

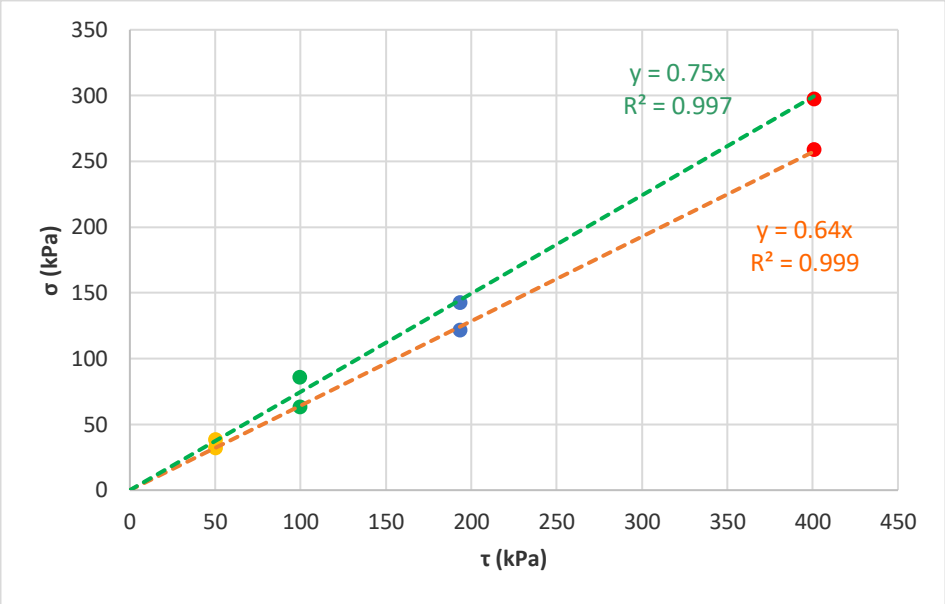

Figure 6.8: Internal shear failure envelopes of soil C. Green envelope refers to peak strength, orange envelope refers to residual strength.

During shearing, soil C showed typical behavior of sand: during the initial stage of testing, specimens contracted to a maximum compaction state and later started to dilate, depending on the applied normal load. Shear resistance is observed to initially reach a peak value, to then stabilize, at larger displacements, to a residual value. Figure 6.8 above shows both peak and residual failure envelopes, computed form the shear tests of soil C. Average peak friction angle $\boldsymbol{\varphi_p}$ is found to be **36.8°**, while average residual friction angle $\boldsymbol{\varphi_r}$ is found to be **32.7°**.

6.1.2 Bentonite

During the laboratory investigation, the bentonite powder used to produce slurry is the Ibeco B1, produced by Imerys. Its typical mixing concentrations and operational parameters are shown in Table 6.3 below:

Table 6.3: Properties of Ibeco B1 (provided by Imerys).

Technical average values	**Valeurs techniques moyennes**		
Water content	Teneur en eau	11 ± 3	%
Specific density	Poids spécifique	2,65	g/cm³
Bulk density	Densité apparente tassée	800 ± 100	g/l
Screen residue on 0,063 mm	Refus au tamis 0,063 mm	20 ± 5	%
Slurry at 50 kg/m³, after 24 hours	**Boue à 50 kg/m³, après 24 heures**		
Slurry density	Densité de Gel	1,028	t/m³
Marsh viscosity	Viscosité Marsh	40	s/l
Liquid limit (ball)	Rigidité (billes)	30 (6)	N/m²
Filtrate volume	Volume de Filtrat	12	ml

6.1.3 Foaming Agent

During the laboratory investigation, the surfactant used to produce foam is the CLB F5, produced by Condat. This additive is specifically designed for tunnelling applications. No technical sheet regarding characteristics and/or dosage of CLB F5 is available.

6.1.4 Shear Apparatus

As discussed previously in paragraph 4, soil interface friction has been investigated using various laboratory equipment. Authors, in fact, report having used both direct ((Potyondy, 1982); (Tsubakihara et al., 1993); (Al-Mhaidib, 2006); etc.) and simple (Rinne, 1989) shear apparatuses, as well as purposely built machinery (Stafford & Tanner, 1982a).
For the thesis laboratory investigation, a direct shear test apparatus is chosen. This apparatus consists of a square shear box housing with nominal size of (60x60x25)mm, which can be seen in Figure 6.9 below:

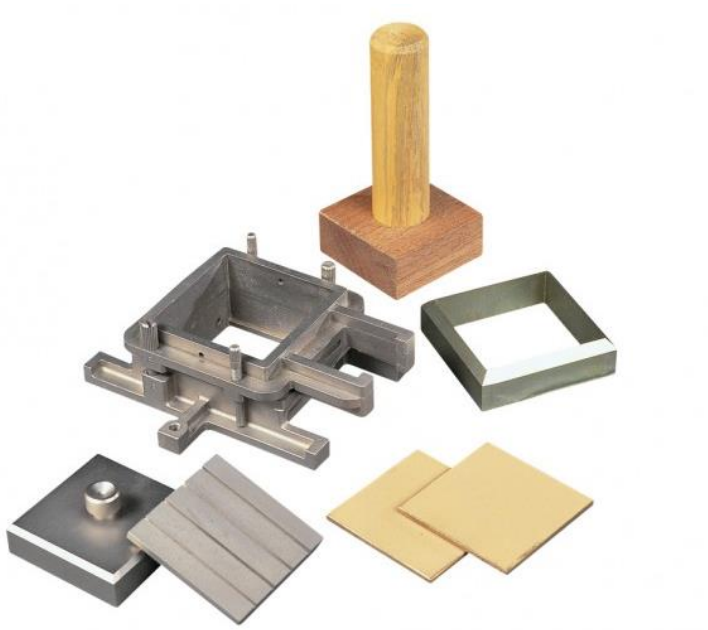

Figure 6.9: Shear box and its accessories [www.ele.com].

The above-mentioned shear box is coupled to an analogic shear machine, which can be seen in Figure 6.10 below:

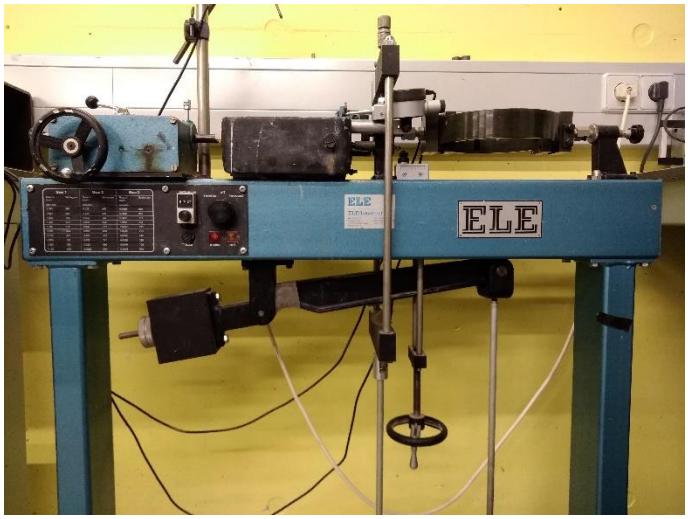

Figure 6.10: Shear machine

Both components are manufactured by ELE International and meet the requirements of standards BS 1377 and ASTM D-3080. Normal load is applied through a system of weights on a lever arm. Vertical and lateral displacements are measured by needle extensometers with accuracy of +/- 0.001mm. A third, identical extensometer measures the radial deformation of a metal ring, due to the force applied by the shear machine. The calibration of such metal ring allows to convert deformation readings into shear loads (Newtons).
A direct shear test apparatus is chosen because of its straightforward adaptability to interface shear tests. Compared to other devices, in fact, including a metal plate in a direct shear apparatus is easier: the lower half of the shear box is

simply replaced by the metal insert, above which the upper shear box housing (containing the soil specimen) slides freely.
A further advantage of the direct shear apparatus is that it enforces failure to occur precisely at the soil-metal interface. The measured friction resistance, therefore, can be attributed exclusively to specimen-metal interaction. This might not be the case using other shear devices, as failure might occur simultaneously along the soil-metal interface and within the specimen.
When performing soil-metal interface shear tests in the laboratory, the lower half of the above-mentioned shear box is replaced with a metal plate, shown in Figure 6.11:

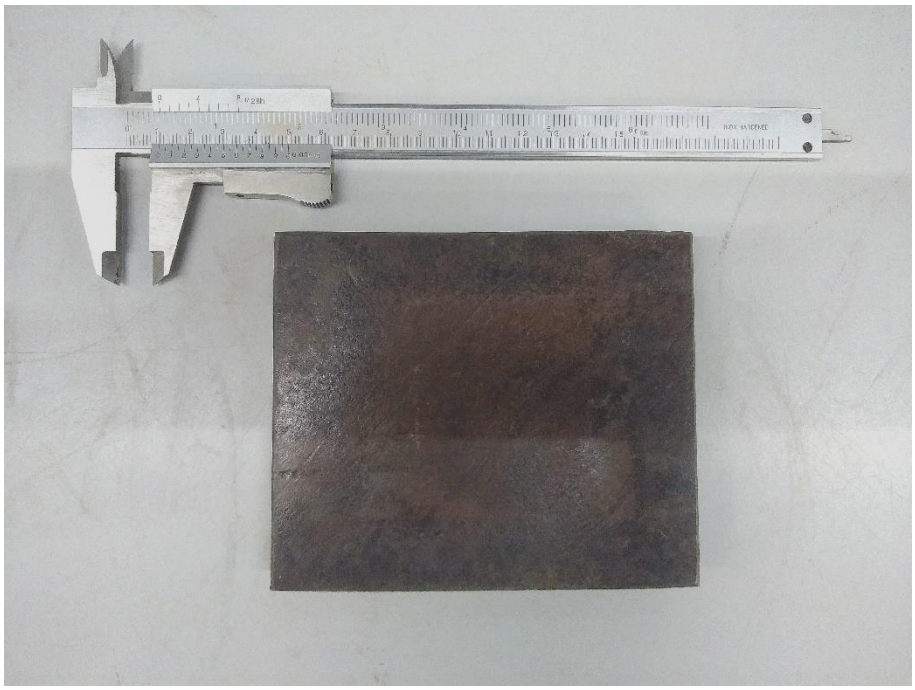

Figure 6.11: Metal plate insert (light surface damage from its previous use can be seen).

Instead of using generic steel, a plate has been purposely cut-out from a used TBM cutterhead and provided by Herrenknecht (Figure 6.11). Using a plate made of genuine TBM componentry means that metal type, surface roughness and wear are the most representative possible of actual operational conditions. The average roughness of the metal plate used in the investigation is measured as 3.12 μm. Additional information on the roughness measurements can be found in Appendix D.
During the laboratory investigation, shear tests are stopped at horizontal displacements of 6mm (equal to 10% of the shear box nominal size). This procedure is prescribed by standard *ASTM D-3080* for conventional shear tests, to avoid an excessive reduction of the specimen shear section. Although this problem does not hold for interface shear tests (as there is no reduction of shear area), the same limit of horizontal displacement is kept for the sake of consistency.

6.1.5 Bentonite Apparatus

Bentonite slurries are prepared using a Hamilton Beach Scovill high speed blender. After the mixing stage, bentonite slurries are transferred into specific buckets and allowed to swell. Similar buckets are also used when combining soil specimens with bentonite slurries, prior to testing in the shear box. Details regarding bentonite slurry preparation and use can be found in paragraph 6.2.2.4.

6.1.6 Foam Apparatus

Foam suspensions are prepared using a Hamilton Beach Scovill high speed blender. An alternative system is sometimes used, consisting of a pressurized air line feeding the surfactant through a porous stone. Graduated plastic containers are used to combine foam suspensions with soil samples. Details regarding foam suspension preparation and use can be found in paragraph 6.2.2.5.

6.2 Methods

The following sub-chapter lists and describes the practical methods and procedures adopted during the laboratory investigation of the thesis. These include set-up and running of multiple tests; assembly of soil specimens; preparation of soil additives.

6.2.1 Shear box set-up

6.2.1.1 Internal Strength

When operating the shear box for testing the internal shear strength of soil specimens, the apparatus set-up is carried according the following procedure:

- The upper and lower halves of the shear box (shown in Figure 6.9) are assembled and placed in the canister, securing them with the registering screws;
- The canister is filled with demineralized water at room temperature;
- After placing the lower porous stone, the soil specimen is transferred into the shear box. This step varies according to the specific soil type and conditioning: soil B and C are pluviated, while specimens made of soil A are consolidated inside the shear box;
- After placing the upper porous stone on the specimen, the loading cap (shown in Figure 6.9) is positioned on the assembly. Afterwards, the loading frame and weights are placed on the loading cap;
- After the consolidation stage (if needed), the shear box halves are un-screwed and play is removed from the apparatus assembly prior to shearing.

6.2.1.2 Interface Friction

When operating the shear box for testing the soil-metal interface friction, the apparatus set-up is carried according the following procedure:

- The metal plate, shown in Figure 6.11, is placed in the canister and secured with the registering screws;
- The upper half of the shear box is placed on the above-mentioned metal plate. The canister is then filled with demineralized water at room temperature;
- The soil specimen is transferred into the shear box. This step varies according to the specific soil type and conditioning: soil B and C are pluviated, while specimens made of soil A are consolidated inside the shear box;
- After placing the upper porous stone on the specimen, the loading cap is positioned on the assembly. When performing tests with bentonite-conditioned specimens, a custom-made rubber gasket is fitted to the loading cap, prior to its instalment. The purpose of this gasket, shown in Figure 6.12, is to prevent slurry from being squeezed out of the sample once load is applied. As can be seen in Figure 6.12, the gasket seats on the shear box edge, creating a seal. To improve the effectiveness of the gasket, as well as to minimize its friction, plenty of impermeable grease is also added. Despite this, some of the normal load applied during shear tests is lost in friction between shear box and gasket. This effect causes an estimated reduction in normal load of 4 kPa, which is the load required to brake the friction between gasket and shear box;
- The loading frame and weights are placed on the loading cap and play is removed from the apparatus assembly prior to shearing.

Figure 6.12: Custom-made rubber gasket fitted to the loading cap.

6.2.2 Preparation Techniques

6.2.2.1 Water-saturated Specimens

Specimens made of soils B and C are prepared according to the following procedure:

- Enough soil is put to dry in the oven, for a period of at least 24 hours;
- The soil is taken out the oven and allowed to cool down;
- After having set-up the shear box apparatus (see paragraph 6.2.1), the soil is gradually transferred with a funnel in the flooded shear box and homogenized with a spoon. This procedure is performed as consistently as possible each time, to guarantee the same specimen characteristics. Care is taken to fully saturate the specimen and to avoid any kind of heterogeneity;
- After installing the porous stone and the loading cap (see paragraph 6.2.1), consolidation is required for specimens of soil B (for internal shear strength tests only). This phase is protracted until vertical displacement stops. The duration of this process depends on the normal load applied and is observed to last between 6 and 14 hours. This step is not necessary in case of specimens consisting of soil C;

Specimens made of soil A are prepared according to the following procedure:

- Enough clay slurry is consolidated in a centrifuge at 100g, for 8-10 hours;
- After having set-up the shear box apparatus (see paragraph 6.2.1), the centrifuge-consolidated clay is transferred with a spatula into the shear box. Care is taken not to include any air within the specimen;
- After installing the porous stone and the loading cap (see paragraph 6.2.1), the specimen is consolidated at the normal load at which it will be tested. This phase is protracted until vertical displacements stop;

6.2.2.2 Conditioned Specimens (Bentonite Slurry)

Specimens made of soils B and C are prepared according to the following procedure:

- Enough soil is put to dry in the oven, for a period of at least 24 hours;
- The soil is taken out the oven and allowed to cool down;
- A known mass of soil is mixed with the slurry. The volume of slurry is 1.75 or 1 times what is required to fill the soil voids, when the specimen density is equivalent to that of water-saturated conditions.
- After having set-up the shear box apparatus (see paragraph 6.2.1), the slurry-conditioned soil is gradually transferred in the shear box and homogenized with a spoon. This procedure is performed as consistently as possible each time, to guarantee the same specimen characteristics. Care is taken to fully saturate the specimen and to avoid any kind of heterogeneity;

Figure 6.13 below shows a sample of soil C, conditioned with tinted bentonite slurry, during specimen preparation:

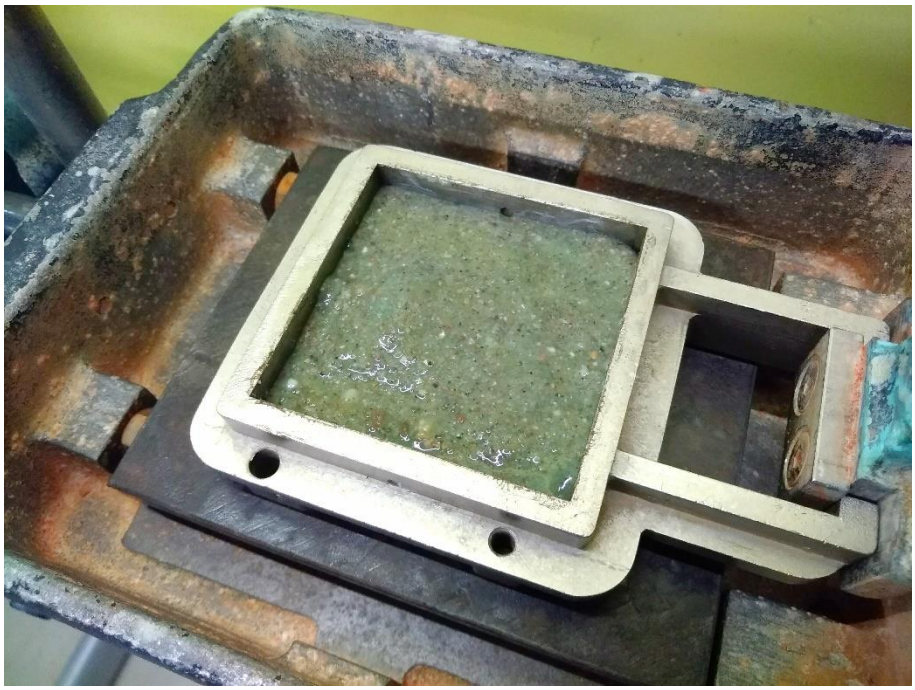

Figure 6.13: Bentonite-conditioned sample of soil C, prior to fitting porous stone and loading cap.

Specimens made of soil A are prepared according to the following procedure:

- Enough clay slurry is consolidated in a centrifuge at 100g, for 8-10 hours;
- After having set-up the shear box apparatus (see paragraph 6.2.1), the centrifuge-consolidated clay is transferred with a spatula into the shear box. Care is taken not to include any air within the specimen;
- After installing the porous stone and the loading cap (see paragraph 6.2.1), the specimen is consolidated at the normal load at which it will be tested. This phase is protracted until vertical displacements stop;
- The setup is momentarily unloaded of the vertical weights. Shear box and metal plate are lifted from the canister, along with the consolidated specimen;
- The shear box is turned upside-down and the specimen is gently pushed in (2-3mm) to create a gap. The latter is filled with bentonite slurry, as pictured in Figure 6.14 below;
- The steel plate is placed on top of the upside-down shear box. The two are firmly held together and then rotated to the ordinary orientation;
- The steel plate and shear box are placed back in the canister, which is then filled with water;
- Finally, after installing the loading cap, normal load can be applied again.

Figure 6.14: Bentonite slurry placed on the underside of clay specimens.

6.2.2.3 Conditioned Specimens (Foam Suspension)

Specimens made of soils B and C are prepared according to the following procedure:

- Enough soil is put to dry in the oven, for a period of at least 24 hours;
- The soil is taken out the oven and allowed to cool down. It is then wetted with demineralized water, to achieve 50% saturation level (corresponding to a W of around 0.2-0.25, depending on soil sample);
- A known mass of wet soil is mixed with the foam suspension. This step is performed inside a small plastic container, by means of agitating the two phases (soil and suspension) until homogeneous. The volumetric ratio between foam and wet soil (FIR) is chosen at 25% for soil C and 50% for soil B. Higher FIR values have been tested during the investigation, but yielded a paste which proved to be extremely difficult to work with;
- After having set-up the shear box apparatus (see paragraph 6.2.1), the foam-conditioned soil is gradually transferred in the shear box and homogenized with a spoon. This procedure is performed as consistently as possible each time, to guarantee the same specimen characteristics;
- The shear box loading cap is installed (see paragraph 6.2.1).

Figure 6.15 below shows a sample of soil C, conditioned with foam suspension, during specimen preparation:

Figure 6.15: Foam-conditioned sample of soil C; prior to fitting porous stone and loading cap.

Specimens made of soil A are prepared according to same procedure followed for bentonite-conditioned specimens. The only difference being that the gap between specimen and metal plate is filled with foam instead of bentonite.

6.2.2.4 Bentonite Slurry

Bentonite slurry is prepared by mixing bentonite powder Ibeco B1 with demineralized water at room temperature. General properties of the bentonite can be found in 6.1.2. The mixing ratio adopted is of 45gr of bentonite powder per liter of solution, yielding a slurry with a density of ρ = 1.028 kg/l and a yield point of 5.5 Pa. Mixing is performed using a high-speed mixer for 10 minutes. Afterwards, bentonite slurry is left undisturbed to swell for 48 hours. Prior to combining bentonite slurry with soil samples, it is pre-sheared for 2 minutes. The procedure described in the lines above takes inspiration from the one of (Kelessidis & Maglione, 2008), (Schosser, Thewes, Budach, & Zenner, 2012) and (API, 2008).

6.2.2.5 Foam Suspension

Foam suspensions for EPB tunnelling are prepared by feeding a surfactant water solution through a pressurized foam generator. Tumblers and swirlers inside the machine agitate the solution, turning it into foam, as described by (Thewes, Budach, & Bezuijen, 2012) and ((Langmaack, 2002)).
The parameters relevant for foam generation and its use with soil are:

- Surfactant concentration, c_f. It is the ratio between mass of surfactant (Q_f) and mass of solution (Q_l), as shown in Equation 13:

Equation 13:

$$c_f = \frac{Q_f}{Q_l} \cdot 100$$

- Foam expansion ratio, FER. It is the ratio between volume of generated foam (Q_F) and volume of generating solution (Q_L), as shown in Equation 14:

Equation 14:

$$FER = \frac{Q_F}{Q_L}$$

- Foam injection ratio, FIR. It is the ratio between volume of injected foam (Q_F) and volume of in situ soil to be excavated (Q_S), as shown in Equation 15:

Equation 15:

$$FIR = \frac{Q_F}{Q_S} \cdot 100$$

According to the guidelines given by (EFNARC, 2005), c_f is typically in the range of 0.5 – 5%. FER should be at 5 – 30, while FIR can be at 10 - 80% (in most cases around 30 – 60%). The specific value for these parameters is chosen based on soil type and condition, as well as machine characteristics and excavation requirements. Table 6.4 below summarizes some combinations of c_f, FER and FIR according to soil type, mentioned in literature:

Table 6.4:

c_f [%]	FER [-]	FIR [%]	Soil	Reference
3 2; 3	17 15; 10	25 20; 50	Silica sand Crushed rock	(Alavi Gharahbagh, Rostami, & Talebi, 2014)*
-	7-10	15-30	Boston blue clay	(Ball, Young, Isaacson, Champa, & Gause, 2009)*
1-3	6-12	25-70	Sandy gravel	(Langmaack, 2002)**
5	10	30; 50; 70	Sand (D_{60}=0.7-0.8mm)	(Mori, Mooney, & Cha, 2018)*
2.5	16	20-50; 30-50	Medium-sized sand; Gravelly-sand	(Peila, Oggeri, & Borio, 2009)*
-	-	50	Gravelly sand	(Y. Peron & Marcheselli, 1994)**
0.5-5	5-30	30-80; 40-60; 20-40; 30-40; 25-50; 30-60	Clay; Sandy clay-silt; Sand-clayey silt; Sand; Clayey gravel; Sandy gravel	(EFNARC, 2005) (General guidelines)

***: From laboratory investigation;**
****: From tunnelling project/s**

In the laboratory investigation, foam suspensions are most commonly prepared by agitating surfactant-water solutions using a high-speed mixer. The surfactant agent used to prepare foam is described in paragraph 6.1.3. Although this method differs from using a purposely-made foam generator, acceptable results can be obtained anyway. c_f is most commonly chosen as 2%. This concentration yields a maximum FER of 11.5 – 12, after a mixing time of 5 minutes. To make sure foam suspensions are prepared consistently every time, mixing of the solution is prolonged until the maximum obtainable of FER 11.5-12 is reached. This value is within the interval suggested in Table 6.4. Figure 6.16 below shows one of the batches of foam prepared during the laboratory investigation:

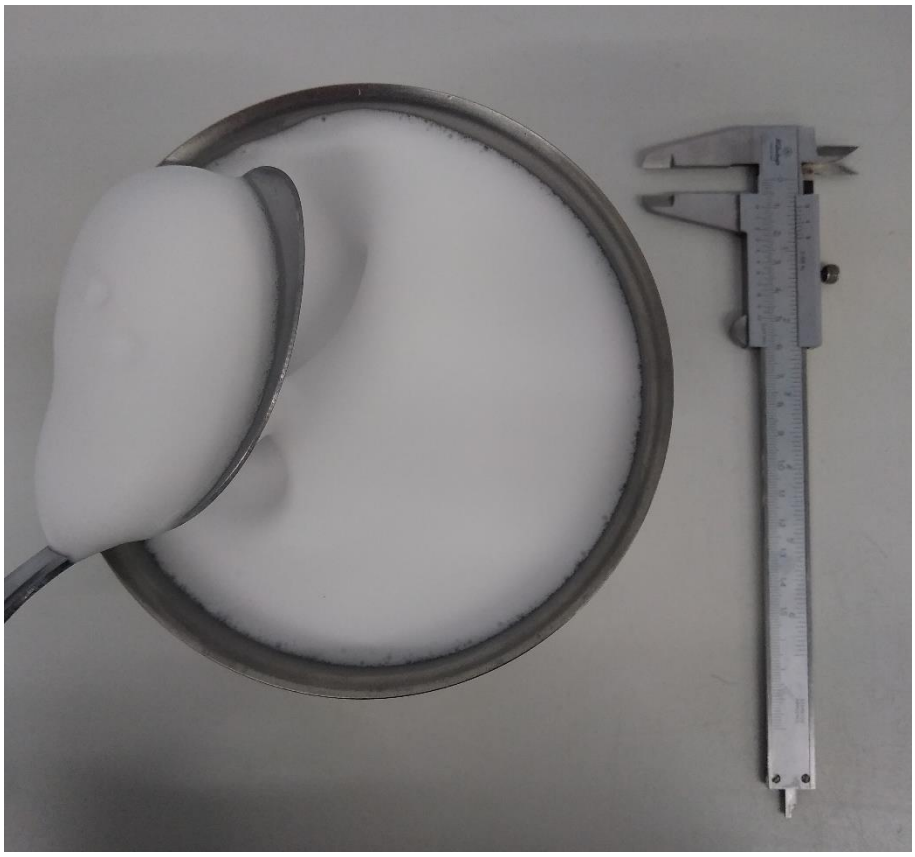

Figure 6.16: Foam suspension (2% surfactant concentration, FER = 11.5-12).

For what concerns FIR, values of up to 50% have been tested during the laboratory investigation. Eventually, FIR = 25% and 50% are chosen for soil C and B, respectively. The first figure, compared to the ones summarized in Table 6.4, sits on the lower boundary of the range. Nonetheless, higher percentages could not be used in practice, as they proved to yield mixtures troublesome to work with. For what concerns soil A, on the other hand, a FIR cannot be defined. As explained in paragraph 6.2.2.3, in fact, foam is not mixed with clay, but rather injected underneath the specimen, along the interface with steel.

7 Experiment Results

The present paragraph reports the results and highlights obtained from interface shear tests performed between soil specimens A, B, and C and steel. For each of the soil types, water-saturated, bentonite-conditioned and foam-conditioned case is discussed.

Before looking at the tests in detail, however, it is necessary to specify how the outcome of each shear test is interpreted.
The interface friction coefficient and angle (μ and δ, respectively) are ultimately the desired outcome of all the interface shear tests. The derivation of δ is performed according to Equation 16:

Equation 16:

$$\delta = tan^{-1}(\mu)$$

While μ is the ratio between measured shear stress and applied normal load (Equation 17):

Equation 17:

$$\mu = \tau/\sigma$$

μ and δ are obtained analysing the shear-displacement curve of each interface shear test: σ is the applied normal load and τ is the measured shear stress. This procedure, however is not standardized and/or unique. While σ is known and unique for each test, τ might be interpreted in various ways, each possibly leading to a different result. All the shear tests performed in the laboratory investigation are interpreted in the following way: only the measurements within 10% of difference from the maximum or residual shear are averaged to obtain a representative shear value. Figure 7.1 visualizes the method just described, using a sample shear test:

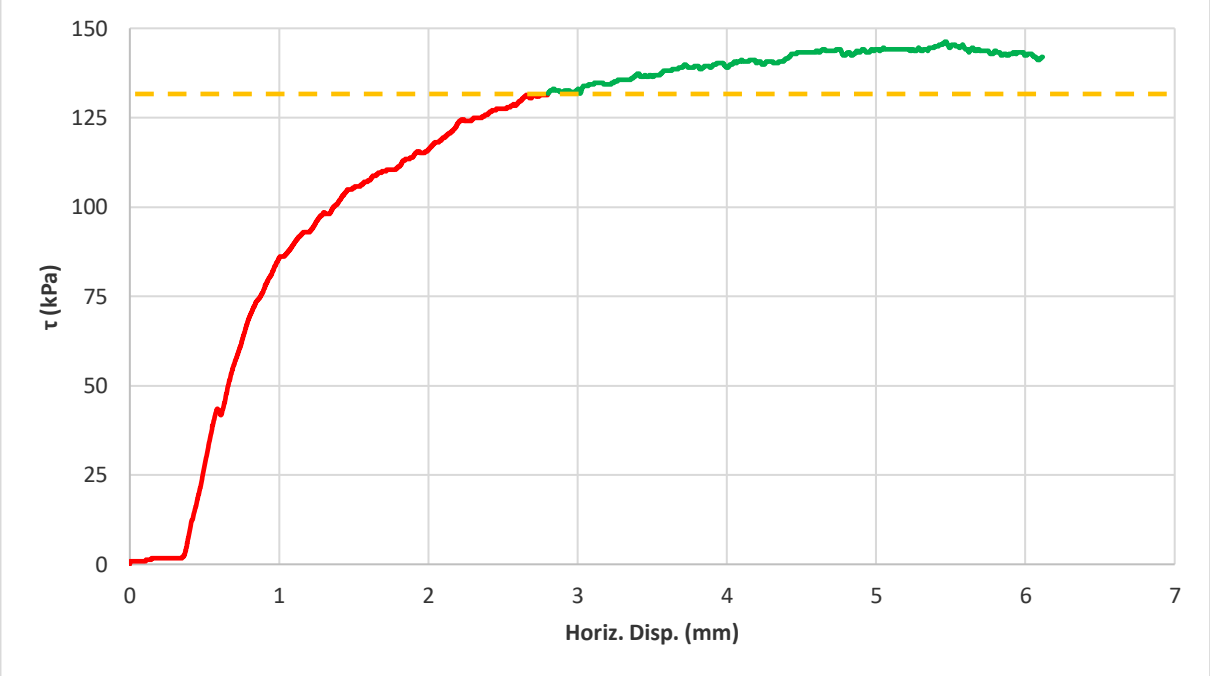

Figure 7.1: In green are the measurements within 10% from the max. shear registered in the test. These values are averaged to obtain a representative τ value.

7.1 Soil A

The following paragraph summarizes results and highlights of interface shear tests performed between steel and soil A (its properties can be found in paragraph 6.1.1.1).

7.1.1 Water-saturated

Interface shear tests between soil A and steel are initially conducted in water-saturated conditions. 4 normal loads are adopted, equal to σ = 50.0, 99.7, 193.4 and 400.7 kPa. Sliding speed is SR = 0.1 mm/min. Further details regarding sample preparation and test set up can be found in paragraph 6.2.
Test evidence shows that clay specimens develop distinct peak and residual interface shear resistance. The post peak shear drop appears to be greater for specimens tested at higher normal loads. Vertical settlements reach an asymptotic value towards the end of shear tests. This general behavior coincides with the one described by (Littleton, 1976). Average residual friction angle and coefficient are respectively found to be $\boldsymbol{\delta_{r,avg}}$ **= 14.6°** and $\boldsymbol{\mu_{r,avg}}$ **= 0.26**. Adhesion between clay and steel is equal to $\boldsymbol{a}$ **= 8.06 kPa.** These values are in accordance with values from literature on clay-steel interface shear tests, as can be seen in Figure 7.2 below:

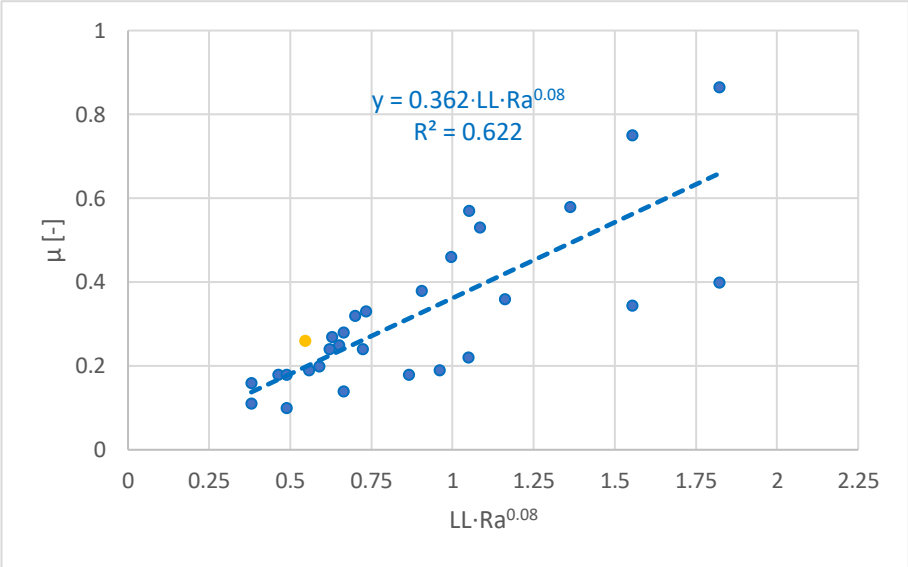

Figure 7.2: Comparison between data from literature (blue) and results from water-saturated interface shear tests of soil A (yellow).

Detailed results and graphs for each test can be found in Appendix E.

7.1.2 Bentonite-conditioned

Interface shear tests between soil A and steel are then conducted for bentonite-conditioned specimens. 4 normal loads are adopted, equal to σ = 50.0, 99.7, 193.4 and 327.3 kPa. Sliding speed is SR = 0.1mm/min. Further details regarding sample preparation and test set up can be found in paragraph 6.2.
Test evidence shows that conditioned clay specimens develop distinct peak and residual interface shear resistance, similarly to non-conditioned clay. Vertical settlements are initially quick but tend to an asymptotic value towards the end of shear tests. The shear friction envelope results to be slightly convex, with friction angles slightly decreasing with increasing normal load. Average residual friction angle and coefficient are respectively found to be $\boldsymbol{\delta_{r,avg}}$ **= 7.5°** and $\boldsymbol{\mu_{r,avg}}$ **= 0.13**. Quadratic interpolation of test results yields null adhesion between clay and steel.

Detailed results and graphs for each test can be found in Appendix E.

7.1.2 Foam-conditioned

Interface shear tests between soil A and steel are then conducted for foam-conditioned specimens. 4 normal loads are adopted, equal to σ = 50.0, 99.7, 193.4 and 327.3 kPa. Sliding speed is SR = 0.1mm/min. Further details regarding sample preparation and test set up can be found in paragraph 6.2.
Specimen behaviour is analogous to that observed for bentonite-conditioned clay. Average residual friction angle and coefficient are respectively found to be $\boldsymbol{\delta_{avg}}$ **= 10.2°** and $\boldsymbol{\mu_{avg}}$ **= 0.18**. Quadratic interpolation of test results yields adhesion between clay and steel equal to $\boldsymbol{a}$ **= 0.5 kPa**.

Detailed results and graphs for each test can be found in Appendix E.

7.2 Soil B

The following paragraph summarizes results and highlights of interface shear tests performed between steel and soil B (its properties can be found in paragraph 6.1.1.2).

7.2.1 Water-saturated

Interface shear tests between soil B and steel are initially conducted in water-saturated conditions. 4 normal loads are adopted, equal to σ = 50.0, 99.7, 193.4 and 400.7 kPa. Sliding speed is SR = 0.1 mm/min. Further details regarding sample preparation and test set up can be found in paragraph 6.2.
Test evidence shows how, once the maximum shear resistance is reached, fluctuation around this value is limited. Specimens show noticeable contraction upon shearing, confirming the behaviour observed from internal shear tests (paragraph 6.1.1.2). If shear tests were not been stopped at 6mm of displacement, specimens would continue to settle. Average friction angle and coefficient are respectively found to be $\boldsymbol{\delta_{avg}}$ **= 26.0°** and $\boldsymbol{\mu_{avg}}$ **= 0.49**. These figures are in accordance with values from literature on sand-steel interface shear tests, as can be seen in Figure 7.3 below:

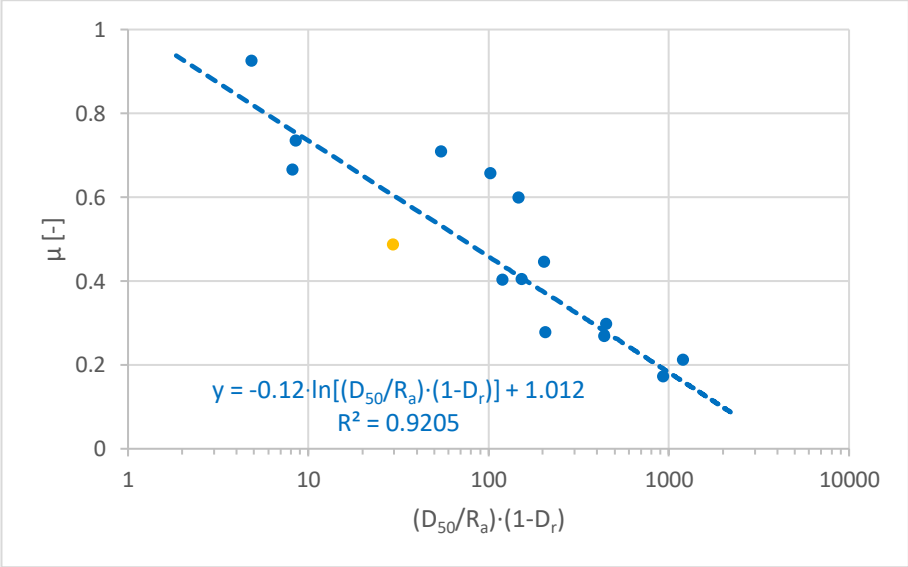

Figure 7.3: Comparison between data from literature (blue) and results from water-saturated interface shear tests of soil B (yellow).

Detailed results and graphs for each test can be found in Appendix F.

7.2.2 Bentonite-conditioned

Interface shear tests between soil B and steel are then conducted for bentonite-conditioned specimens. 4 normal loads are adopted, equal to σ = 50.0, 99.7, 193.4 and 327.3 kPa. Sliding speed is SR = 0.1 mm/min. Further details regarding sample preparation and test set up can be found in paragraph 6.2.
Test evidence shows how shear resistance requires higher horizontal displacement to reach a stable value, compared to the water-saturated case. The peak shear resistance ultimately developed, moreover, is found to be lower than for

water-saturated conditions. The contractive behaviour observed for water-saturated conditions is accentuated. This is likely because bentonite-conditioned samples have lower density and compaction, compared to water-saturated ones. Average friction angle and coefficient are respectively found to be $\boldsymbol{\delta_{avg}}$ **= 23.1°** and $\boldsymbol{\mu_{avg}}$ **= 0.43.**

Detailed results and graphs for each test can be found in Appendix F.

7.2.3 Foam-conditioned

Interface shear tests between soil C and steel are then conducted for foam-conditioned specimens. 4 normal loads are adopted, equal to σ = 50.0, 99.7, 193.4 and 327.3 kPa. Sliding speed is SR = 0.1 mm/min. Further details regarding sample preparation and test set up can be found in paragraph 6.2.
Test evidence shows how the contractive behaviour observed for water-saturated conditions is accentuated. Foam conditioning does not seem to noticeably reduce friction, compared to the water-saturated case. Average friction angle and coefficient are respectively found to be $\boldsymbol{\delta_{avg}}$ **= 25.2°** and $\boldsymbol{\mu_{avg}}$ **= 0.47.**

Detailed results and graphs for each test can be found in Appendix F.

7.3 Soil C

The following paragraph summarizes results and highlights of interface shear tests performed between steel and soil C (its properties can be found in paragraph 6.1.1.3).

7.3.1 Water-saturated

Interface shear tests between soil C and steel are initially conducted in water-saturated conditions. 4 normal loads are adopted, equal to σ = 50.0, 99.7, 193.4 and 400.7 kPa. Sliding speed is SR = 0.50 mm/min. Further details regarding sample preparation and test set up can be found in paragraph 6.2.
Test evidence shows how shear resistance is fully mobilized already after very little horizontal displacement (fractions of mm). Once the maximum shear resistance is reached, fluctuation around this value is limited. Specimen show modest dilation upon shearing, confirming the behaviour observed from internal shear tests (paragraph 6.1.1.3). Average friction angle and coefficient are respectively found to be $\boldsymbol{\delta_{avg}}$ **= 23.9°** and $\boldsymbol{\mu_{avg}}$ **= 0.44**. These figures are in accordance with values from literature on sand-steel interface shear tests, as can be seen in Figure 7.4 below:

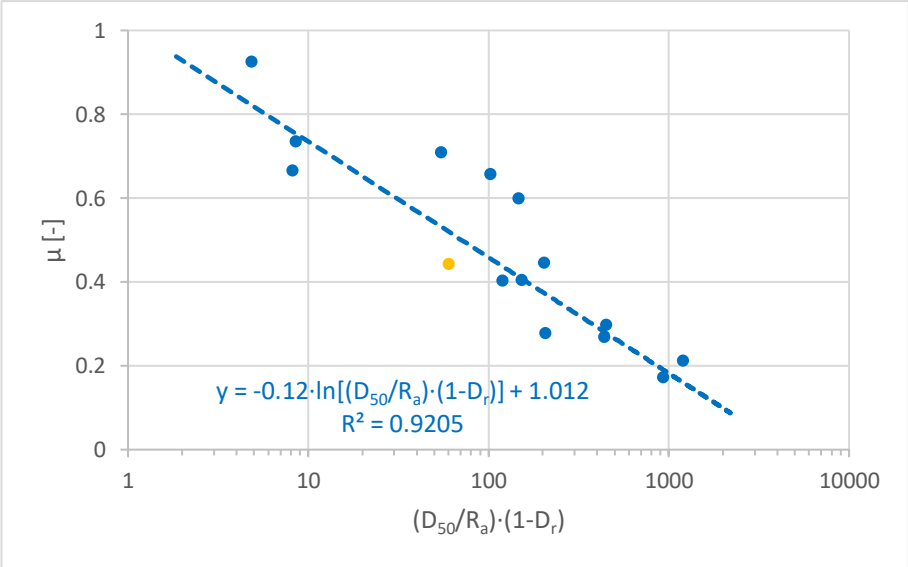

Figure 7.4: Comparison between data from literature (blue) and results from water-saturated interface shear tests of soil C (yellow).

Detailed results and graphs for each test can be found in Appendix G.

7.3.2 Bentonite-conditioned

Interface shear tests between soil C and steel are then conducted for bentonite-conditioned specimens. 4 normal loads are adopted, equal to σ = 50.0, 99.7, 193.4 and 327.3 kPa. Sliding speed is SR = 0.5 mm/min. Further details regarding sample preparation and test set up can be found in paragraph 6.2.
Shear resistance, compared to water-saturated conditions, appears to require slightly higher horizontal displacement to develop. The peak shear resistance, moreover, is found to be lower than for water-saturated conditions. The slight dilation observed for water-saturated conditions is replaced by evident contraction of specimens. This is likely because bentonite-conditioned samples have considerably lower density and compaction, compared to water-saturated ones. Average friction angle and coefficient are respectively found to be $\boldsymbol{\delta_{avg}}$ **= 19.4°** and $\boldsymbol{\mu_{avg}}$ **= 0.35**.
A second series of tests is performed later, adopting a lower bentonite/soil ratio. This allows the relative density of specimens to be analogous to the one of water-saturated conditions. Shear resistance, compared to water-saturated conditions, does not appear to be reduced. Average friction angle and coefficient are respectively found to be $\boldsymbol{\delta_{avg}}$ **= 23.5°** and $\boldsymbol{\mu_{avg}}$ **= 0.44**.

Detailed results and graphs for each test can be found in Appendix G.

7.3.3 Foam-conditioned

Interface shear tests between soil C and steel are then conducted for foam-conditioned specimens. 4 normal loads are adopted, equal to σ = 50.0, 99.7, 193.4 and 327.3 kPa. Sliding speed is SR = 0.5 mm/min. Further details regarding sample preparation and test set up can be found in paragraph 6.2.
Shear resistance appears to be affected by sudden spike fluctuations, which become more frequent and intense with increasing applied normal load. Each shear spike corresponds to a sudden vertical settlement: every time the specimen contracts, shear drops and immediately goes back to the previous value. The reason to why foam could induce this tendency is not clear. It is to be noted, however, that such shear fluctuations are not random singularities of few tests, as they also manifest during additional trial shear tests (performed in the same conditions).
The slight dilation observed for water-saturated conditions is replaced by evident contraction of foam-conditioned specimens. This is because foam bubbles capture soil grains and hold them in suspension, yielding a “paste” with a loose compaction state which tends to contract extremely easily.
For what concerns peak shear resistance, foam conditioning does not seem to noticeably reduce friction, compared to the water-saturated case. Average friction angle and coefficient are respectively found to be $\boldsymbol{\delta_{avg}}$ **= 22.4°** and $\boldsymbol{\mu_{avg}}$ **= 0.41**.
A second series of tests is performed later, adopting a thicker foam suspension (i.e. prepared with a c_f = 5% surfactant solution, rather than c_f = 2%). These tests are meant to assess whether increasing the foam density can yield lubrication effects.

Detailed results and graphs for each test can be found in Appendix G.

Part 3: Analysis and Discussion

8 Bentonite Conditioning

The present paragraph analyses and discusses the effects of bentonite conditioning on soil interface friction. The analysis initially focuses on bentonite-conditioned sands (soil B and C). The effects on clay (soil A) are studied afterwards.

8.1 Sand

Bentonite-conditioned sands are tested using the custom shear box gasket (introduced in paragraph 6.2.1). If the gasket was not adopted, most of the slurry would be expelled from the shear box, nullifying the point of treating soil with bentonite in the first place. Test evidence shows that the gasket performs effectively: upon loading of conditioned specimens, part of the pressure is transferred to the slurry, which would tend to permeate through the shear box. The seal created between gasket, loading cap and shear box, however, prevents this from happening.
For normal loads of approximately 200-300 kPa and above, some bentonite leakage is observed, as can be seen in Figure 8.1 below. The amount of leakage also depends on the viscosity/consistency of conditioned specimens: the less viscous is the mixture, the likelier is the occurrence of leakage. Specimen viscosity decreases with increasing bentonite concentration. Consequently, the bentonite-dry soil ratio of sand specimens is limited to approximately 0.3-0.4 by mass, depending on the specific soil considered.
Overall, the normal loads adopted (approximately 50-330 kPa) and the sufficient viscosity of specimens tested allow enough slurry to endure in the shear box assembly.

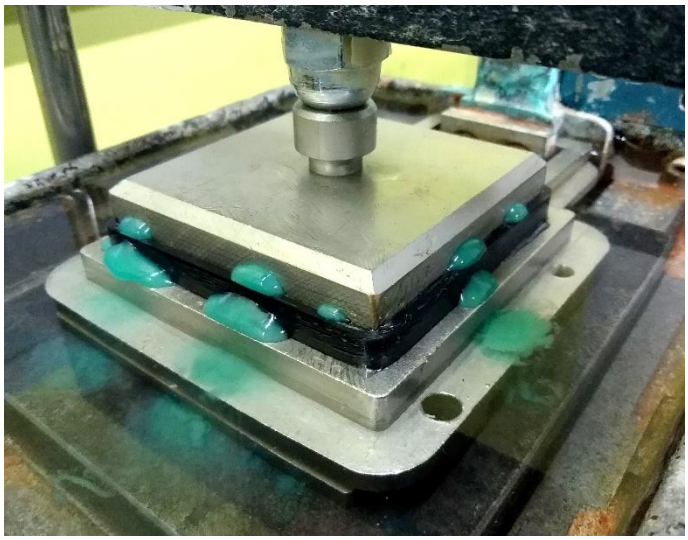

Figure 8.1: Leakage of tinted bentonite highlights the serviceability limit of the shear box gasket (approx. 200-300 kPa).

For what concerns bentonite-conditioned tests between clay and steel, the above-mentioned gasket is not required. In fact, the volume of bentonite used to condition clay is considerably lower than for sand. Moreover, the low permeability of clay and its tight fit in the shear box already provide satisfactory sealing against bentonite leaks.

Figure 8.2 below compares results of interface shear tests between water-saturated and bentonite-conditioned samples of soil B, sliding against steel:

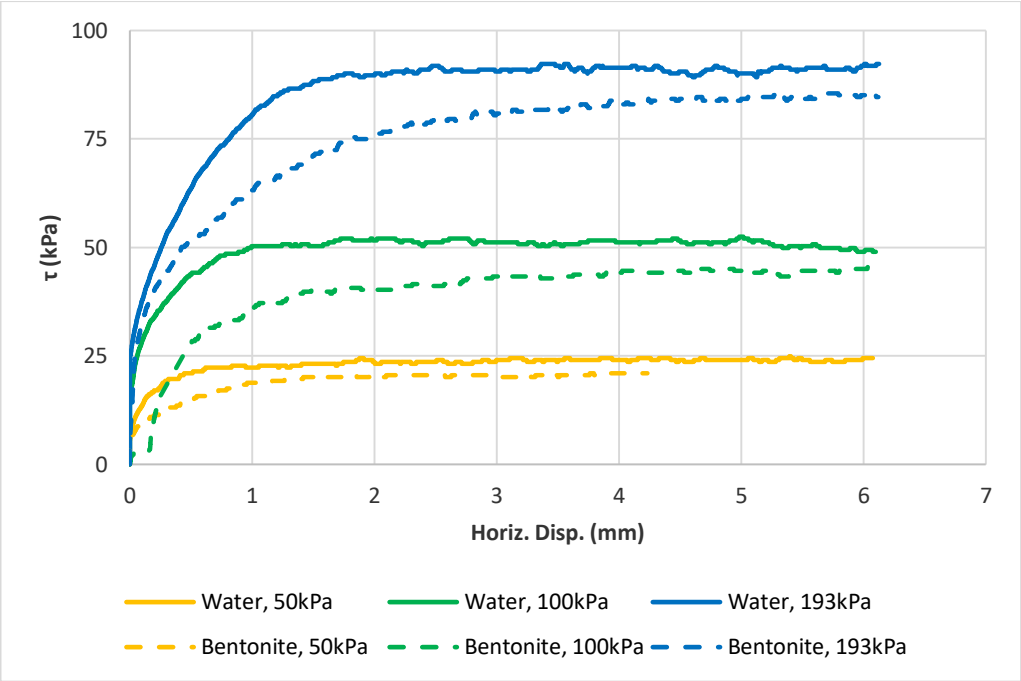

Figure 8.2: Comparison of interface shear tests (soil B). Water-saturated tests in solid lines, bentonite-conditioned tests in dashed lines. Normal loads are of 50.0, 99.7 and 193.4 kPa. Note: additional tests at normal loads of 400.7 and 327.3 kPa are not shown (mutual comparison of shear not possible).

When analysing tests performed at equal normal load, it is evident how shear resistance developed by bentonite-conditioned specimens is lower than that developed by water-saturated ones.
Table 8.1 below shows, for each test, the reduction in interface friction observed when testing bentonite-conditioned and water-saturated specimens of soil B:

Table 8.1: Interface friction angle reduction due to bentonite conditioning (soil B). The last line shows values averaged over all tests (including those at 327.3 and 400.7 kPa).

σ [kPa]	δ_{water}; $\delta_{bent.}$ [°]
50.0	25.4, 22.4 13.7% reduction
99.7	27.0, 23.8 13.3% reduction
193.4	25.1, 23.2 8.8% reduction
Whole shear envelope	26.0, 23.1 **12.5% reduction**

Figure 8.3 below compares results of interface shear tests between water-saturated and bentonite-conditioned samples of soil C, sliding against steel:

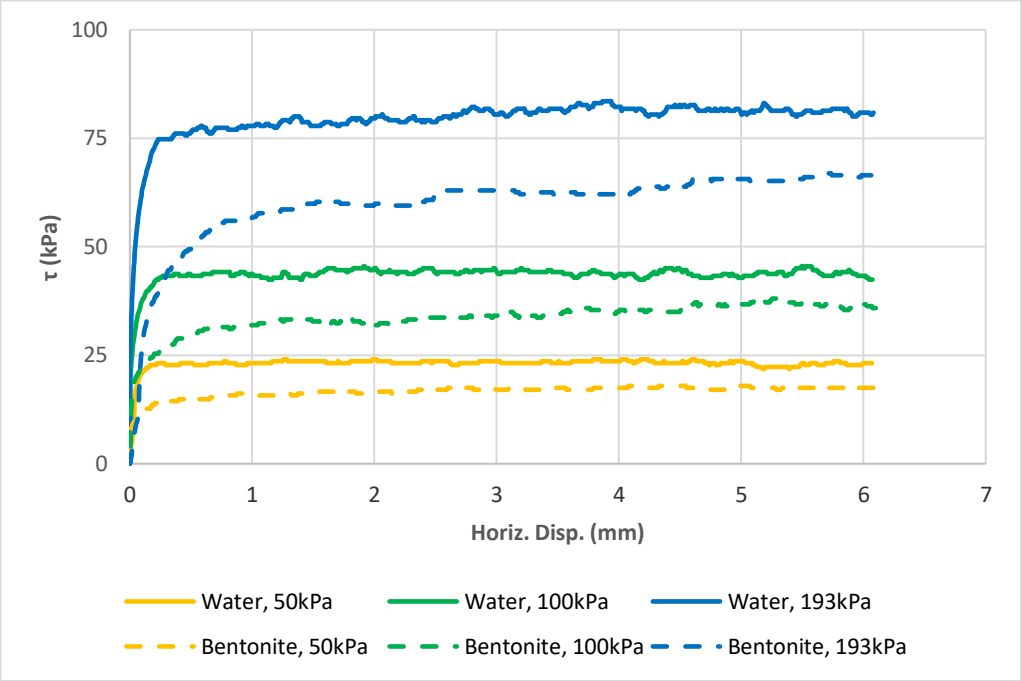

Figure 8.3: Comparison of interface shear tests (soil C). Water-saturated tests in solid lines, bentonite-conditioned tests in dashed lines. Normal loads are of 50.0, 99.7 and 193.4 kPa. Note: additional tests at normal loads of 400.7 and 327.3 kPa are not shown (mutual comparison of shear not possible).

When analysing tests performed at equal normal load, it is evident how the shear resistance developed by bentonite-conditioned specimens is lower than that developed by water-saturated ones. This reduction is more pronounced than that of soil B (Figure 8.2).
Table 8.2 below shows, for each test, the reduction in interface friction observed when testing bentonite-conditioned and water-saturated specimens of soil C:

Table 8.2: Interface friction angle reduction due to bentonite conditioning (soil C). The last line shows values averaged over all tests (including those at 327.3 and 400.7 kPa).

σ [kPa]	δ_{water}; $\delta_{bent.}$ [°]
50.0	24.9, 18.9 32.2% reduction
99.7	23.7, 19.7 20.4% reduction
193.4	22.5, 18.3 23.3% reduction
Whole shear envelope	23.9, 19.4 **23.5% reduction**

To formulate a hypothesis as to why bentonite lowers frictional resistance between sand and steel, it is useful to examine soil density, prior and after shearing.
For soil B, as can be seen in Table 0.4 (Appendix F), the initial average density of water-saturated specimens is $\rho_{dry,0}$ = 1.95 g/cm^3 which slightly increases to $\rho_{dry,f}$ = 1.98 g/cm^3 after testing. For bentonite-conditioned specimens, as can be seen in Table 0.5 (Appendix F), the initial average density is $\rho_{dry,0}$ = 1.65 g/cm^3 which increases to $\rho_{dry,f}$ = 1.85 g/cm^3 after testing.
For soil C, as can be seen in Table 0.7 (Appendix G), the initial average density of water-saturated specimens is $\rho_{dry,0}$ = 1.81 g/cm^3 which is virtually unchanged after testing (Soil C, in fact, undergoes hardly any contraction/expansion).

For bentonite-conditioned specimens, as can be seen in Table 0.8 (Appendix G), the initial average density is $\rho_{dry,0}$ = 1.55 g/cm^3 which slightly increases to $\rho_{dry,f}$ = 1.59 g/cm^3 after testing.

As the values reported above suggest, the density of bentonite conditioned sand specimens is lower than that of water-saturated ones. Depending on sand properties and on bentonite/sand ratio, conditioned specimens can easily reach negative relative density. When sand is mixed with bentonite, in fact, soil grains get suspended in the slurry and "float" further apart from each other, yielding a loose yet stable structure. The latter is depicted in Figure 8.4 and Figure 8.5 below and compared with the structure of water-saturated sand:

Figure 8.4: Equal amounts of sand (100 gr of soil C) mixed with bentonite (left) and water (right).

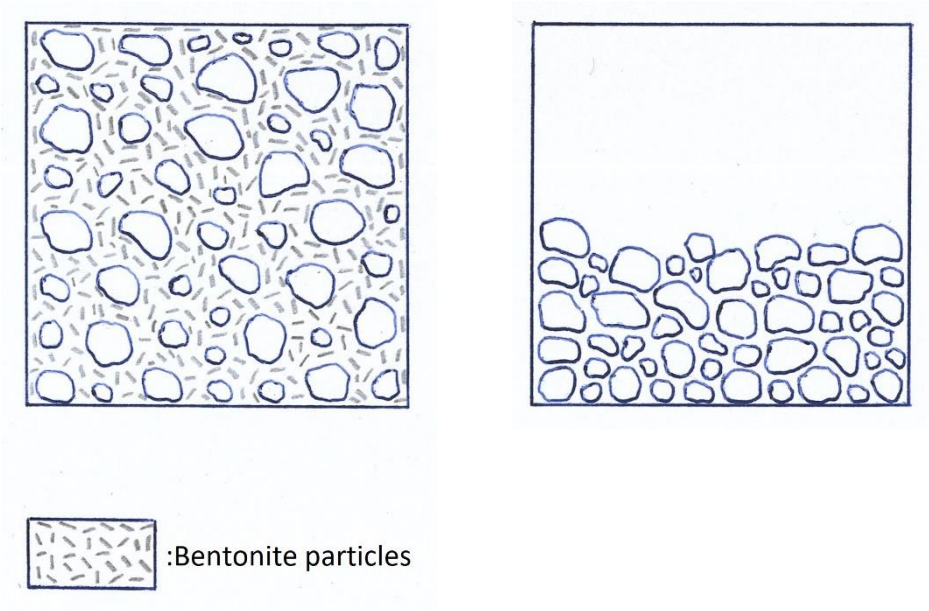

Figure 8.5: Schematization of equal amounts of sand, conditioned with bentonite (left) and saturated with water (right).

The density of conditioned specimens maintains lower than that of water-saturated ones, even after shearing. Their loose structure, therefore, proves to withstand the loads applied during testing, without densifying excessively. Such low density is believed to be the reason of lower interface friction coefficients developed by bentonite-conditioned sand.

As mentioned in paragraph 7.3, a second series of interface shear tests is performed between soil C and steel, adopting a lower bentonite/soil ratio. The amount of bentonite used is such that it just fills the soil voids, keeping the density of conditioned specimens approximately equivalent to that of water-saturated ones. The aim of these tests is to assess

whether bentonite can have lubrication effects (i.e. reduction of friction coefficients), independently of the bulking effect it generates when used at high concentrations.
Figure 8.6 below depicts the results obtained from these tests. Water-saturated and "mild" bentonite-conditioned samples of soil C are compared:

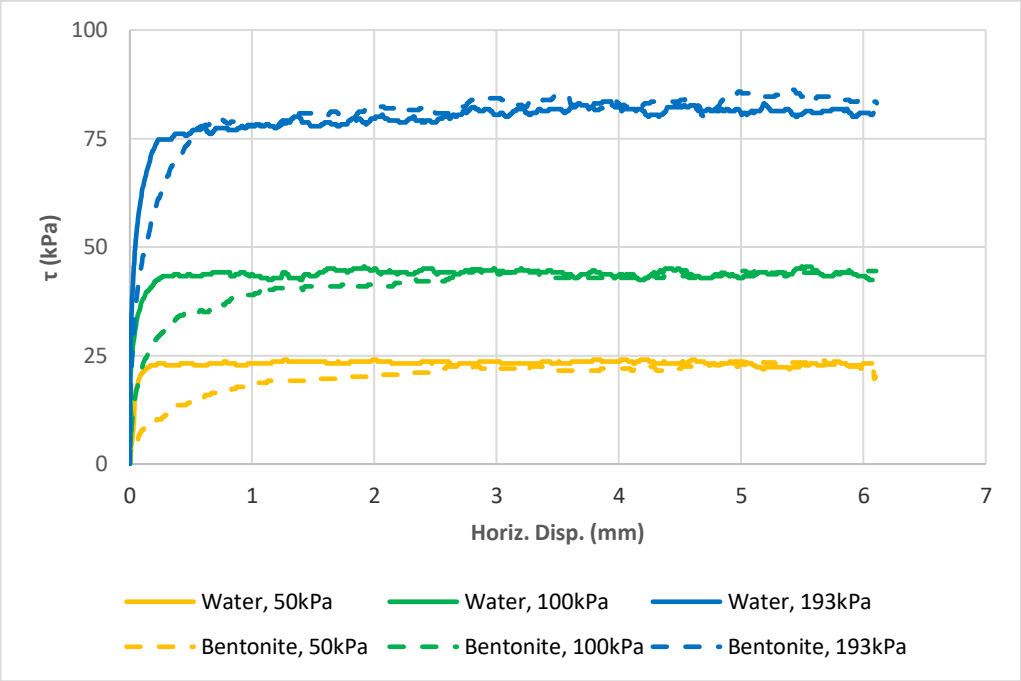

Figure 8.6: Comparison of interface shear tests (soil C). Water-saturated tests in solid lines, mild bentonite-conditioned tests in dashed lines. Normal loads are of 50.0, 99.7 and 193.4 kPa.

When analysing tests performed at equal normal load, it can be seen how shear resistance developed by "mild" bentonite-conditioned specimens of soil C is ultimately equivalent to that developed by water-saturated ones.
Table 8.3 below shows, for each test, the difference in interface friction observed when testing "mild" bentonite-conditioned and water-saturated specimens of soil C:

Table 8.3: Interface friction angle difference between mild bentonite-conditioned and water-saturated specimens (soil C). The last line shows values averaged over all tests.

σ [kPa]	δ_{water}; $\delta_{bent.}$ [°]
50.0	24.9, 24.1 3.3 % reduction
99.7	23.7, 23.3 6.0% reduction
193.4	22.5, 23.1 1.9% reduction
Whole shear envelope	23.9, 23.5 **1.8% reduction**

As can be seen in Table 0.7 and Table 0.9 (Appendix G), the density of "mild" bentonite-conditioned and water-saturated specimens is approximately equivalent, as is, accordingly, their compaction state. The shear resistance they develop during tests is also analogous.
Tests performed at different bentonite concentrations show that the reduction in interface friction observed for bentonite-conditioned sand is not due to lubrication of soil grain-steel contacts. The reduction in friction is rather because bentonite considerably lowers specimen compaction and density throughout testing (bulking effect). The

higher is the bentonite/soil ratio of conditioned specimens, the lower their density and interface friction with steel are. As explained at the beginning of this paragraph, the amount of bentonite which can be added to sand is limited by the apparatus, as is, therefore, the measurable reduction in soil-steel friction. If higher bentonite/soil ratios could be adopted in the laboratory (possibly replicating the conditions typical of excavation), the reduction of soil-steel friction is expected to be larger.

8.2 Clay

Figure 8.7 below compares results of interface shear tests between water-saturated and bentonite-conditioned samples of soil A (clay), sliding against steel:

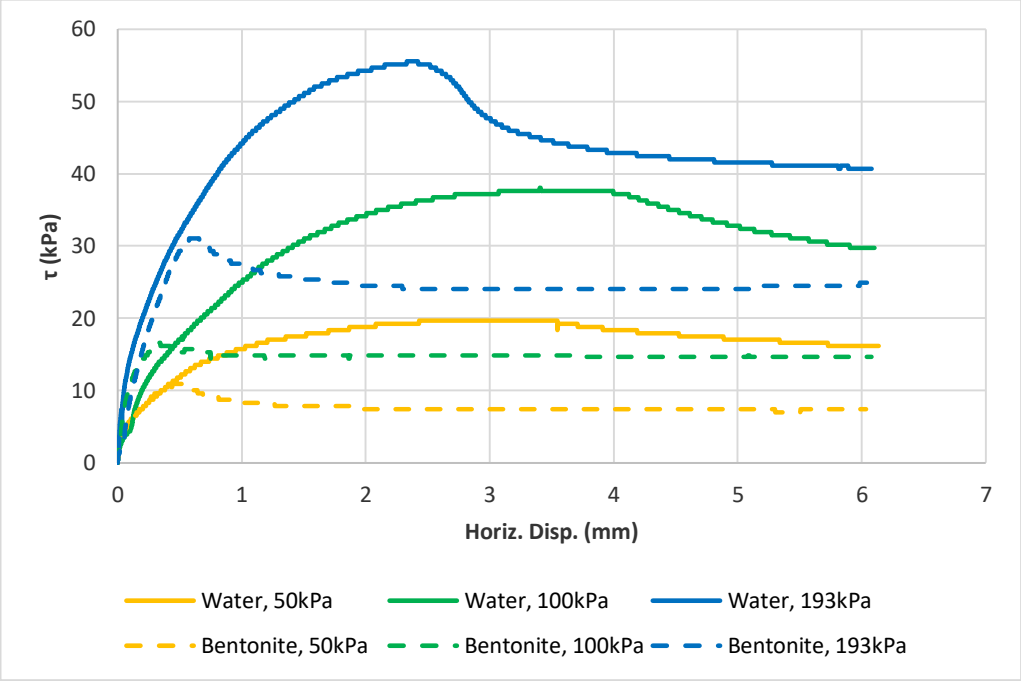

Figure 8.7: Comparison of interface shear tests (soil A). Water-saturated tests in solid lines, bentonite-conditioned tests in dashed lines. Normal loads are of 50.0, 99.7 and 193.4 kPa. Note: additional tests at normal loads of 400.7 and 327.3 kPa are not shown (mutual comparison of shear not possible).

When analysing tests performed at equal normal load, it is evident how the shear resistance developed by bentonite-conditioned clay specimens is lower than that developed by ordinary ones. The difference is considerable and is shown in Table 8.4 below, comparing residual friction angles measured for the two conditions:

Table 8.4: Residual interface friction angle difference between bentonite-conditioned and ordinary specimens (soil A). The last line shows values averaged over all tests.

σ [kPa]	δ_{water}; $\delta_{bent.}$ [°]
50.0	17.9, 8.5 52.8% reduction
99.7	16.6, 8.4 49.6% reduction
193.4	12.1, 7.3 39.1% reduction
Whole shear envelope	14.6, 7.5 **48.8% reduction**

The bentonite layer placed between clay specimen and steel plate considerably reduces friction between the two. Unlike for sand, the observed reduction in interface friction is due to actual clay-steel lubrication, rather than to particle bulking. In fact, bentonite does not permeate through the clay (thanks to the low porosity of the latter), meaning that slurry and specimen remain separated. Consequently, a bentonite film endures at the interface between clay and steel during testing, lubricating their relative motion and reducing interface shear resistance.

9 Foam Conditioning

The present paragraph analyses and discusses the effects on soil interface friction caused by conditioning specimens with foam. The analysis initially focuses on foam-conditioned sands (soil B and C). The effects on clay (soil A) are studied afterwards.

Evidence from bentonite-conditioned sand tests encourages to use the custom shear box gasket also for foam-conditioned sand tests. Unfortunately, the gasket results uncapable of preventing foam from leaking out of the shear box. While slurry has considerable viscosity and is, thus, relatively easy to contain, foam is much thinner and manages to permeate through the seal. Alternative test setups able to prevent/limit foam leakage are not found. Consequently, all foam-conditioned sand tests are hindered by this problem, which occurs even at low normal loads. Figure 9.1 below depicts a typical foam leakage observed during tests:

Figure 9.1: Foam leaking out of shear box assembly.

For what concerns foam-conditioned tests between clay and steel, the above-mentioned gasket is not required. In fact, the volume of foam used to condition clay is considerably lower than for sand. Moreover, the low permeability of clay and its tight fit in the shear box already provide satisfactory sealing against foam leaks.

9.1 Sand

Figure 9.2 below compares results of interface shear tests of water-saturated and foam-conditioned samples of soil B, sliding against steel:

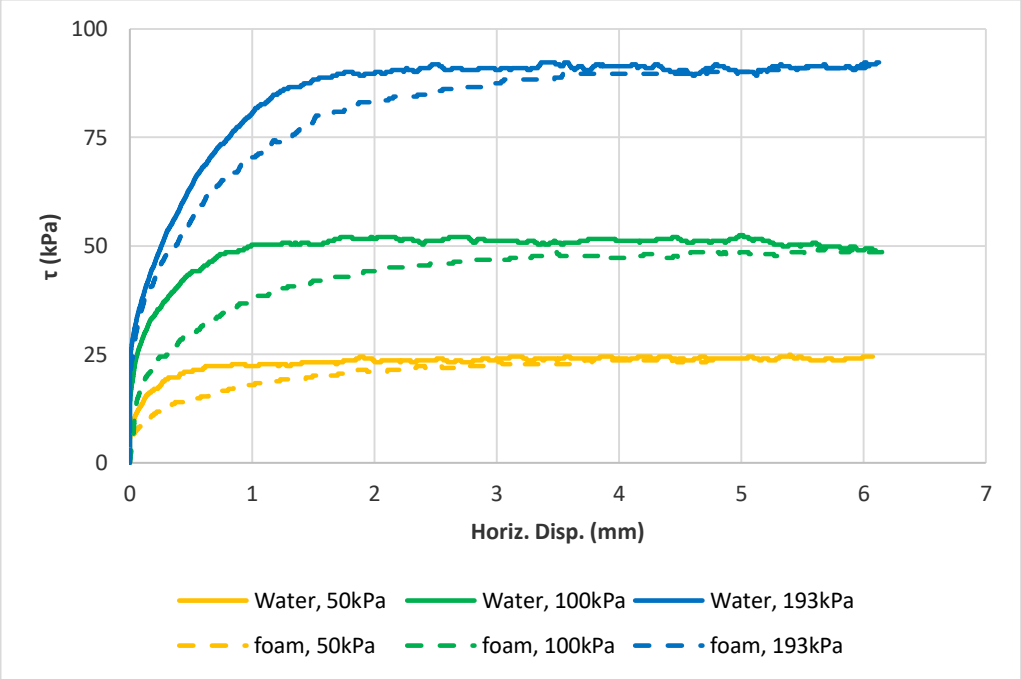

Figure 9.2: Comparison of interface shear tests (soil B). Water-saturated tests in solid lines, foam-conditioned tests in dashed lines. Normal loads are of 50.0, 99.7 and 193.4 kPa. Note: additional tests at normal loads of 400.7 and 327.3 kPa are not shown (mutual comparison of shear not possible).

When analysing tests performed at equal normal load, it can be seen how the shear resistance developed by foam-conditioned specimens of soil B is ultimately equivalent to that developed by water-saturated ones.
Table 9.1 below shows, for each test, the difference in interface friction observed when testing foam-conditioned and water-saturated specimens of soil B:

Table 9.1: Interface friction angle difference between foam-conditioned and water-saturated specimens (soil B). The last line shows values averaged over all tests (including those at 327.3 and 400.7 kPa).

σ [kPa]	δ_{water}; δ_{foam} [°]
50.0	25.4, 24.4 4.2% reduction
99.7	27.0, 25.5 6.0% reduction
193.4	25.1, 24.6 1.9% reduction
Whole shear envelope	26.0, 25.2 **3.1% reduction**

Figure 9.3 below compares results of interface shear tests of water-saturated and foam-conditioned samples of soil C, sliding against steel:

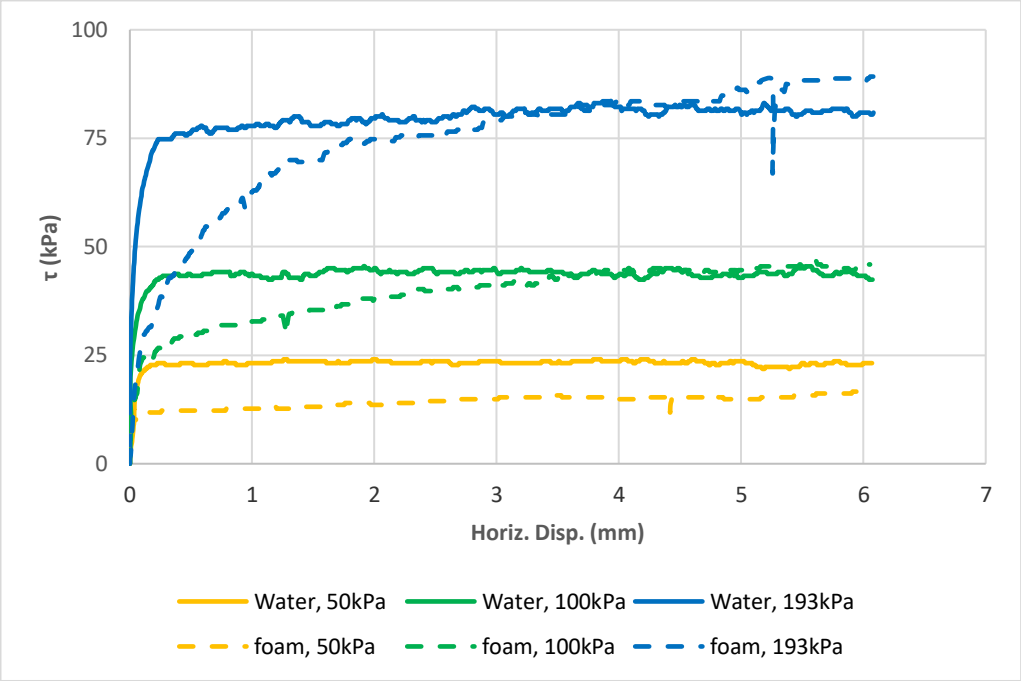

Figure 9.3: Comparison of interface shear tests (soil C). Water-saturated tests in solid lines, foam-conditioned tests in dashed lines. Normal loads are of 50.0, 99.7 and 193.4 kPa. The foam-conditioned test at 50.0 kPa is an outlier but is reported anyway. Note: additional tests at normal loads of 400.7 and 327.3 kPa are not shown (mutual comparison of shear not possible).

Analogously to soil B, tests reveal how the shear resistance developed by foam-conditioned specimens of soil C is ultimately equivalent to that developed by water-saturated ones.
Table 9.2 below shows, for each test, the difference in interface friction observed when testing foam-conditioned and water-saturated specimens of soil C:

Table 9.2: Interface friction angle difference between foam-conditioned and water-saturated specimens (soil C). The last line shows values averaged over all tests (including those at 327.3 and 400.7 kPa).

σ [kPa]	δ_{water}; δ_{foam} [°]
99.7	23.7, 24.1 1.5% increase
193.4	22.5, 23.5 4.4% increase
Whole shear envelope	23.9, 22.4 **2.6% increase***

*Test at 50.0 not considered

(Duarte, 2007) performed direct shear tests on foam-conditioned sands, using a direct shear apparatus of large size. The study shows that conditioned sand specimens have considerably lower density than ordinary ones, due to foam bubbles replacing sand grains in the soil structure.
Table 0.6 (Appendix F) and Table 0.10 (Appendix G) show how the density of foam-conditioned specimens tested in the laboratory is considerably lower than that of water-saturated ones (for both soil B and C). This evidence is in accordance with the observations from (Duarte, 2007) discussed above.
The internal friction angle of specimens tested by (Duarte, 2007) is reported to decrease between 23-70% when they are conditioned with foam. A comparable decrease, on the other hand, is not observed from tests performed in the laboratory: unexpectedly, the interface friction angle between foam-conditioned sand and steel is virtually unchanged from that of water-saturated conditions.

As mentioned in paragraph 7.3, a second series of conditioned interface shear tests is performed between soil C and steel, adopting a thicker foam suspension (i.e. with a c_f = 5%). This surfactant concentration is higher than the values used in practice. Nonetheless, such c_f is chosen to assess whether a denser and possibly more resilient foam can make up for the shortcomings of the test apparatus and yield lower friction coefficients. Figure 9.4 below depicts the results obtained from these tests. Water-saturated and thick foam-conditioned samples of soil C are compared:

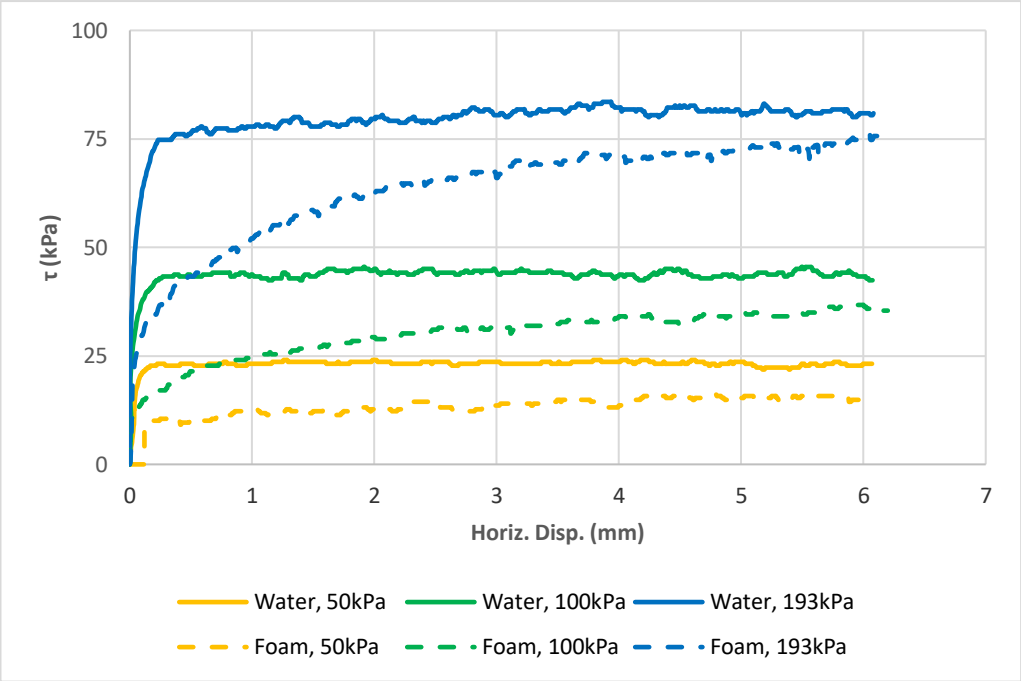

Figure 9.4: Comparison of interface shear tests (soil C). Water-saturated tests in solid lines, foam-conditioned tests in dashed lines (thick foam). Normal loads are of 50.0, 99.7 and 193.4 kPa

Figure 9.4Figure 9.3 show how the samples conditioned with the thick foam develop lower shear resistance than that of samples conditioned with regular foam, at equal normal load. Table 9.3 below shows, for each test, the difference in interface friction observed when testing thick foam-conditioned and water-saturated specimens of soil C:

Table 9.3: Interface friction angle difference between thick foam-conditioned and water-saturated specimens (soil C). The last line shows values averaged over all tests

σ [kPa]	δ_{water}; δ_{foam} [°]
50.0	25.4, 16.8 32.8% reduction
99.7	27.0, 19.0 29.6% reduction
193.4	25.1, 20.4 18.7% reduction
Whole shear envelope	26.0, 18.7 **27.9% reduction**

Albeit limited in number, this second series of tests shows that conditioning sand samples with foam can indeed lead to a reduction of their interface friction with steel, as previously observed by (Duarte, 2007). A reduced in friction between foam-conditioned sand and steel should, in principle, be observable even for lower surfactant concentrations. As shown in Figure 9.2 Figure 9.3, however, foam with c_f = 2% (reflecting the values adopted in practice) does not yield noticeable effects.

The reason for these unforeseen results is possibly poor foam quality. To verify whether the foam used in the laboratory has satisfactory characteristics, it is compared with foam made with a pressurized system. This consists of a pressurized air line, feeding the water-surfactant solution through a porous media. This system mimics the foam apparatuses used in tunnelling excavation and should therefore provide a reference for satisfactory foam. Figure 9.5 below shows the main components of this system:

Figure 9.5: Schematization of pressurized foam apparatus. The surfactant solution (contained in the syringe on the left) is pushed by pressurized air through the porous stone (enclosed in the metal housing on the right).

Evidence shows that foam suspensions produced with the high-speed mixer (see paragraphs 6.1.6 and 6.2.2.5) do not differ noticeably from those produced with the pressurized system: bubble size and expansion ratio are comparable, while lifetime is longer for foams made with the mixer. Accordingly, the quality of the foam produced with the mixer can be considered adequate (in the context of a basic laboratory investigation).

Since foam quality is ascertained to be satisfactory, the un-expected outcome of foam-conditioned tests must be caused by a different reason. This is, presumably, the inability of the test apparatus to maintain the foam-sand mixture pressurized, as mentioned at the beginning of this paragraph. The point of adding foam to soil, in fact, is to obtain a "paste" which can withstand the excavation pressure, thus creating an air "cushion" in the excavation chamber. If upon loading of specimens foam is expelled from the shear box, the stresses transmitted during testing have necessarily to be borne by the soil grains. Consequently, the resulting interface friction is virtually identical to that of un-conditioned soil. The thicker foam (i.e. c_f = 5%) shows to be more resilient, resulting in slightly reduced leakage from the shear box. Since more foam bubbles endure through testing, some lubricating effects can be seen (Figure 9.4).

9.2 Clay

Figure below compares results of interface shear tests between water-saturated and foam-conditioned samples of soil A (clay), sliding against steel:

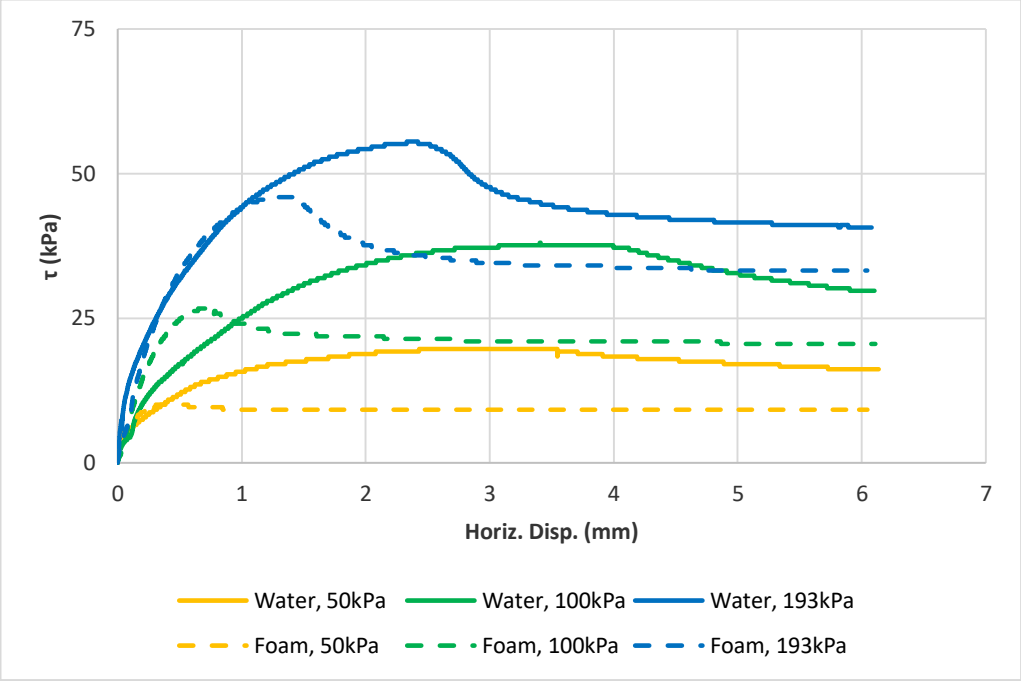

Figure 9.4: Comparison of interface shear tests (soil A). Water-saturated tests in solid lines, foam-conditioned tests in dashed lines. Normal loads are of 50.0, 99.7 and 193.4 kPa. Note: additional tests at normal loads of 400.7 and 327.3 kPa are not shown (mutual comparison of shear not possible).

When analysing tests performed at equal normal load, it is evident how the shear resistance developed by foam-conditioned clay specimens is lower than that developed by ordinary ones. The difference is shown in Table below, comparing residual friction angles measured for the two conditions:

Table 9.3: Residual interface friction angle difference between foam-conditioned and ordinary specimens (soil A). The last line shows values averaged over all tests.

σ [kPa]	δ_{water}; δ_{foam} [°]
50.0	17.9, 10.4 42.0% reduction
99.7	16.6, 11.6 29.9% reduction
193.4	12.1, 9.8 19.1% reduction
Whole shear envelope	14.6, 10.2 **29.9% reduction**

During consolidation, clay is moulded precisely to the inner dimensions of the shear box and a tight fit is established between them. This, combined with the low permeability of clay, allows reduced foam leakage, compared to tests for sand. Consequently, a film of foam endures at the interface between clay and steel during shearing, lubricating their relative motion and reducing their shear resistance, somewhat similarly to bentonite-conditioned clay (paragraph 8),

Part 4: Conclusions and Recommendations

10 Conclusions

Four main thesis objectives have been defined in the introduction (paragraph 1.3). The present paragraph addresses these four research targets, based on the results obtained from theoretical studies and laboratory investigations.

- **Objective nr° 1:** to classify and examine the available scientific sources reporting:
  - Theoretical or empirical friction coefficients between excavating machine and ground;
  - Empirical friction coefficients between soil and steel obtained from laboratory studies

  and to investigate a relation between friction coefficients belonging to these two groups.

  Friction coefficients between excavating machine and ground reported by literature are summarized in Figure 10.1 below. Additional details about the data displayed in Figure 10.1 can be found in Table 3.3.

*Figure 10.1: Soil-machine friction coefficients from tunneling literature. **Square** datapoints: non-lubricated conditions; **circular** datapoints: lubricated conditions. **Green** datapoints: values measured/back-figured; **Blue** datapoints: values as generic guideline. Note: positioning of datapoints along the horizontal axis is arbitrary (but within the correct soil type), due to lack of information. Thesis results depicted in **red**.*

Friction coefficients between soil and steel obtained from previous laboratory studies are summarized in Figure 10.2 and Figure 10.3 below, for sand and clay respectively. Additional details about data displayed in Figure 10.2 and Figure 10.3 can be found in Table 4.3.

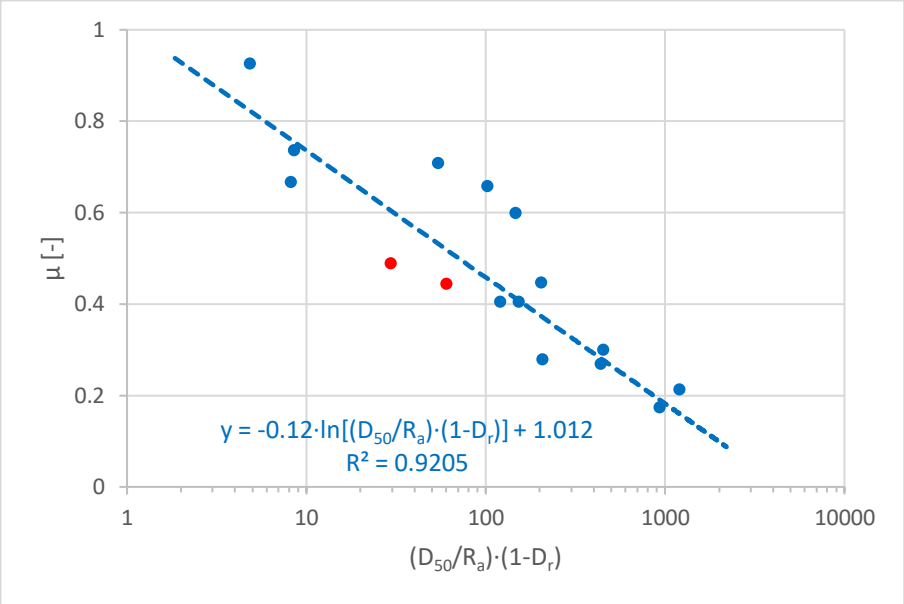

*Figure 10.2: Sand-steel friction coefficients from laboratory studies (Table 4.3). Thesis results depicted in **red**.*

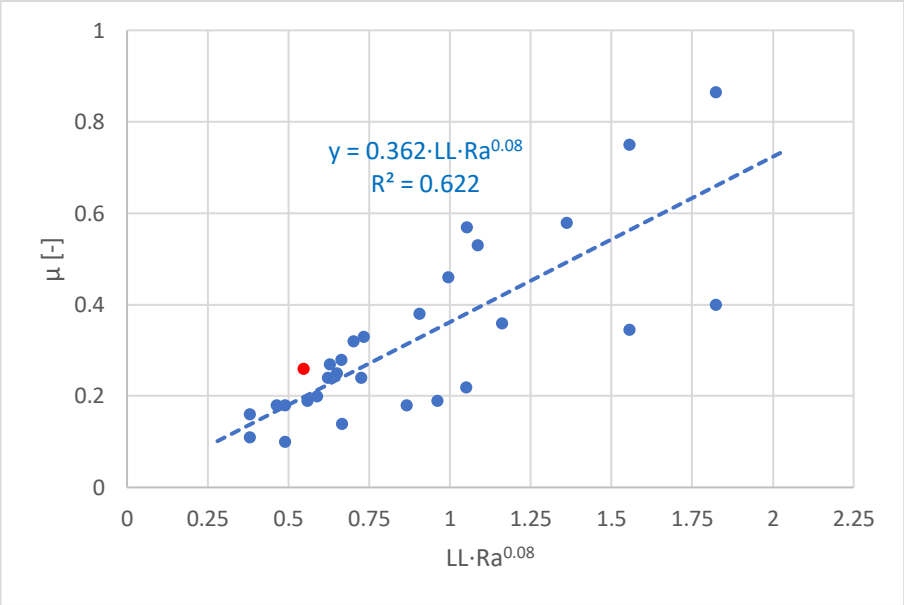

*Figure 10.3: Clay-steel friction coefficients from laboratory studies (Table 4.3). Thesis results depicted in **red**.*

Clays with low LL (< 0.75) tested in laboratory studies and clays excavated without soil lubricants develop analogous friction coefficients. On the contrary, clays with high LL (> 0.75) tested in laboratory studies show higher and more scattered friction coefficients than clays excavated without soil lubricants.

Sands tested in laboratory studies and sands excavated without soil lubricants develop analogous friction coefficients.

Comparison of conditioned interface friction coefficients between tunneling literature and laboratory studies is not possible, as the latter do not make use of foam or bentonite.

- **Objective nr° 2:** to perform interface shear tests between various soils and steel and to determine soil-steel friction coefficients from the outcome of these tests.

  Interface shear tests have been performed on two sands and clay, adopting a direct shear apparatus and a steel plate. The two sands (soil B and C) show average friction coefficients of μ = 0.49 and μ = 0.44, respectively.

The clay (soil A) shows average friction coefficient of $\mu = 0.26$. Additional information can be found in paragraph 7 and Appendices E, F and G.

- **Objective nr° 3:** to quantify the influence of soil additives on the friction coefficients determined from interface shear tests performed between soil and steel.

  The addition of bentonite slurry to soil specimens noticeably lowers soil-steel friction coefficients:
  Bentonite-conditioned tests show soil-steel friction coefficients which are up to 25% and 50% lower than without lubrication, for sands and clay respectively. For conditioned sand, the reduction in friction is attributed to the "bulking" effect of bentonite (i.e. lower specimen compaction and density). When excavating through sand, therefore, slurry should be injected extensively, to minimize soil density and lower friction. For conditioned clay, the reduction in friction is attributed to a lubricating bentonite film at the soil-steel interface. When excavating through clay, therefore, conditioning can be optimized to spraying the excavation face with bentonite, to create a slurry film at the soil-metal interface.

  The addition of foam to sand specimens does not convincingly lower measured soil-steel friction coefficients. This shortcoming is attributed to the test apparatus, which cannot replicate the confined/pressurized conditions of TBM excavation. If sand is treated with especially thick foam, some lubrication effects can be observed.
  The addition of foam suspension to clay specimens reduces soil-steel friction coefficients by 30% on average. This reduction in friction is attributed to a lubricating foam layer at the soil-steel interface.

  Figure 10.4, Figure 10.5 and Figure 10.6 below depict the overall shear envelopes of the soils tested, for every test condition:

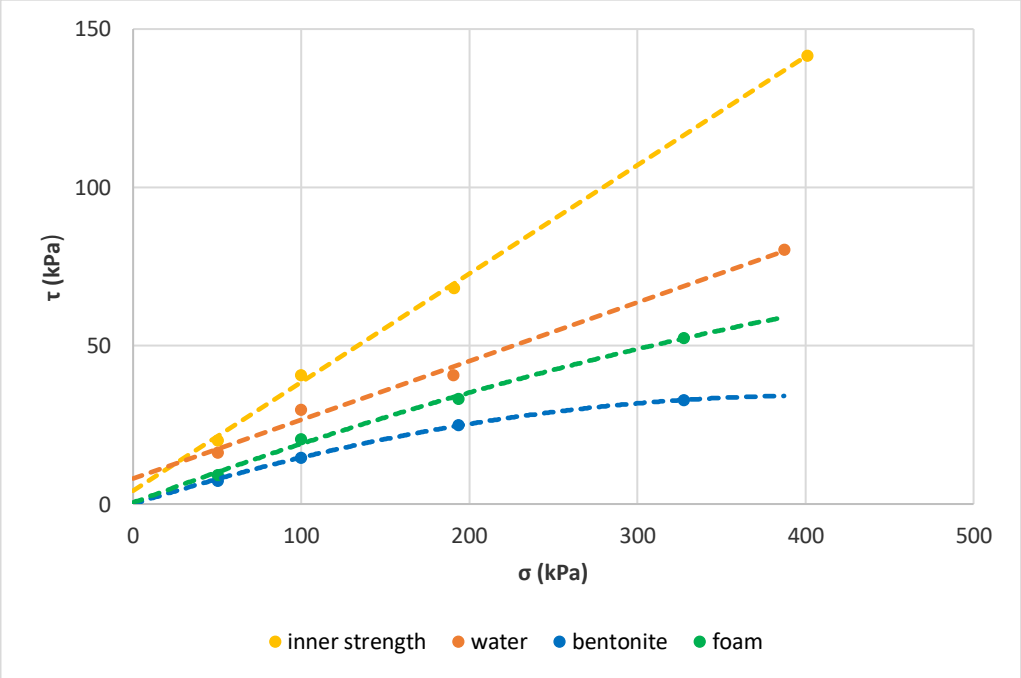

Figure 10.4: Shear envelopes of soil A (kaolin). Yellow depicts soil inner shear strength. Orange, Green and Blue depict respectively water-saturated, foam-conditioned and bentonite-conditioned interface shear strength.

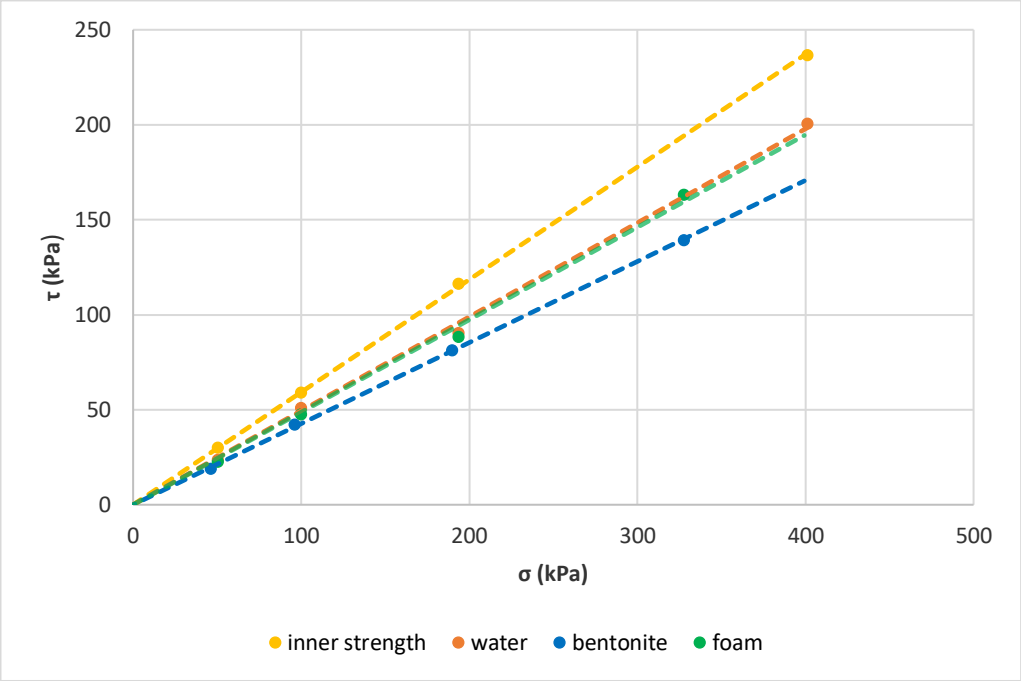

*Figure 10.5: Shear envelopes of soil B (fine sand). **Yellow** depicts soil inner shear strength. **Orange**, **Green** and **Blue** depict respectively water-saturated, foam-conditioned and bentonite-conditioned interface shear strength.*

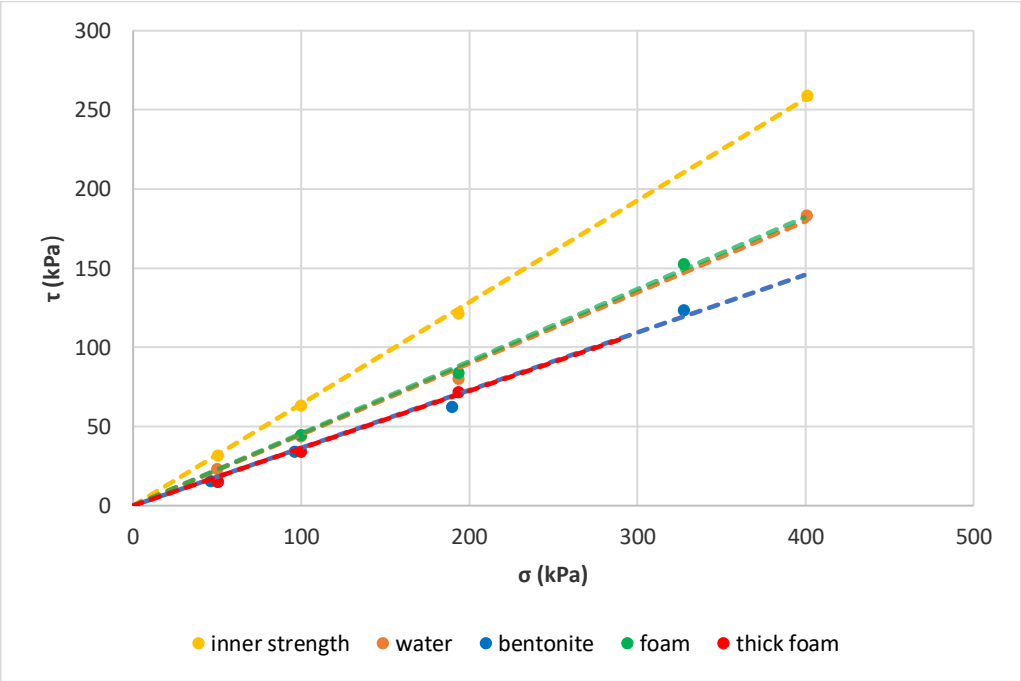

*Figure 10.6: Shear envelopes of soil C (coarse sand). **Yellow** depicts soil inner shear strength. **Orange**, **Green**, **Blue** and **Red** depict respectively water-saturated, foam-conditioned, bentonite-conditioned and thick foam-conditioned interface shear strength.*

- **Objective nr° 4:** to assess whether a direct shear apparatus, along with ordinary geotechnical investigations, can provide results which are satisfactory and useful for TBM design and use.

  Tests performed for non-lubricated specimens provide interface friction coefficients which closely match those reported by tunnelling literature, for all tested soils.
  Tests performed for bentonite-conditioned sand tend to over estimate the interface friction coefficients reported by tunnelling literature. Tests for bentonite-conditioned clay provide interface friction coefficients matching those reported by tunnelling literature.
  Tests performed for foam-conditioned sand cannot convincingly reproduce the interface fricton coefficients reported by tunnelling literature. Tests performed for foam-conditioned clay slightly over estimate the interface friction coefficients reported by tunnelling literature.

  Accordingly, an ordinary direct shear apparatus can be succesfully used to predict non-lubricated soil-TBM friction coefficients. The same apparatus, however, can at its basic design provide only an estimation of lubricated soil-TBM friction coefficients. Accurate prediction of lubricated friction coefficients in the laboratory requires more advanced equipment, or possibly extended modifications to the direct shear apparatus.

11 Recommendations

The present paragraph discusses about recommendation for further studies, as well as limits of the thesis investigation, considering both theoretical and practical aspects.

Existing soil-TBM friction coefficients (Figure 10.1) have been collected from heterogeneous sources, including laboratory studies, general guidelines on tunnelling excavation and specific excavation data. These sources often result to be generic and/or conflicting, especially regarding soil characterization. The information provided, therefore, is somewhat vague and only qualitative: rigorous analysis and forecast of soil-TBM friction coefficients result not to be possible.

Soil sample selection aimed at choosing the most relevant soils possible to the research field of the thesis. Nonetheless, however relevant and varied soils A, B and C can be, it is not possible to extend the results obtained for these three soils to the whole soil spectrum. If more reliable and detailed results are desired, additional soils of different nature and characteristics should be tested. Focus should especially go to rock aggregates, which have been disregarded completely from the thesis and might yield different outcomes.

Overall, in excess of 60 interface shear tests have been performed, considering various permutations of soil, load and conditioning. Some tests have occasionally been repeated, showing satisfactory consistency and reproducibility. Nonetheless, the number of tests conducted is too low to determine rigorously the accuracy of the thesis results. If results of probabilistic/stochastic nature want to be obtained, it is recommended to perform and repeat tests in higher numbers.

Choosing an ordinary direct shear apparatus allows to perform tests analogous to those of the thesis in any laboratory and to make results comparable. However, a direct shear device approximates simplistically the shearing mechanisms occurring in excavation. Moreover, bentonite and foam leakage from the shear box does not allow to test highly-conditioned samples.
To improve the test apparatus while maintaining a simple design, the shear box could be replaced by a cylinder-piston assembly from a small ordinary engine: the cylinder would be facing downwards, resting on the TBM metal plate. The piston would act as the shear box loading cap. The elastic segments of the piston would provide good sealing against foam and bentonite leaks, while maintaining low wall friction.

Finally, conditioning of soil specimens should in principle be performed via a pressurised system, simulating the apparatuses used in tunnelling. During the laboratory investigation, on the contrary, soil is mixed with bentonite or foam prior to its setup in the shear box. Moreover, foam is produced using a high-speed blender, rather than with a specifically-built system. These practical simplifications inevitably introduce inaccuracies and approximations.

Bibliography

Al-Mhaidib, A. I. (2006). Influence of shearing rate on interfacial friction between sand and steel.

Alavi Gharahbagh, E., Rostami, J., & Talebi, K. (2014). Experimental study of the effect of conditioning on abrasive wear and torque requirement of full face tunneling machines. *Tunnelling and Underground Space Technology, 41*, 127-136. doi:10.1016/j.tust.2013.12.003

Antonio Cavallaro, Michele Maugeri, & Mazzarella, R. Static and dynamic properties of Leighton Buzzard sand from laboratory tests.

API. (2008). Recommended Practice for Field Testing Water-based Drilling Fluids.

Ates, U., Bilgin, N., & Copur, H. (2014). Estimating torque, thrust and other design parameters of different type TBMs with some criticism to TBMs used in Turkish tunneling projects. *Tunnelling and Underground Space Technology, 40*, 46-63. doi:10.1016/j.tust.2013.09.004

Ball, R. P. A., Young, D. J., Isaacson, J., Champa, J., & Gause, C. (2009). Research in Soil Conditioning for Epb Tunneling through Difficult Soils. *2009 Rapid Excavation and Tunneling Conference, Proceedings*, 320-333. Retrieved from <Go to ISI>://WOS:000270588000026.

Boukpeti, N., & White, D. J. (2017). Interface shear box tests for assessing axial pipe–soil resistance. *Géotechnique, 67*(1), 18-30. doi:10.1680/jgeot.15.P.112

Butterfield, R., & Andrawes, Z. (1972). On the angles of friction between sand and plane surfaces.

Cui, K., & Lin, W. (2016). Muck Problems in Subway Shield Tunneling in Sandy Cobble Stratum. *Polish Maritime Research, 23*(s1), 175-179. doi:10.1515/pomr-2016-0062

Duarte, M. Á. P. (2007). *Foam as a soil conditioner in tunnelling: physical and mechanical properties of conditioned sands.* (Thesis of Doctor of Philosophy), University of Oxford, ST. Catherine's College.

EFNARC. (2005). Specification and Guidelines for the use of specialist products for Mechanised Tunnelling (TBM) In.

Feligha, M., Hammoud, F., Belachia, M., & Nouaouria, M. S. (2015). Experimental Investigation of Frictional Behavior Between Cohesive Soils and Solid Materials Using Direct Shear Apparatus. *Geotechnical and Geological Engineering, 34*(2), 567-578. doi:10.1007/s10706-015-9966-5

Festa, D. (2015). *On the interaction between a Tunnel Boring Machine and the surrounding soil.*

Gehring, K. H. (1995). DESIGN CRITERIA FOR TBMS WITH RESPECT TO REAL ROCK PRESSURE. *Tunnel Boring Machines*, 43-53.

Giang, P. H. H., Haegeman, W., Impe, P. V., Impe, W. V., & Menge, P. Shear and interface shear strengths of calcareous sand.

Godinez, R., Yu, H., & Mooney, M. Earth Pressure Balance machine cutterhead torque modelling learning from machine data.

Herzog, M. (1985). Die Pressenkrafte bei Schildvortrieb und Rohrvorpressung im Lockergestein. *Baumachine und Bautechnik*, 236-238.

Jancsecz, S. (1991). Definition geotechnischer Parameter für den Einsatz von Schildvortriebsmachinen mit suspensionsgestutzter Ortsbrust.

Japan Society of Civil Engineers, J. (2007). *Standard specifications for tunnelling - 2006: Shield Tunnels*.

Kelessidis, V. C., & Maglione, R. (2008). Yield stress of water–bentonite dispersions. *Colloids and Surfaces A: Physicochemical and Engineering Aspects, 318*(1-3), 217-226. doi:10.1016/j.colsurfa.2007.12.050

Kooistra, A., Verhoef, P. N. W., Broere, W., Ngan-Tillard, D. J. M., & F., V. T. A. (1998). Appraisal of stickyness of natual clays from laboratory tests.

Krause, T. (1987). *Schildvortrieb mit flüssigkeits - und erdgestützter Ortsbrust.* (Ph.D.), Technische Universitat Braunschweig,

Langmaack, L. (2002). Advanced technology of soil conditioning in EPB shield tunnelling.

Littleton, I. (1976). An Experimental Study of the Adhesion Between Clay and Steel.

Lunardi, P., Gatti, M., & Cassani, G. (2011). *The largest TBM-EPB machine in the world, designed to the Apennines. The experience of the Sparvo tunnel*. Paper presented at the 1st International Congress on Tunnels and Underground Structures in South-East Europe, Dubrovnik, Croatia.

Maidl, B., Thewes, M., & Maidl, U. (2013). *Handbook of Tunnel Engineering, vol 1 Structures and Methods*: Ernst & Sohn.

Mori, L., Mooney, M., & Cha, M. (2018). Characterizing the influence of stress on foam conditioned sand for EPB tunneling. *Tunnelling and Underground Space Technology, 71*, 454-465. doi:10.1016/j.tust.2017.09.018

Ngan-Tillard, D. J. M., & Verhoef, P. N. W. The adherence of clay to steel surfaces.

Peila, D., Oggeri, C., & Borio, L. (2009). Using the Slump Test to Assess the Behavior of Conditioned Soil for EPB Tunneling. *Environmental & Engineering Geoscience, 15*(3), 167-174. Retrieved from <Go to ISI>://WOS:000271317400004. doi:DOI 10.2113/gseegeosci.15.3.167

Potyondy, J. G. (1982). Skin friction between various soils and construction materials.

Ramoni, M. (2010). *On the feasibility of TBM drives in squeezing ground and the risk of shield jamming.* ETH Zurich,

Rinne, N. F. (1989). *Evaluation of interface friction coefficients between cohesionless soils and common building materials.*

Schosser, B., Thewes, M., Budach, C., & Zenner, B. (2012). Professional production of bentonite.

Shi, H., Yang, H., Gong, G., & Wang, L. (2011). Determination of the cutterhead torque for EPB shield tunneling machine. *Automation in Construction, 20*(8), 1087-1095. doi:10.1016/j.autcon.2011.04.010

Song, X., Liu, J., & Guo, W. (2010). *A Cutter Head Torque Forecast Model Based on Multivariate Nonlinear Regression for EPB Shield Tunneling*. Paper presented at the 2010 International Conference on Artificial Intelligence and Computational Intelligence.

Spagnoli, G., Feinendegen, M., Ernst, R., & Weh, M. (2012). Manipulations of the sticky clays regarding EPB tunnel driving. *Geotechnical Aspects of Underground Construction in Soft Ground, 7th International Symposium*, 111-118. Retrieved from <Go to ISI>://WOS:000329585400010.

Stafford, J. V., & Tanner, D. W. (1982a). Effect of rate on soil shear strength and soil-metal friction (I. Shear Strength).

Stafford, J. V., & Tanner, D. W. (1982b). Effect of rate on soil shear strength and soil-metal friction (II. Soil-Metal Friction).

Thewes, M. (2007). *TBM tunnelling challenges - redefining the state of the art*. Paper presented at the ITA-AITES WTC, Prague.

Thewes, M., Budach, C., & Bezuijen, A. (2012). Foam conditioning in EPB tunnelling. In *Geotechnical Aspects of Underground Construction in Soft Ground* (pp. 127-135).

Tiwari, B., & Al-Adhadh, A. R. (2013). Influence of Relative Density on Static Soil–Structure Frictional Resistance of Dry and Saturated Sand. *Geotechnical and Geological Engineering, 32*(2), 411-427. doi:10.1007/s10706-013-9723-6

Tokarz, S. (2014). *Evaluation of the sticking potential of clays to a tunnell boring machine cutterhead.*

Tomlison, M. J. (1969). *Foundation Design and Construction*. London.

Tsubakihara, Y., Kishida, H., & Nishiyama, T. (1993). Friction between cohesive soils and steel.

Vangla, P., & Latha, G. M. (2015). Influence of Particle Size on the Friction and Interfacial Shear Strength of Sands of Similar Morphology. *International Journal of Geosynthetics and Ground Engineering, 1*(1). doi:10.1007/s40891-014-0008-9

Y. Peron, J., & Marcheselli, P. (1994). Construction of the 'Passante Ferroviario' link in Milan, Italy, lots 3P, 5P and 6P: excavation by large earth pressure balanced shield with chemical foam injection. In (pp. 679-707).

Yusu, Y. D., Z. (1990). Investigation of the relationship between soil-metal friction and sliding speed. *Journal of Terramechanics, 27*, 283-290.

Zhang, Q., Qu, C., Cai, Z., Kang, Y., & Huang, T. (2014). Modeling of the thrust and torque acting on shield machines during tunneling. *Automation in Construction, 40*, 60-67. doi:10.1016/j.autcon.2013.12.008

Zhou, X.-P., & Zhai, S.-F. (2018). Estimation of the cutterhead torque for earth pressure balance TBM under mixed-face conditions. *Tunnelling and Underground Space Technology, 74*, 217-229. doi:10.1016/j.tust.2018.01.025

Part 5: Appendices

A. Soil A Classification Tests

I. Density (Pycnometer):

Run	Volume [cc]	Density [g/cc]
1	13.7251	2.6521
2	13.7199	2.6531
3	13.7564	2.6460
4	13.7325	2.6507
5	13.7707	2.6433
6	13.7817	2.6412
7	13.8143	2.6350
8	13.8031	2.6371
9	13.8137	2.6351
10	13.8387	2.6303
Sample Mass:	36.40 g	
Avg. Density:	**2.6342 g/cc**	

II. Plastic Limit:

Test n°: 1
Date: 16/01/19

Sample n°	Tare [g]	Wet Clay & Tare [g]	Dry Clay & Tare [g]	*PL* [%]	PL_{avg} [%]
1	46.30	54.39	52.49	30.64	**30.71**
2	49.35	55.85	54.32	30.77	

Test n°: 2
Date: 17/01/19

Sample n°	Tare [g]	Wet Clay & Tare [g]	Dry Clay & Tare [g]	*PL* [%]	PL_{avg} [%]
1	46.30	53.87	52.12	30.00	**30.24**
2	49.35	56.10	54.52	30.48	

Test n°: 3
Date: 22/01/19

Sample n°	Tare [g]	Wet Clay & Tare [g]	Dry Clay & Tare [g]	*PL* [%]	PL_{avg} [%]
1	43.32	50.05	48.50	29.90	**30.02**
2	43.81	49.24	47.98	30.13	

III. Liquid Limit:

Test n°: 1
Date: 17/01/19
Cone: 30°, 80g

Sample n°	Tare [g]	Wet Clay & Tare [g]	Dry Clay & Tare [g]	Water Content [%]	Cone Penetration [mm]
1	46.66	79.04	67.05	58.80	34.87
2	46.00	83.11	69.97	54.82	26.06
3	44.82	62.81	56.64	52.20	23.81
4	43.79	78.21	67.38	45.91	16.68
5	43.70	72.77	62.70	53.00	16.00

Liquid Limit: **48.98 %**

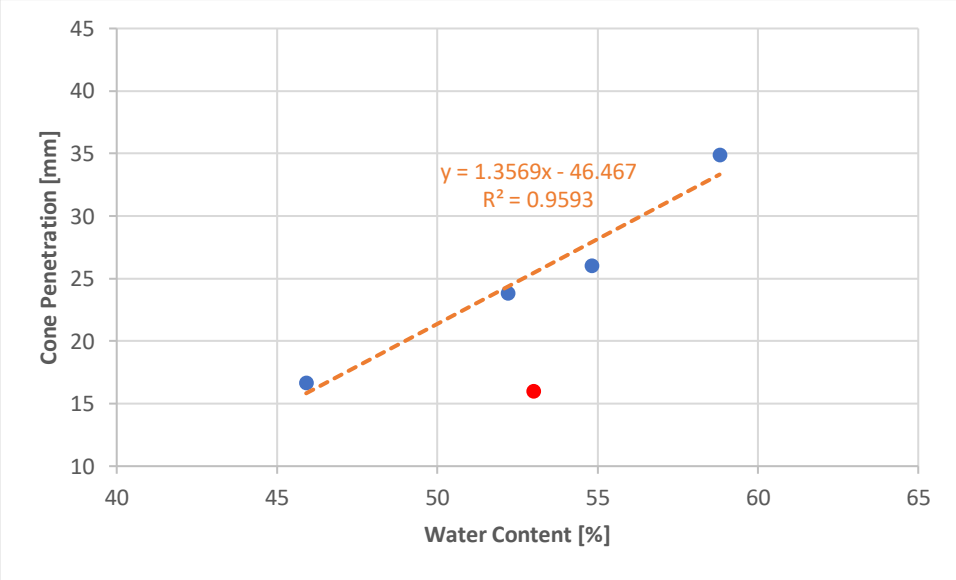

Figure 0.1: Fall cone test 1.

Test n°: 2
Date: 18/01/19
Cone: 30°, 80g

Sample n°	Tare [g]	Wet Clay & Tare [g]	Dry Clay & Tare [g]	Water Content [%]	Cone Penetration [mm]
1	49.35	72.60	63.91	59.68	35.11
2	46.29	65.04	58.40	54.83	25.19
3	47.44	67.24	60.36	53.25	21.66
4	44.99	70.03	61.55	51.21	20.07
5	45.75	67.80	60.62	48.29	17.14

Liquid Limit: **51.04 %**

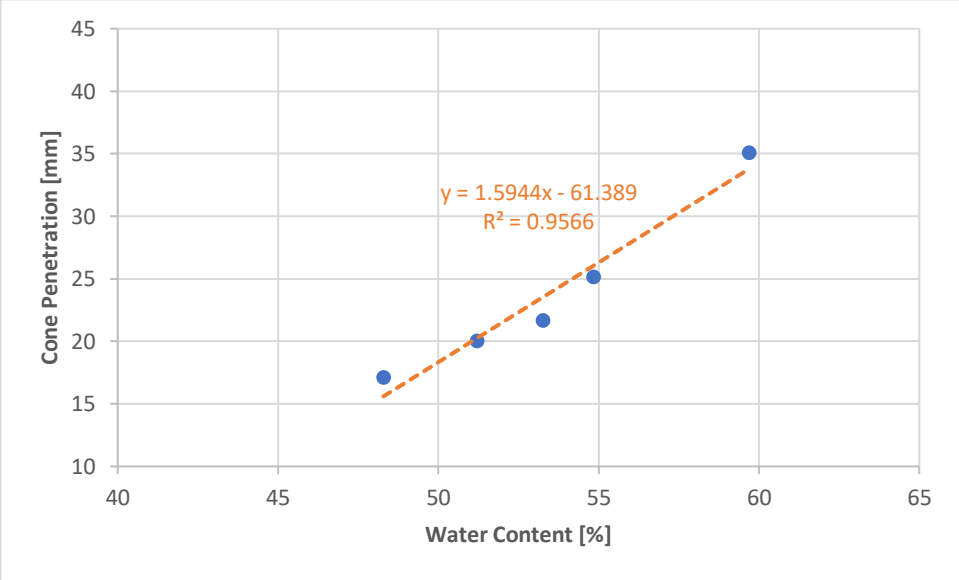

Figure 0.2: Fall cone test 2.

Test n°: 3
Date: 22/01/19
Cone: 30°, 80g

Sample n°	Tare [g]	Wet Clay & Tare [g]	Dry Clay & Tare [g]	Water Content [%]	Cone Penetration [mm]
1	44.27	63.08	56.16	58.20	32.94
2	49.25	78.22	68.11	53.61	28.12
3	45.77	68.02	60.72	48.83	18.55
4	48.68	79.87	69.92	46.85	15.95
5	42.80	84.65	71.76	44.51	13.68
Liquid Limit:	**49.16 %**				

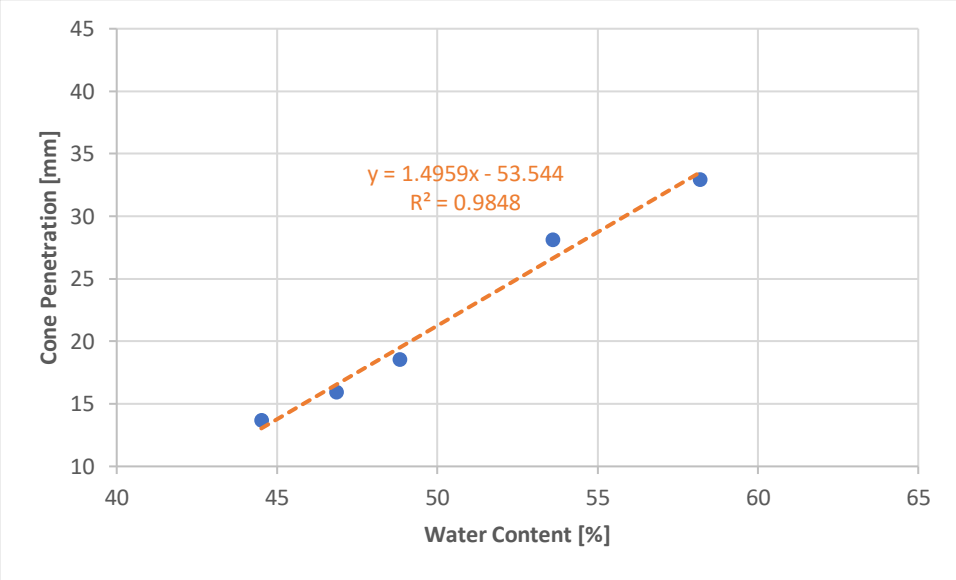

Figure 0.3: Fall cone test 3.

IV. Internal Shear Strength

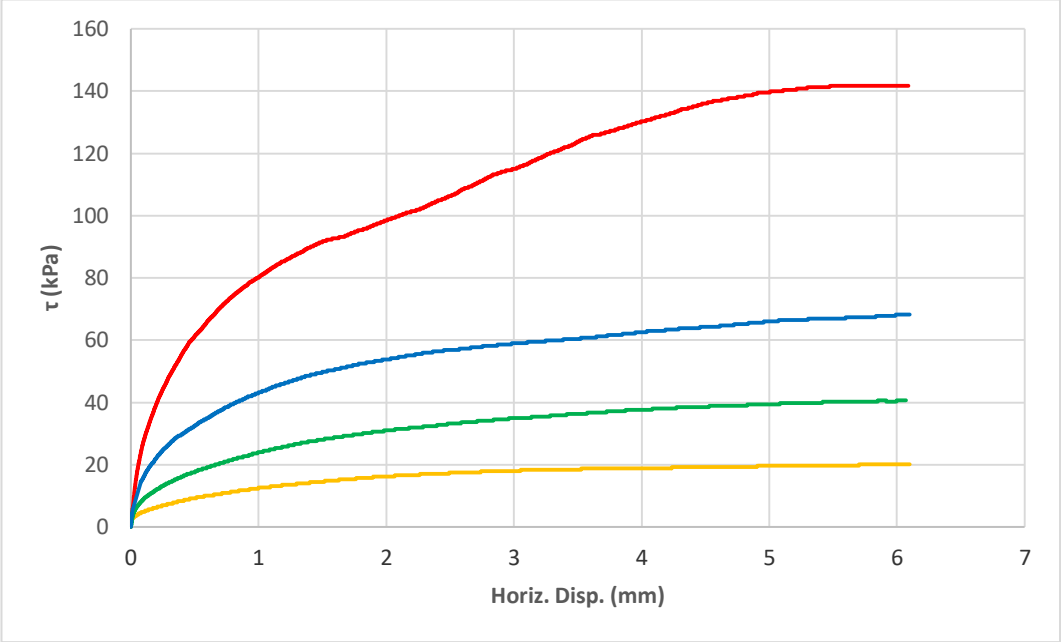

Figure 0.4: Plots from internal shear tests of soil A (water-saturated), conducted at normal loads of 50.0, 99.7, 193.4 and 400.7 kPa. Shear resistance is shown function of horizontal displacement.

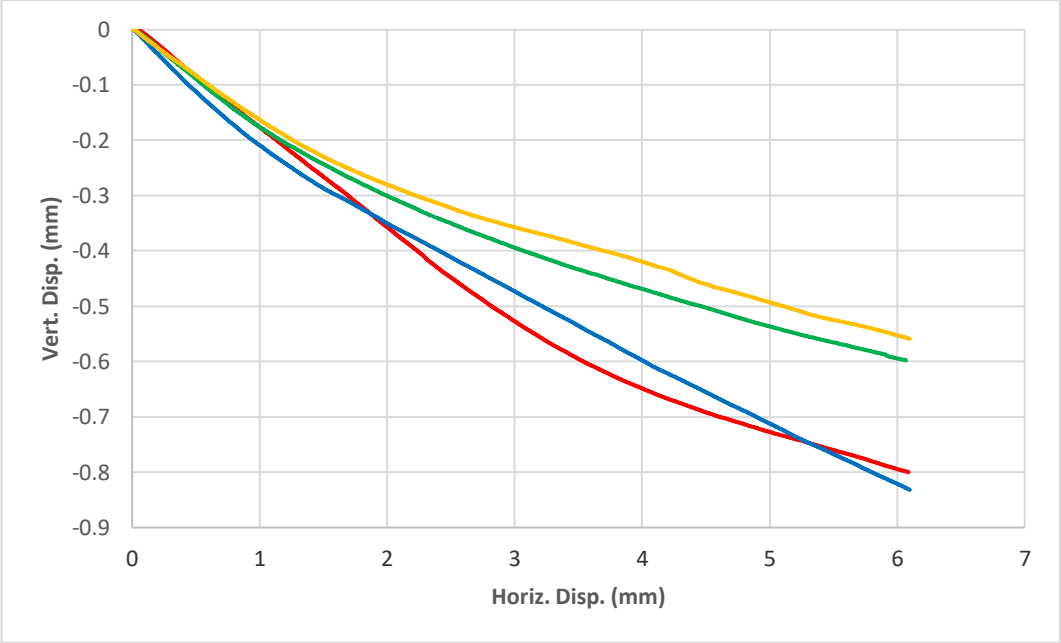

Figure 0.5: Plots from internal shear tests of soil A (water-saturated), conducted at normal loads of 50.0, 99.7, 193.4 and 400.7 kPa. Shear resistance is shown function of vertical displacement.

B. Soil B Classification Tests

I. Density (Pycnometer):

Run	Volume [cc]	Density [g/cc]
1	16.8491	2.6470
2	16.9316	2.6341
3	16.9762	2.6272
4	16.9815	2.6264
5	17.0044	2.6228
6	16.9933	2.6241
7	17.0203	2.6204
8	17.0070	2.6225
9	16.9992	2.6237
10	17.0131	2.6215
Sample Mass:	44.60 g	
Avg. Density:	**2.6225 g/cc**	

II. Internal Shear Strength

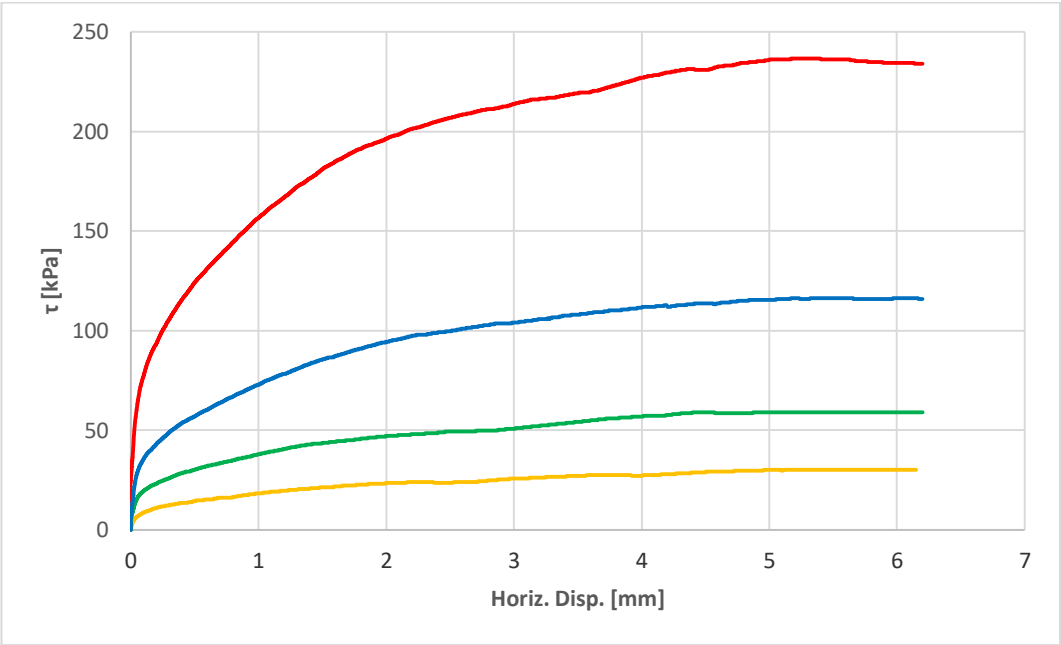

Figure 0.6: Plots from internal shear tests of soil B (water-saturated), conducted at normal loads of 50.0, 99.7, 193.4 and 400.7 kPa. Shear resistance is shown function of horizontal displacement.

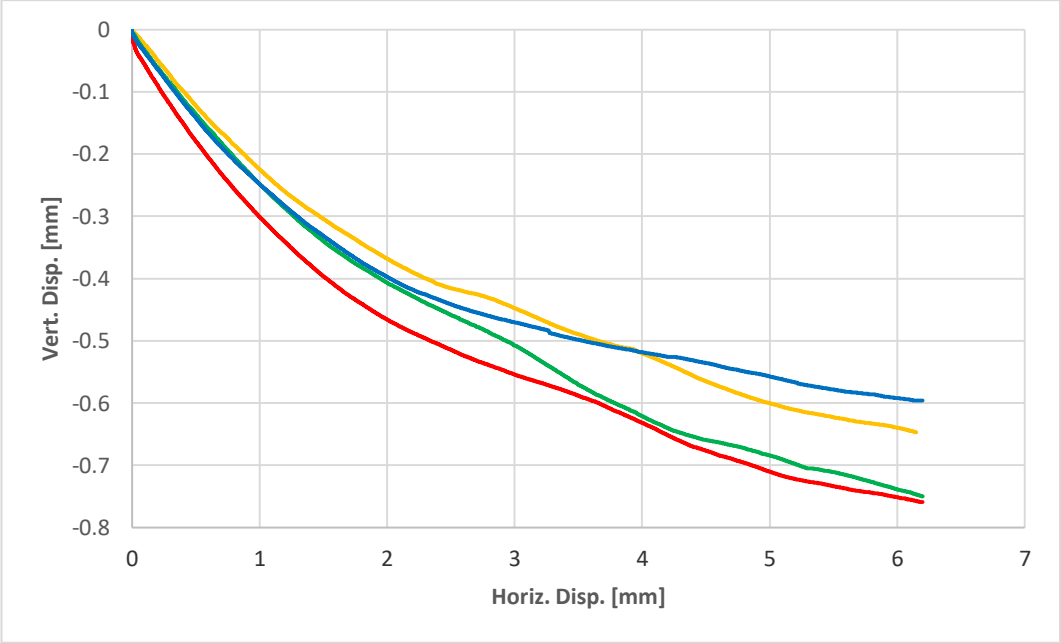

Figure 0.7: Plots from internal shear tests of soil B (water-saturated), conducted at normal loads of 50.0, 99.7, 193.4 and 400.7 kPa. Shear resistance is shown function of vertical displacement.

C. Soil C Classification Tests

I. Density (Pycnometer):

Run	Volume [cc]	Density [g/cc]
1	24.6915	2.6361
2	24.6322	2.6425
3	24.5983	2.6461
4	24.6110	2.6448
5	24.6328	2.6424
6	24.6119	2.6447
7	24.6251	2.6432
8	24.6301	2.6427
9	24.6497	2.6406
10	24.6414	2.6415
Sample Mass:	65.09 g	
Avg. Density:	**2.6416 g/cc**	

II. Max/Min Void Ratio and Density

Test Configuration: Dense
Test n°: 1
Date: 24/01/19

Sample n°	Sample mass [g]	Cylinder Volume [cm^3]	ρ_{max} [g/cm^3]	$\rho_{max,avg}$ (g/cm^3)	e_{min} [-]	$e_{min,avg}$ [-]
1	205.19		1.826		0.446	
2	208.73		1.858		0.422	
3	205.34	112.35	1.828	1.840	0.445	0.436
4	208.03		1.852		0.427	
5	206.11		1.835		0.440	

Test Configuration: Loose
Test n°: 2
Date: 24/01/19

Sample n°	Sample mass [g]	Cylinder Volume [cm^3]	ρ_{min} [g/cm^3]	$\rho_{min,avg}$ [g/cm^3]	e_{max} [-]	$e_{max,avg}$ [-]
1	181.75		1.618		0.633	
2	180.90		1.610		0.641	
3	183.41	112.345	1.633	1.622	0.618	0.629
4	181.97		1.620		0.631	
5	182.84		1.627		0.623	

Test Configuration: Dense
Test n°: 3
Date: 25/01/19

Sample n°	Sample mass [g]	Cylinder Volume [cm^3]	ρ_{max} [g/cm^3]	$\rho_{max,avg}$ [g/cm^3]	e_{min} [-]	$e_{min,avg}$ [-]
1	212.13		1.888		0.399	
2	212.17		1.889		0.399	
3	210.14	112.345	1.870	1.881	0.412	0.404
4	210.69		1.875		0.409	
5	211.64		1.884		0.402	

Test Configuration: Loose
Test n°: 4
Date: 25/01/19

Sample n°	Sample mass [g]	Cylinder Volume [cm^3]	ρ_{min} [g/cm^3]	$\rho_{min,avg}$ [g/cm^3]	e_{max} [-]	$e_{max,avg}$ [-]
1	182.25		1.622		0.628	
2	180.42		1.606		0.645	
3	180.74	112.345	1.609	1.617	0.642	0.633
4	182.67		1.626		0.625	
5	182.44		1.624		0.627	

Test Configuration: Dense
Test n°: 5
Date: 28/01/19

Sample n°	Sample mass [g]	Cylinder Volume [cm^3]	ρ_{max} [g/cm^3]	$\rho_{max,avg}$ [g/cm^3]	e_{min} [-]	$e_{min,avg}$ [-]
1	211.15		1.879		0.405	
2	213.55		1.901		0.390	
3	212.74	112.345	1.894	1.891	0.395	0.397
4	212.14		1.888		0.399	
5	212.52		1.892		0.396	

Test Configuration: Loose
Test n°: 6
Date: 28/01/19

Sample n°	Sample mass [g]	Cylinder Volume [cm^3]	ρ_{min} [g/cm^3]	$\rho_{min,avg}$ [g/cm^3]	e_{max} [-]	$e_{max,avg}$ [-]
1	185.30		1.649		0.602	
2	184.70		1.644		0.607	
3	184.16	112.345	1.639	1.641	0.611	0.610
4	184.67		1.644		0.607	
5	182.92		1.628		0.622	

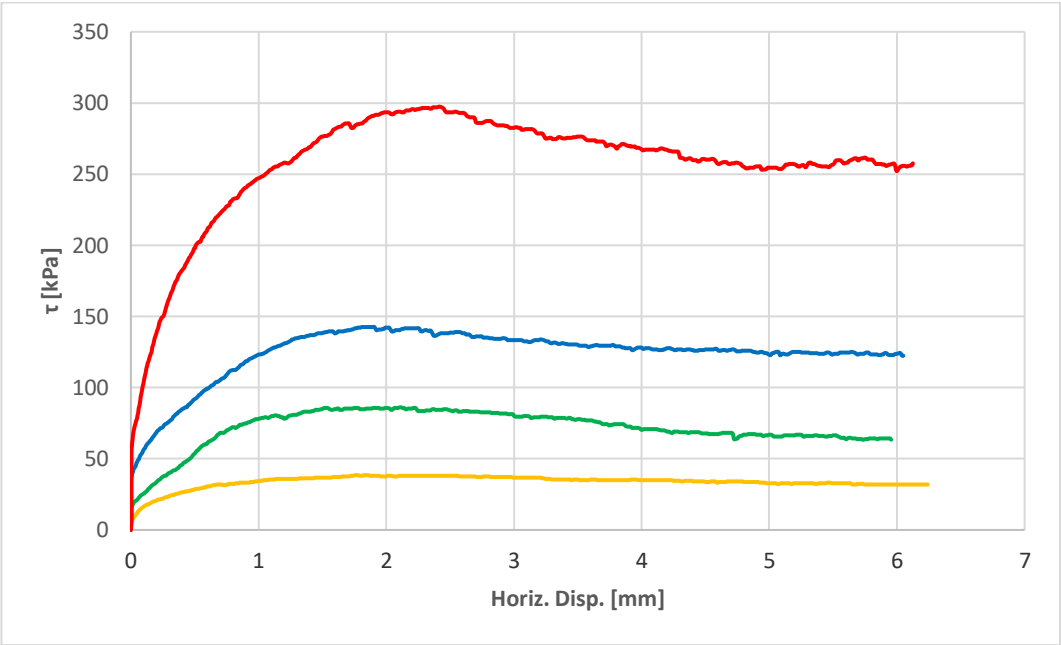

Figure 0.8: Plots from internal shear tests of soil C (water-saturated), conducted at normal loads of 50.0, 99.7, 193.4 and 400.7 kPa. Shear resistance is shown function of horizontal displacement.

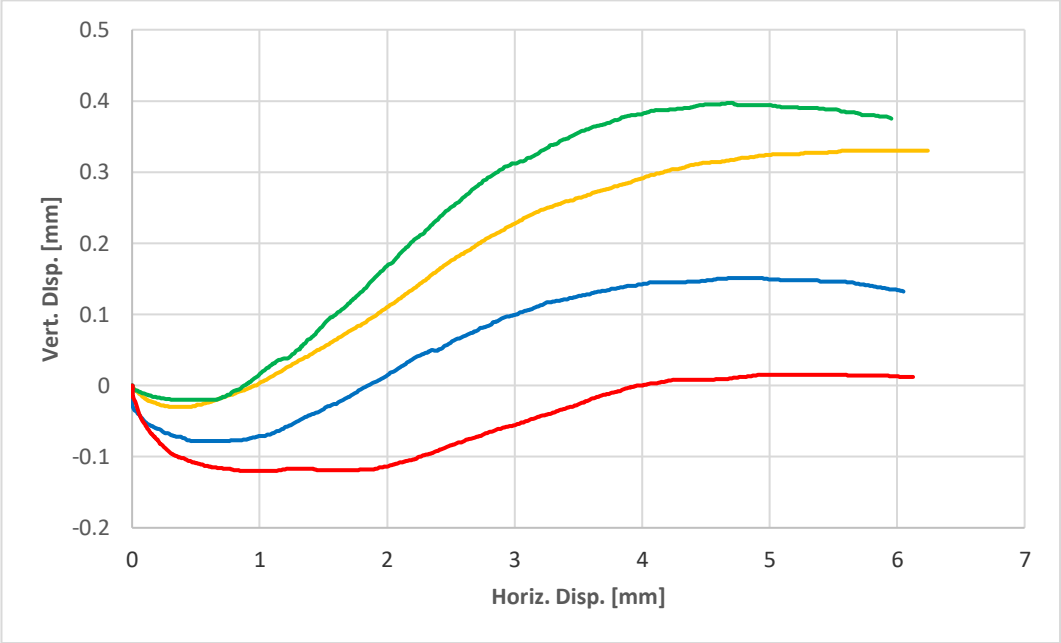

Figure 0.9: Plots from internal shear tests of soil C (water-saturated), conducted at normal loads of 50.0, 99.7, 193.4 and 400.7 kPa. Shear resistance is shown function of vertical displacement.

D. Surface Roughness Measurements

Date: 17/05/19

Reading n°	Average Surface Roughness, R_a [μm]
1	3.09
2	2.92
3	3.55
4	2.06
5	3.05
6	3.95
7	3.45
8	2.88
	Avg. R_a = 3.12 μm

Figure 0.10 below shows where each of the 8 roughness readings is taken on the metal plate surface:

Figure 0.10: Metal plate from TBM cutterhead.

Figure 0.11: Results of roughness measurement tests. R_a: arithmetical mean height of surface asperities; R_y/R_z: maximum height/width of the surface asperities; R_q: root mean square deviation of the surface asperities.

E. Interface Shear Tests, soil A

I. Water-saturated

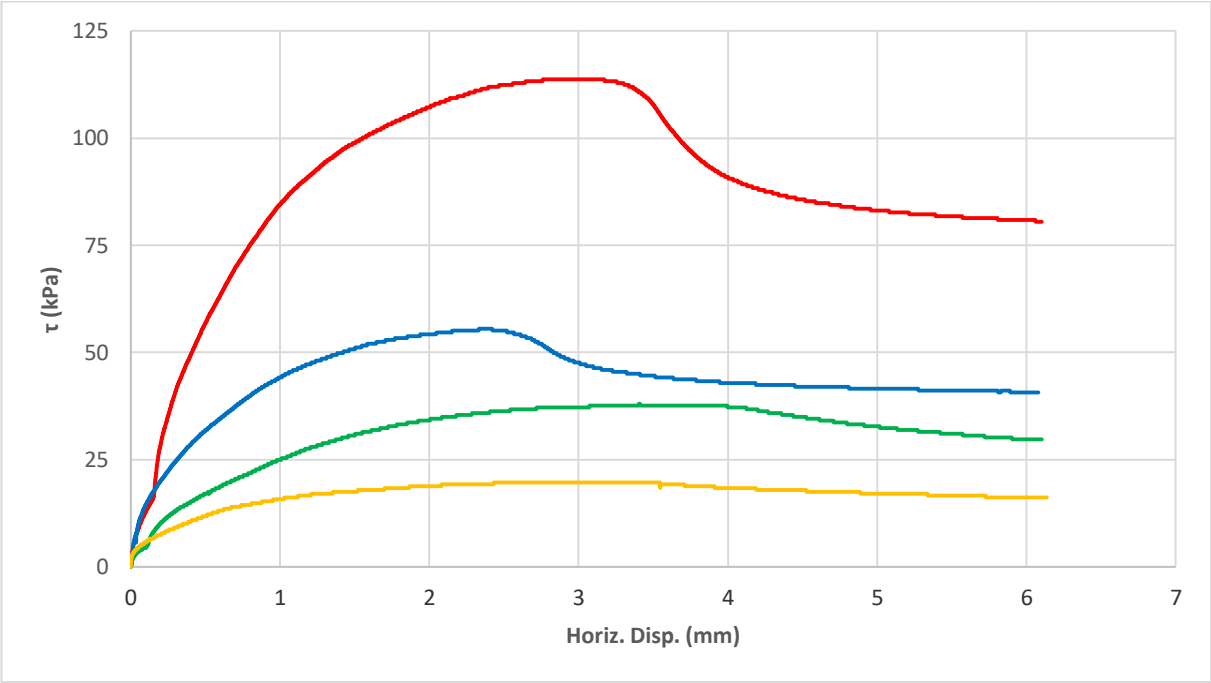

Figure 0.12: Plots from interface shear tests of soil A (water-saturated), conducted at normal loads of 50.0, 99.7, 193.4 and 400.7 kPa. Shear resistance is shown function of horizontal displacement.

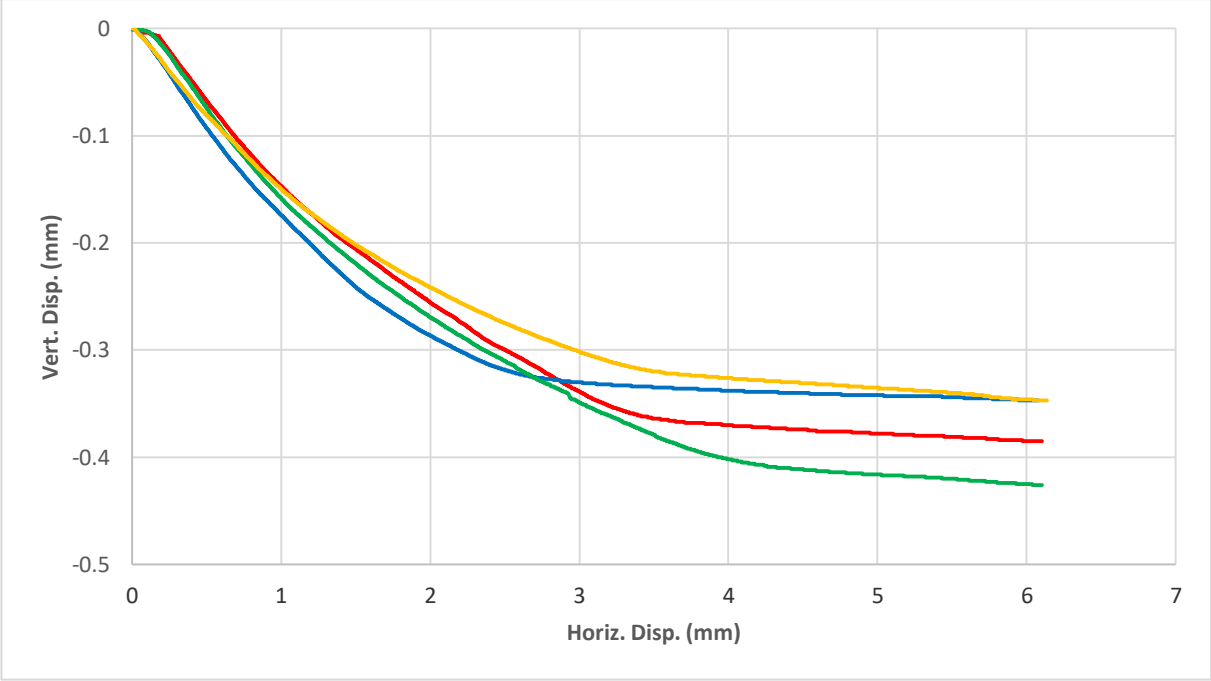

Figure 0.13: Plots from interface shear tests of soil A (water-saturated), conducted at normal loads of 50.0, 99.7, 193.4 and 400.7 kPa. Vertical displacement is shown function of horizontal displacement (starting point is at end of consolidation).

Table 0.1: Results of interface shear tests of soil A (water-saturated).

σ [kPa]	CI_f [-]	δ_p[°]; μ_p[-]	$\delta_{p,avg}$[°]; $\mu_{p,avg}$ [-]	δ_r [°]; μ_r [-]	$\delta_{r,avg}$ [°]; $\mu_{r,avg}$ [-]
50.0	0.386	20.788; 0.380	18.114; 0.328	17.932; 0.324	14.584; 0.261
99.7	0.482	20.181; 0.368		16.601; 0.298	
193.4	0.541	15.705; 0.281		12.057; 0.214	
400.7	0.568	15.783; 0.283		11.745; 0.208	

II. Bentonite-conditioned

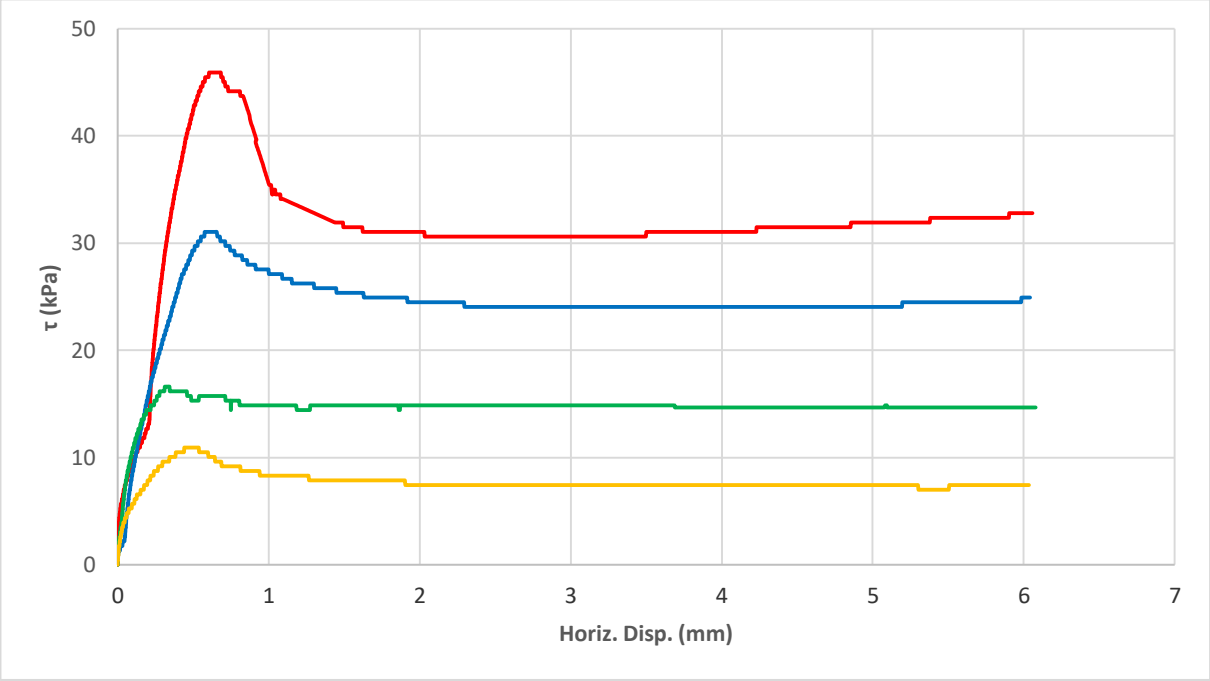

Figure 0.14: Plots from interface shear tests of soil A (bentonite-conditioned), conducted at normal loads of 50.0, 99.7, 193.4 and 327.3 kPa. Shear resistance is shown function of horizontal displacement.

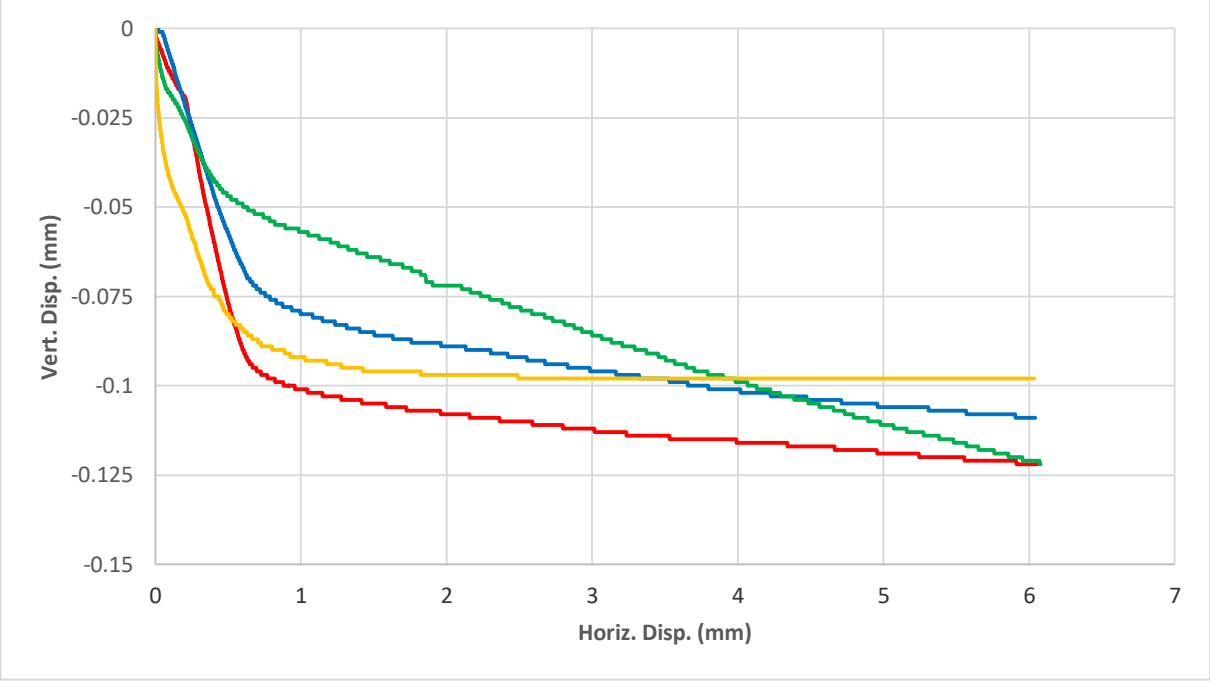

Figure 0.15: Plots from interface shear tests of soil A (bentonite-conditioned), conducted at normal loads of 50.0, 99.7, 193.4 and 400.7 kPa. Vertical displacement is shown function of horizontal displacement.

Table 0.2: Results of interface shear tests of soil A (bentonite-conditioned).

σ [kPa]	CI_f [-]	δ_p[°]; μ_p[-]	$\delta_{p,avg}$[°]; $\mu_{p,avg}$ [-]	δ_r [°]; μ_r [-]	$\delta_{r,avg}$ [°]; $\mu_{r,avg}$ [-]
50.0	0.394	11.881; 0.210	9.162; 0.161	8.457; 0.149	7.473; 0.131
99.7	0.489	8.386; 0.147		8.368; 0.147	
193.4	0.543	8.685; 0.153		7.345; 0.129	
327.3	0.571	7.694; 0.135		5.723; 0.100	

III. Foam-conditioned

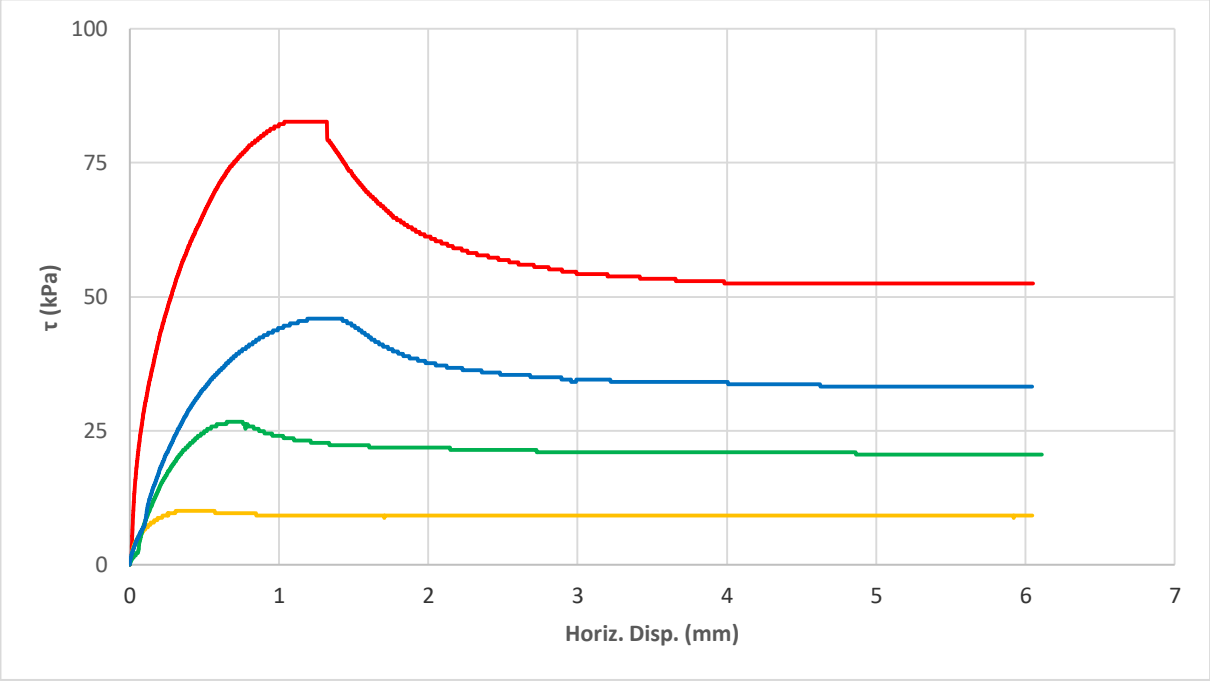

Figure 0.16: Plots from interface shear tests of soil A (foam-conditioned), conducted at normal loads of 50.0, 99.7, 193.4 and 327.3 kPa. Shear resistance is shown function of horizontal displacement.

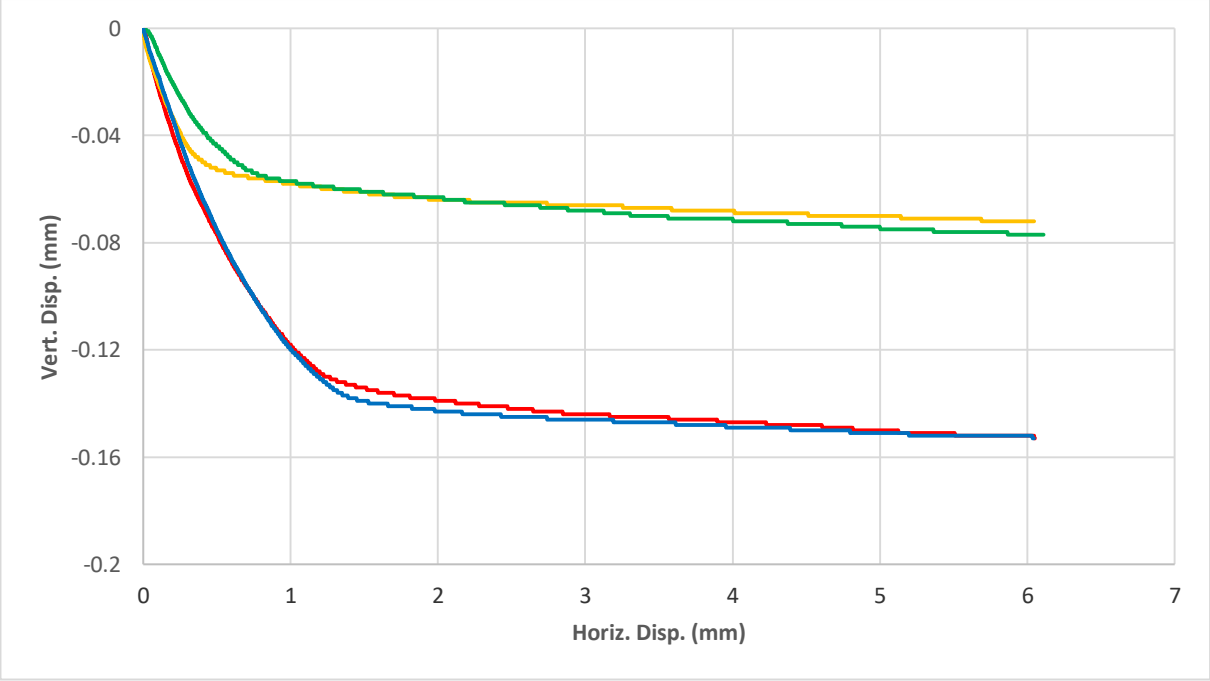

Figure 0.17: Plots from interface shear tests of soil A (foam-conditioned), conducted at normal loads of 50.0, 99.7, 193.4 and 400.7 kPa. Vertical displacement is shown function of horizontal displacement.

Table 0.3: Results of interface shear tests of soil A (foam-conditioned).

σ [kPa]	CI_f [-]	δ_p[°]; μ_p[-]	$\delta_{p,avg}$[°]; $\mu_{p,avg}$ [-]	δ_r [°]; μ_r [-]	$\delta_{r,avg}$ [°]; $\mu_{r,avg}$ [-]
50.0	0.398	10.479; 0.185	12.971; 0.231	10.408; 0.184	10.229; 0.181
99.7	0.501	14.300; 0.255		11.644; 0.206	
193.4	0.546	12.918; 0.229		9.753; 0.172	
327.3	0.586	14.186; 0.253		9.110; 0.160	

F. Interface Shear Tests, soil B

I. Water-saturated

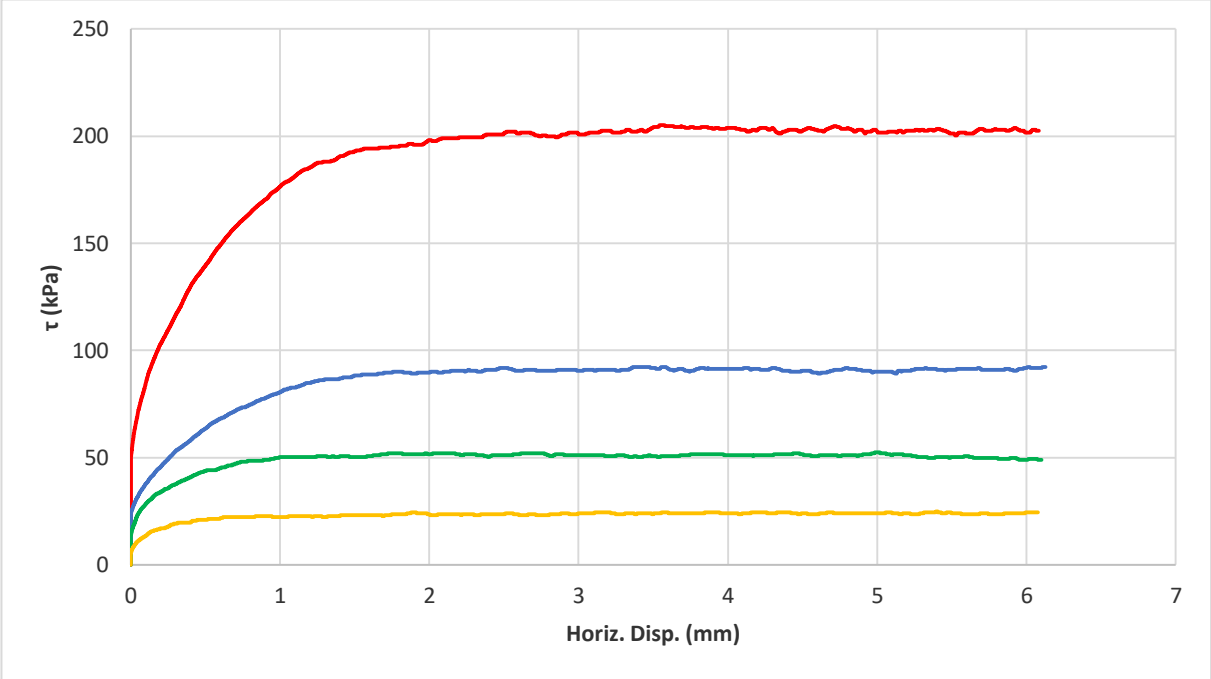

Figure 0.18: Plots from interface shear tests of soil B (water-saturated), conducted at normal loads of 50.0, 99.7, 193.4 and 400.7 kPa. Shear resistance is shown function of horizontal displacement.

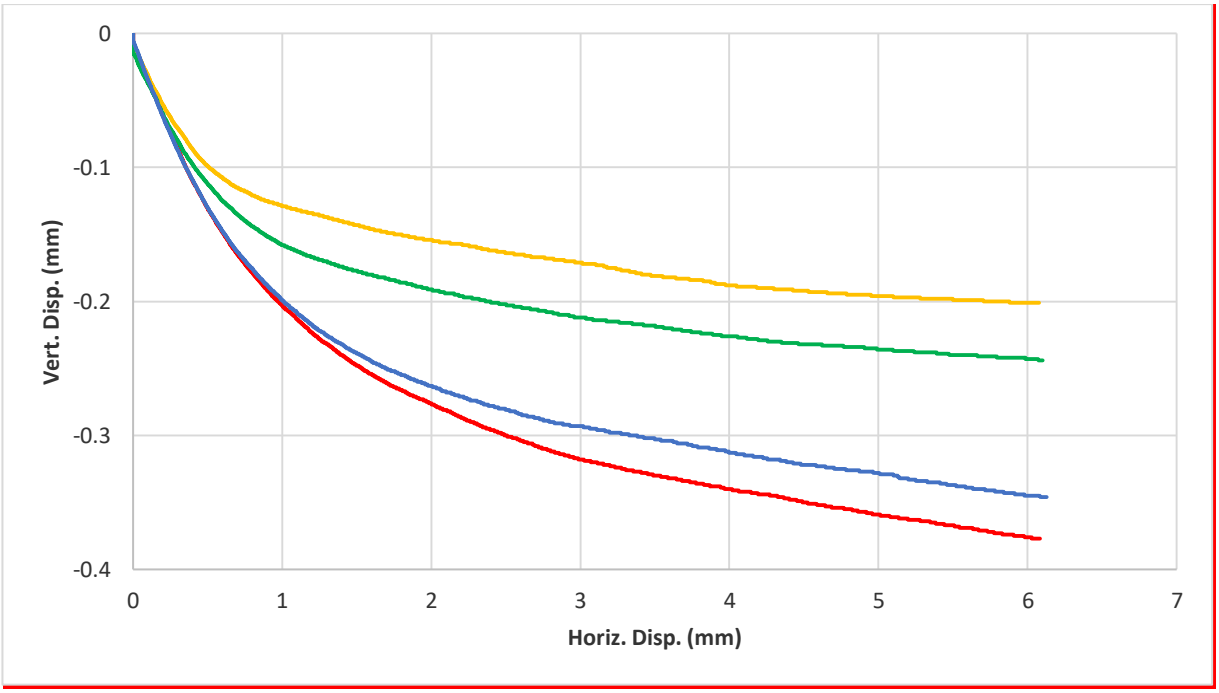

Figure 0.19: Plots from interface shear tests of soil B (water-saturated), conducted at normal loads of 50.0, 99.7, 193.4 and 400.7 kPa. Vertical displacement is shown function of horizontal displacement.

Table 0.4: Results of interface shear tests of soil B (water-saturated).

σ [kPa]	$\rho_{dry,0}$; $\rho_{sat,0}$ [g/cm^3]	$\rho_{dry,f}$; $\rho_{sat,f}$ [g/cm^3]	δ [°]; μ [-]	δ_{avg} [°]; μ_{avg} [-]
50.0	1.904; 2.178	1.926; 2.192	25.412; 0.475	26.015; 0.488
99.7	1.983; 2.227	2.011; 2.244	27.011; 0.510	
193.4	1.957; 2.228	1.985; 2.224	25.055; 0.467	
400.7	1.949; 2.206	1.993; 2.233	26.581; 0.500	

II. Bentonite-conditioned

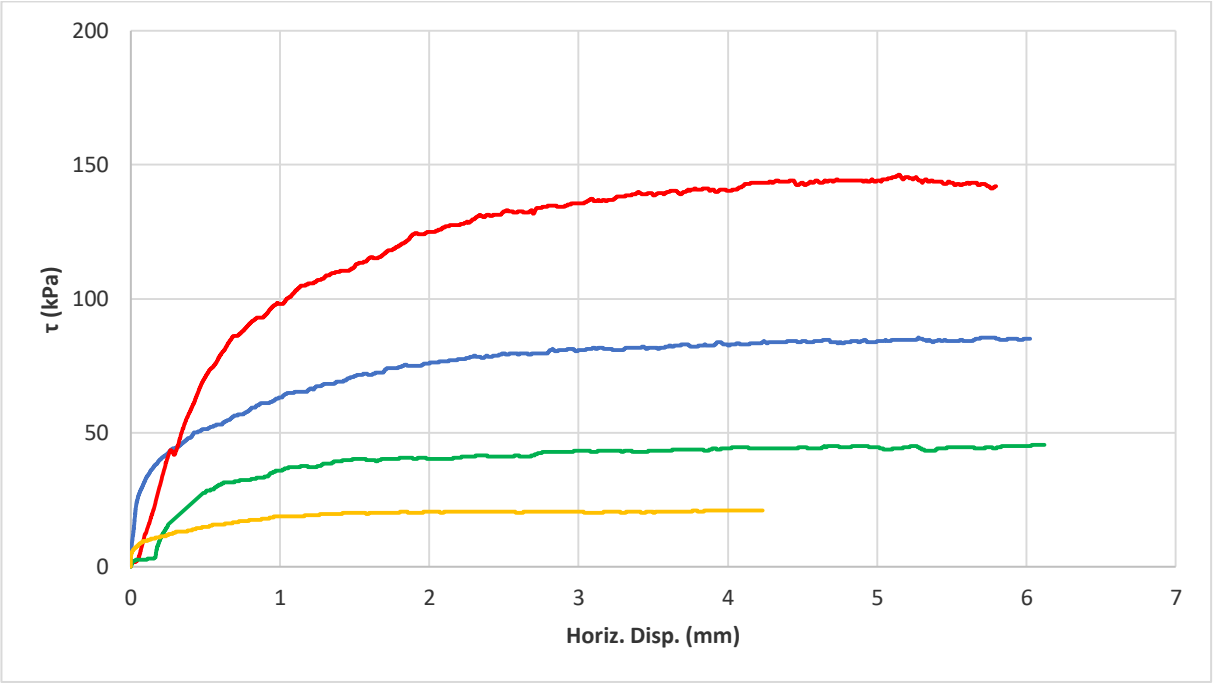

Figure 0.20: Plots from interface shear tests of soil B (bentonite-conditioned), conducted at normal loads of 50.0, 99.7, 193.4 and 327.3 kPa. Shear resistance is shown function of horizontal displacement.

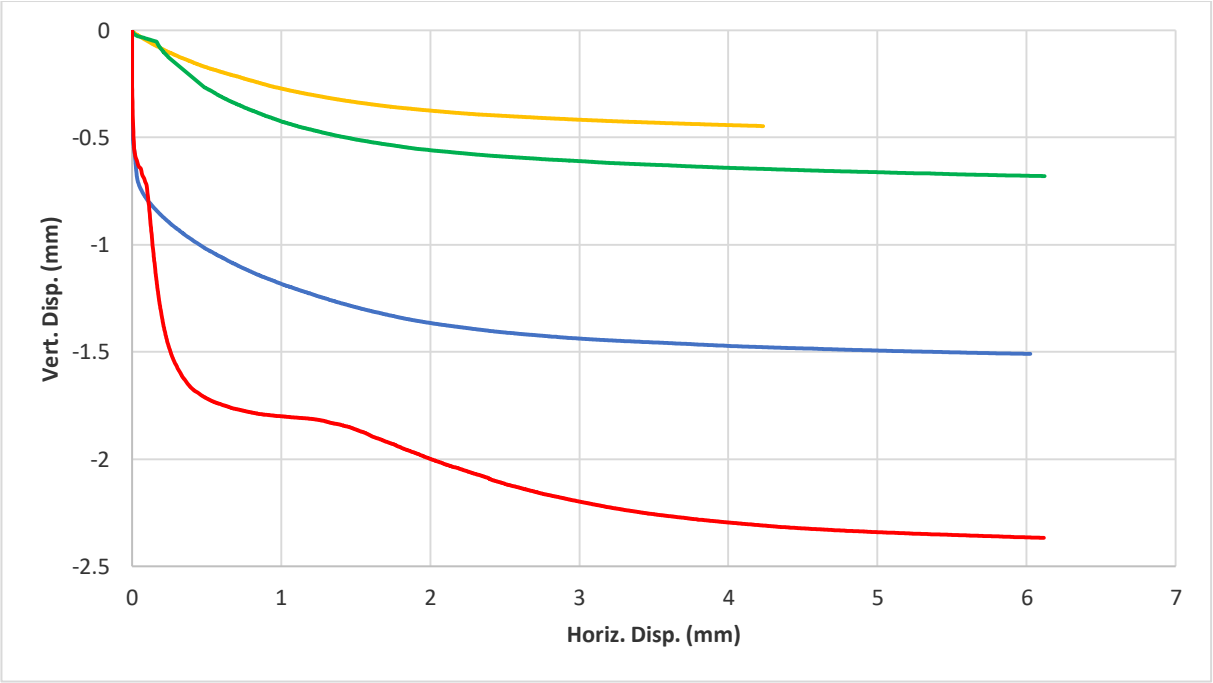

Figure 0.21: Plots from interface shear tests of soil B (bentonite-conditioned), conducted at normal loads of 50.0, 99.7, 193.4 and 327.3 kPa. Vertical displacement is shown function of horizontal displacement.

Table 0.5: Results of interface shear tests of soil B (bentonite-conditioned).

σ [kPa]	$\rho_{dry,0}$; $\rho_{sat,0}$ [g/cm^3]	$\rho_{dry,f}$; $\rho_{sat,f}$ [g/cm^3]	δ [°]; μ [-]	δ_{avg} [°]; μ_{avg} [-]
50.0	1.615; 1.961	1.806; 2.183	22.435; 0.413	23.130; 0.427
99.7	1.674; 2.033	1.837; 2.246	23.839; 0.442	
193.4	1.651; 2.005	1.852; 2.250	23.209; 0.429	
327.3	1.670; 2.028	1.887; 2.293	23.036; 0.425	

III. Foam-conditioned

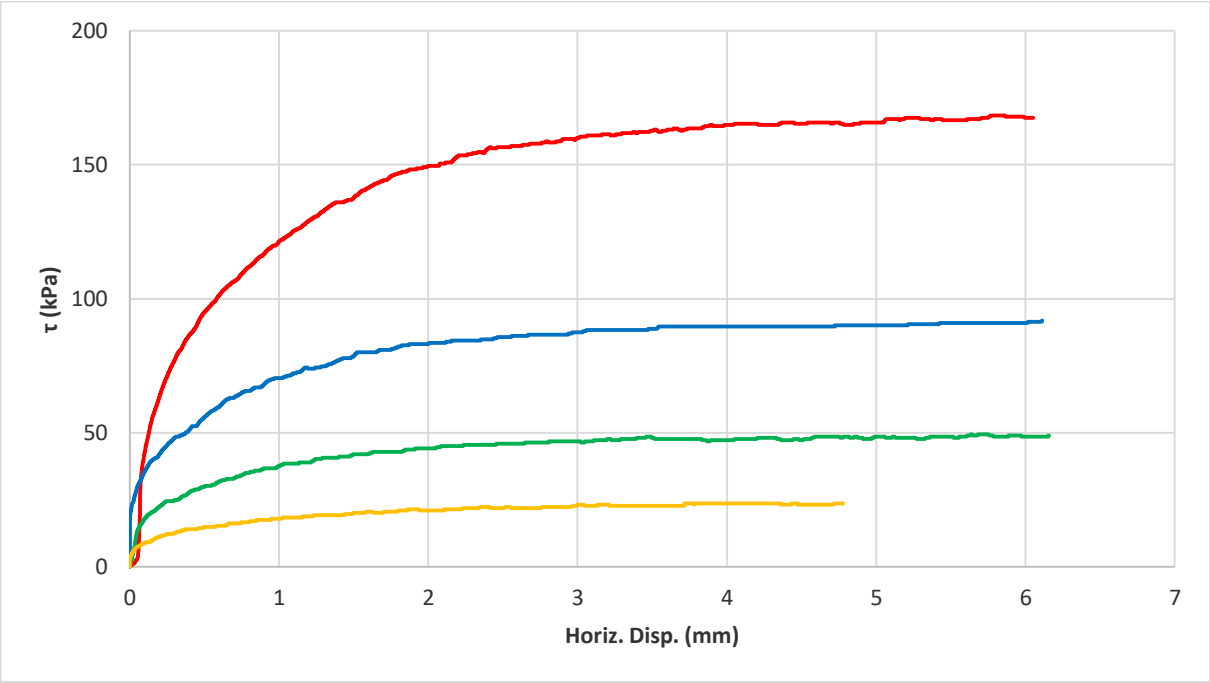

Figure 0.22: Plots from interface shear tests of soil B (foam-conditioned), conducted at normal loads of 50.0, 99.7, 193.4 and 327.3 kPa. Shear resistance is shown function of horizontal displacement.

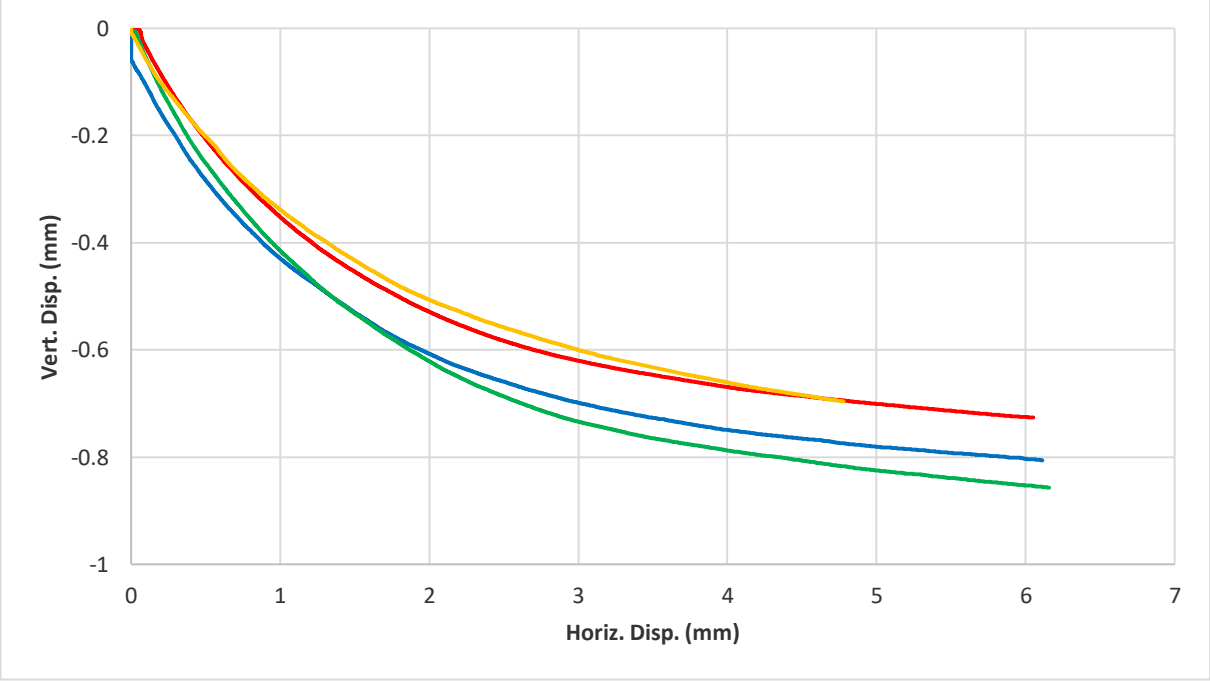

Figure 0.23: Plots from interface shear tests of soil B (foam-conditioned), conducted at normal loads of 50.0, 99.7, 193.4 and 327.3 kPa. Vertical displacement is shown function of horizontal displacement.

Table 0.6: Results of interface shear tests of soil B (foam-conditioned).

σ [kPa]	$\rho_{dry,0}$; $\rho_{sat,0}$ [g/cm^3]	$\rho_{dry,f}$; $\rho_{sat,f}$ [g/cm^3]	δ [°]; μ [-]	δ_{avg} [°]; μ_{avg} [-]
50.0	1.450; 1.692	1.519; 1.772	24.391; 0.453	25.245; 0.472
99.7	1.473; 1.721	1.567; 1.830	25.484; 0.477	
193.4	1.528; 1.783	1.617; 1.887	24.598; 0.458	
327.3	1.596; 1.860	1.680; 1.958	26.508; 0.499	

G. Interface Shear Tests, soil C

I. Water-saturated

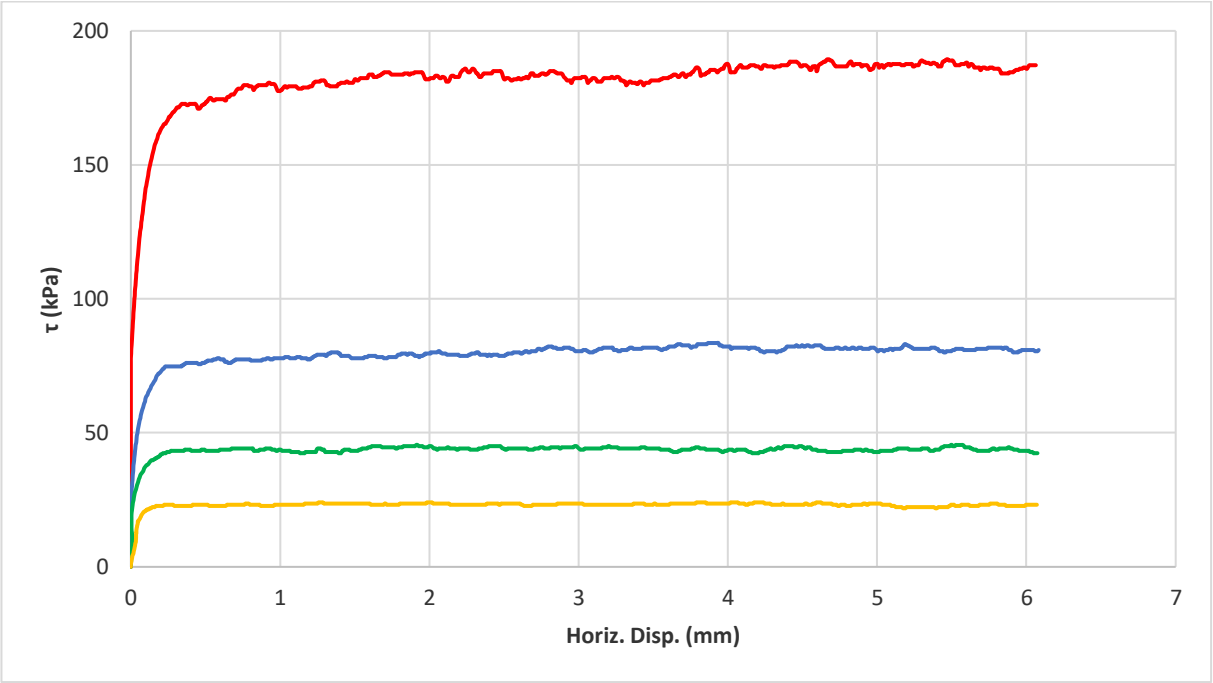

Figure 0.24: Plots from interface shear tests of soil C (water-saturated), conducted at normal loads of 50.0, 99.7, 193.4 and 400.7 kPa. Shear resistance is shown function of horizontal displacement.

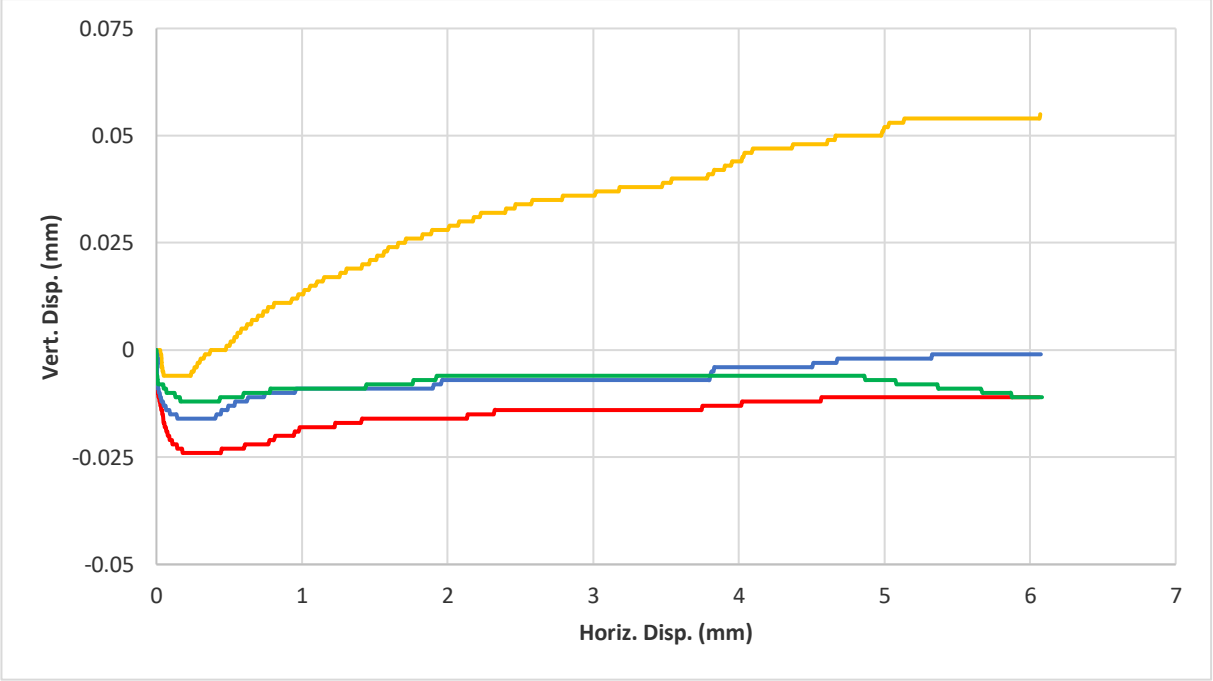

Figure 0.25: Plots from interface shear tests of soil C (water-saturated), conducted at normal loads of 50.0, 99.7, 193.4 and 400.7 kPa. Vertical displacement is shown function of horizontal displacement.

Table 0.7: Results of interface shear tests of soil C (water-saturated).

σ [kPa]	$\rho_{dry,0}$; $\rho_{sat,0}$ [g/cm^3]	$\rho_{dry,f}$; $\rho_{sat,f}$ [g/cm^3]	δ [°]; μ [-]	δ_{avg} [°]; μ_{avg} [-]
50.0	1.846; 2.141	1.840; 2.144	24.933; 0.465	23.946; 0.444
99.7	1.795; 2.115	1.795; 2.115	23.744; 0.440	
193.4	1.814; 2.128	1.816; 2.128	22.530; 0.415	
400.7	1.784; 2.109	1.785; 2.109	24.576; 0.457	

II. Bentonite-conditioned (high bentonite/soil ratio)

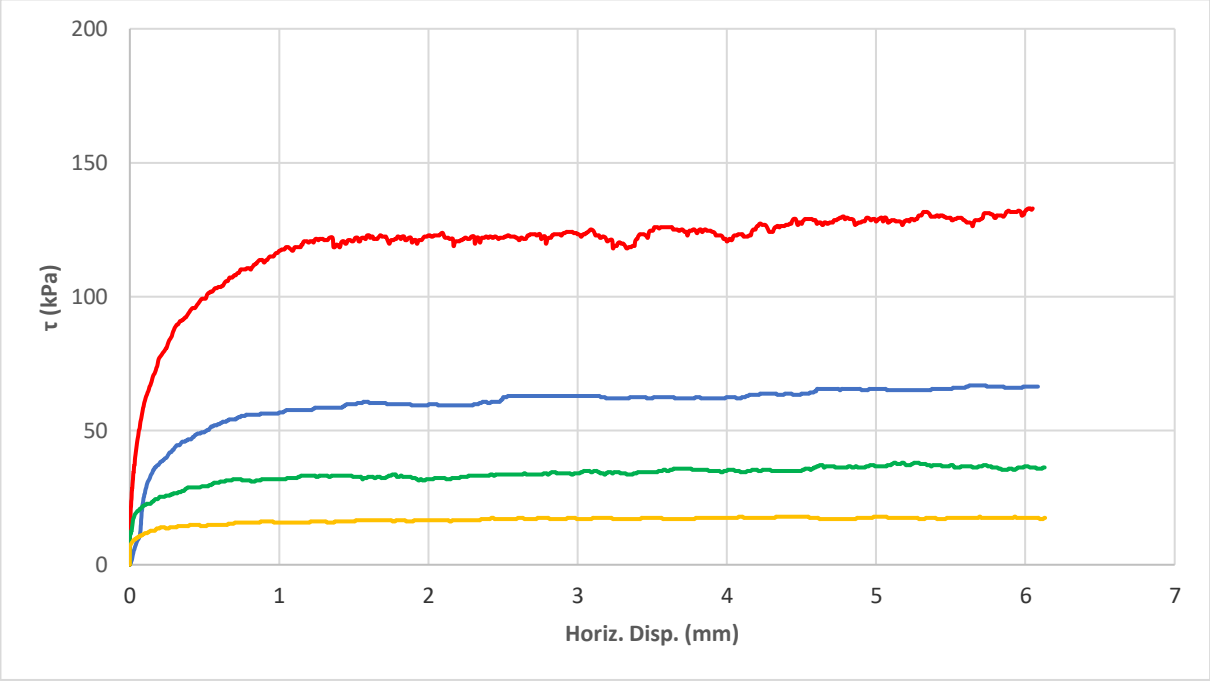

Figure 0.26: Plots from interface shear tests of soil C (bentonite-conditioned), conducted at normal loads of 50.0, 99.7, 193.4 and 327.3 kPa. Shear resistance is shown function of horizontal displacement.

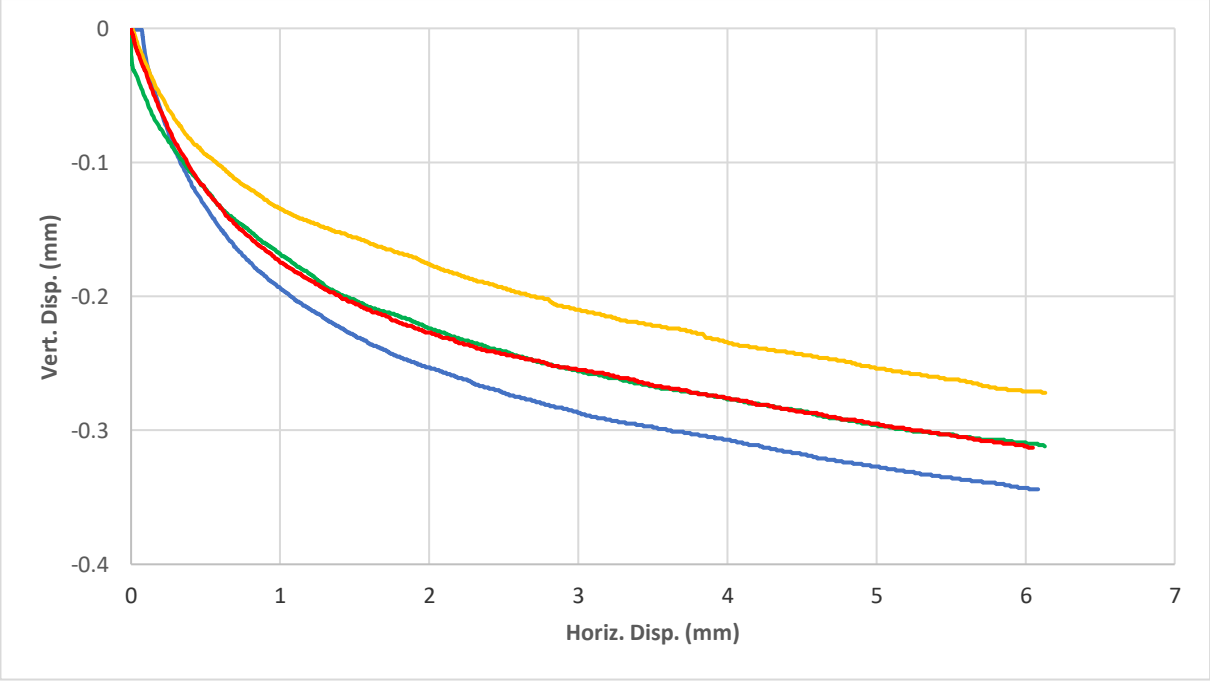

Figure 0.27: Plots from interface shear tests of soil C (bentonite-conditioned), conducted at normal loads of 50.0, 99.7, 193.4 and 327.3 kPa. Vertical displacement is shown function of horizontal displacement.

Table 0.8: Results of interface shear tests of soil C (bentonite-conditioned).

σ [kPa]	$\rho_{dry,0}$; $\rho_{sat,0}$ [g/cm^3]	$\rho_{dry,f}$; $\rho_{sat,f}$ [g/cm^3]	δ [°]; μ [-]	δ_{avg} [°]; μ_{avg} [-]
50.0	1.591; 2.138	1.623; 2.181	18.857; 0.342	19.383; 0.352
99.7	1.468; 1.972	1.501; 2.017	19.741; 0.359	
193.4	1.557; 2.092	1.597; 2.146	18.273; 0.330	
327.3	1.599; 2.149	1.636; 2.198	20.660; 0.377	

III. Bentonite-conditioned (low bentonite/soil ratio)

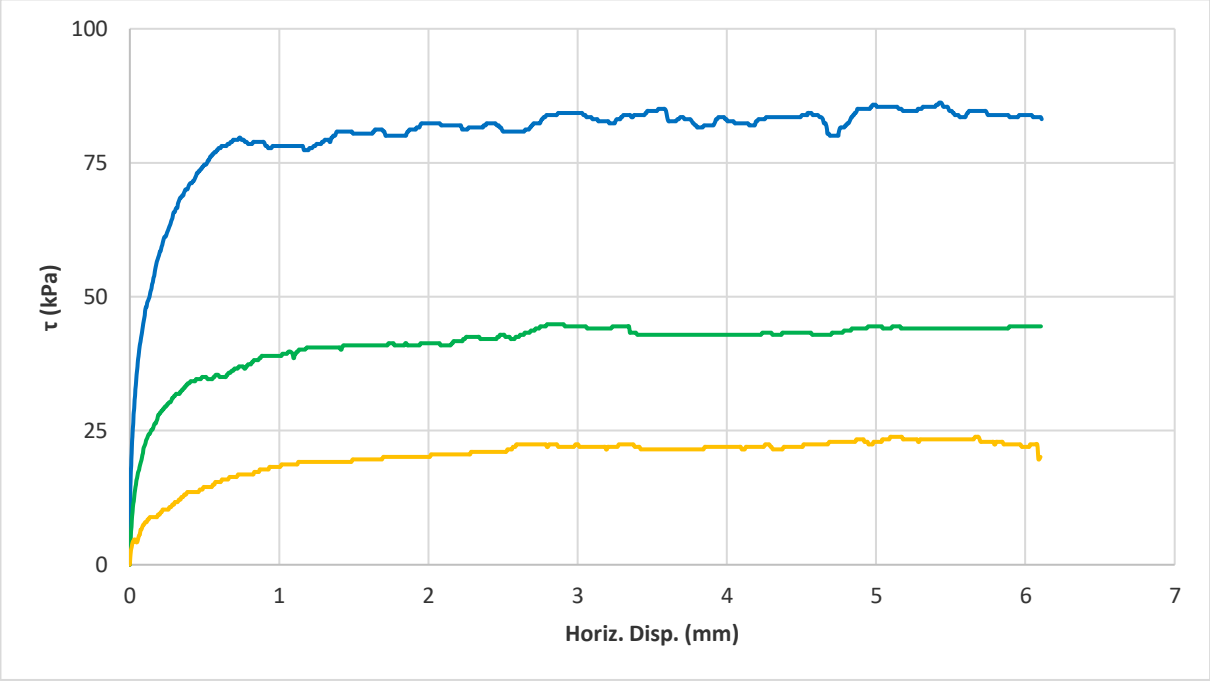

Figure 0.28: Plots from interface shear tests of soil C ("mild" bentonite-conditioned), conducted at normal loads of 50.0, 99.7 and 193.4 kPa. Shear resistance is shown function of horizontal displacement.

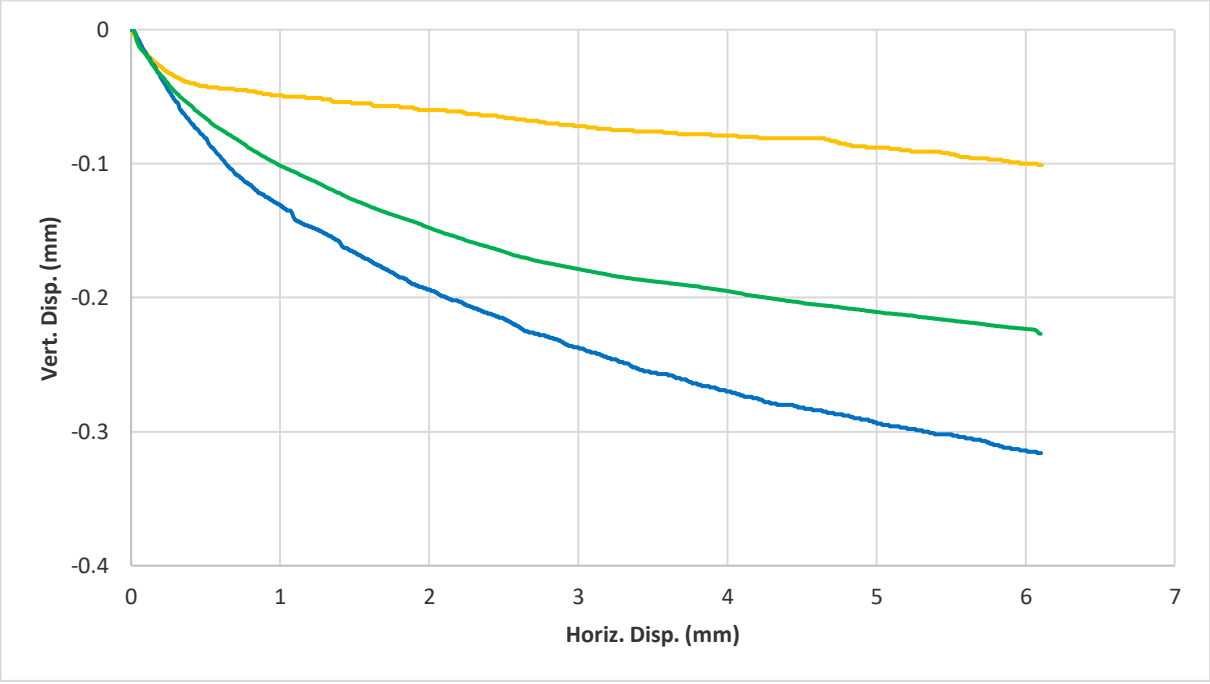

Figure 0.29: Plots from interface shear tests of soil C ("mild" bentonite-conditioned), conducted at normal loads of 50.0, 99.7 and 193.4 kPa. Vertical displacement is shown function of horizontal displacement.

Table 0.9: Results of interface shear tests of soil C ("mild" bentonite-conditioned).

σ [kPa]	$\rho_{dry,0}$; $\rho_{sat,0}$ [g/cm^3]	$\rho_{dry,f}$; $\rho_{sat,f}$ [g/cm^3]	δ [°]; μ [-]	δ_{avg} [°]; μ_{avg} [-]
50.0	1.749; 2.083	1.838; 2.189	24.138; 0.448	
99.7	1.750; 2.085	1.785; 2.126	23.333; 0.431	23.513; 0.435
193.4	1.802; 2.146	1.812; 2.159	23.069; 0.426	

IV. Foam-conditioned

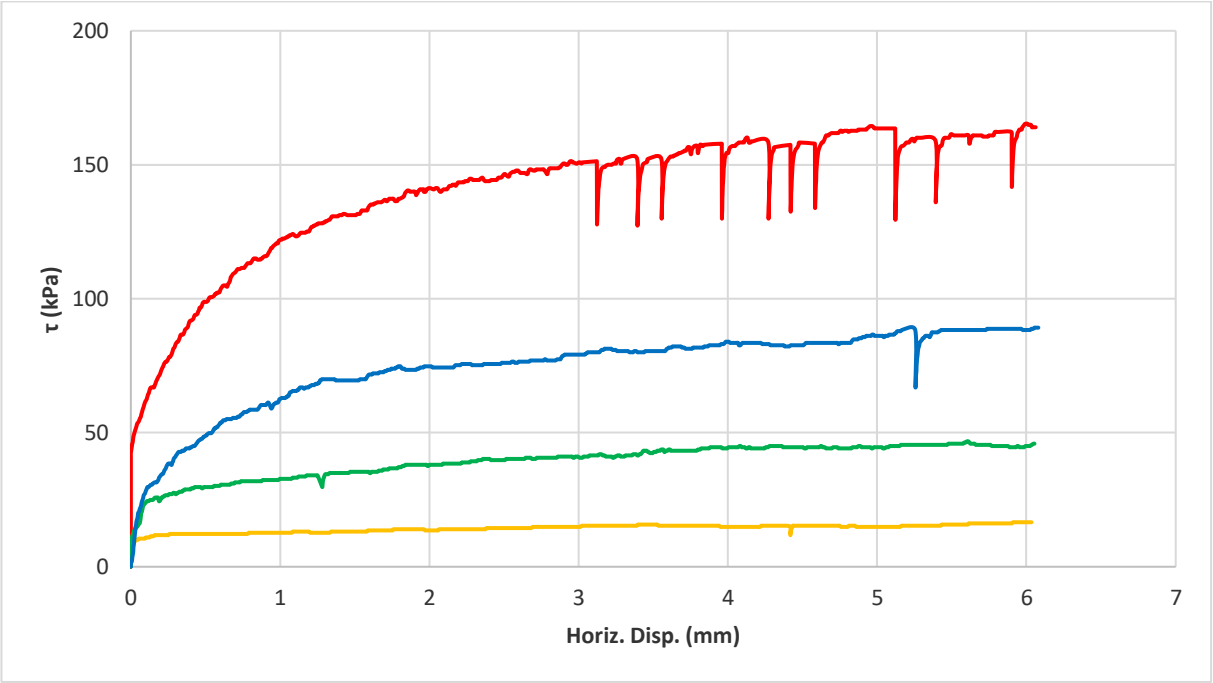

Figure 0.30: Plots from interface shear tests of soil C (foam-conditioned), conducted at normal loads of 50.0, 99.7, 193.4 and 327.3 kPa. Shear resistance is shown function of horizontal displacement.

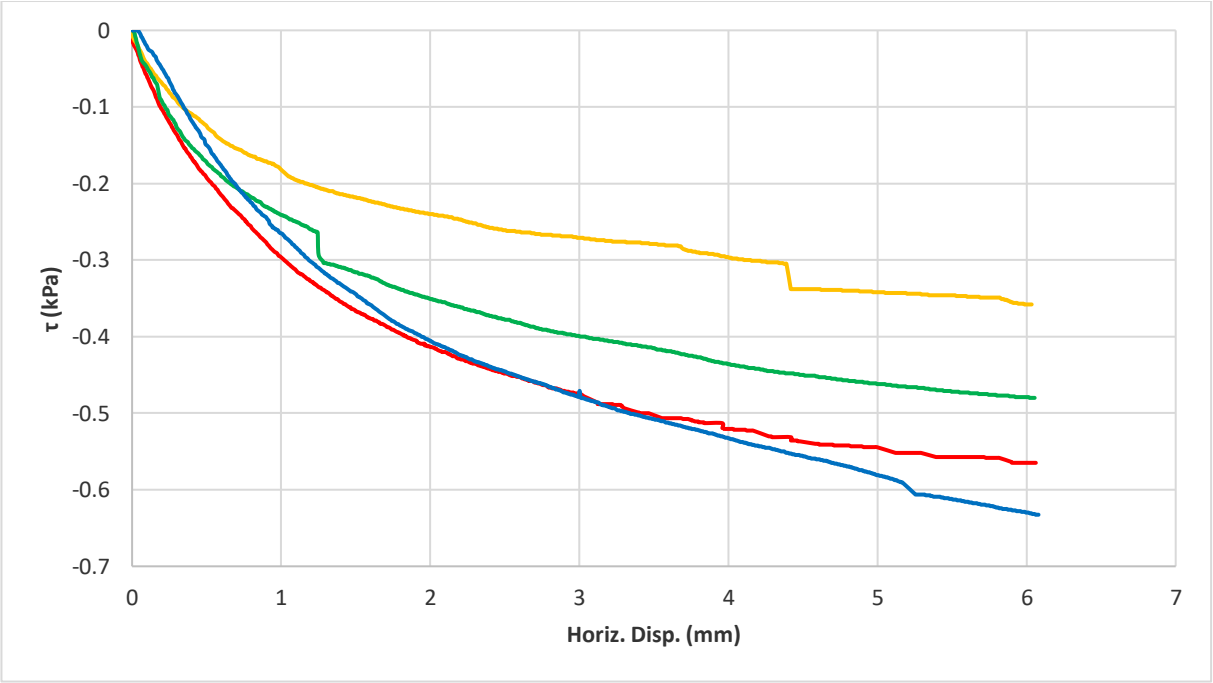

Figure 0.31: Plots from interface shear tests of soil C (foam-conditioned), conducted at normal loads of 50.0, 99.7, 193.4 and 327.3 kPa. Vertical displacement is shown function of horizontal displacement.

Table 0.10: Results of interface shear tests of soil C (foam-conditioned).

σ [kPa]	$\rho_{dry,0}$; $\rho_{sat,0}$ [g/cm^3]	$\rho_{dry,f}$; $\rho_{sat,f}$ [g/cm^3]	δ [°]; μ [-]	δ_{avg} [°]; μ_{avg} [-]
50.0	1.435; 1.607	1.472; 1.648	17.096; 0.308	22.439; 0.413
99.7	1.474; 1.652	1.586; 1.777	24.108; 0.447	
193.4	1.625; 1.818	1.706; 1.909	23.512; 0.435	
327.3	1.518; 1.697	1.580; 1.767	25.040; 0.467	

V. Foam-conditioned (thicker foam)

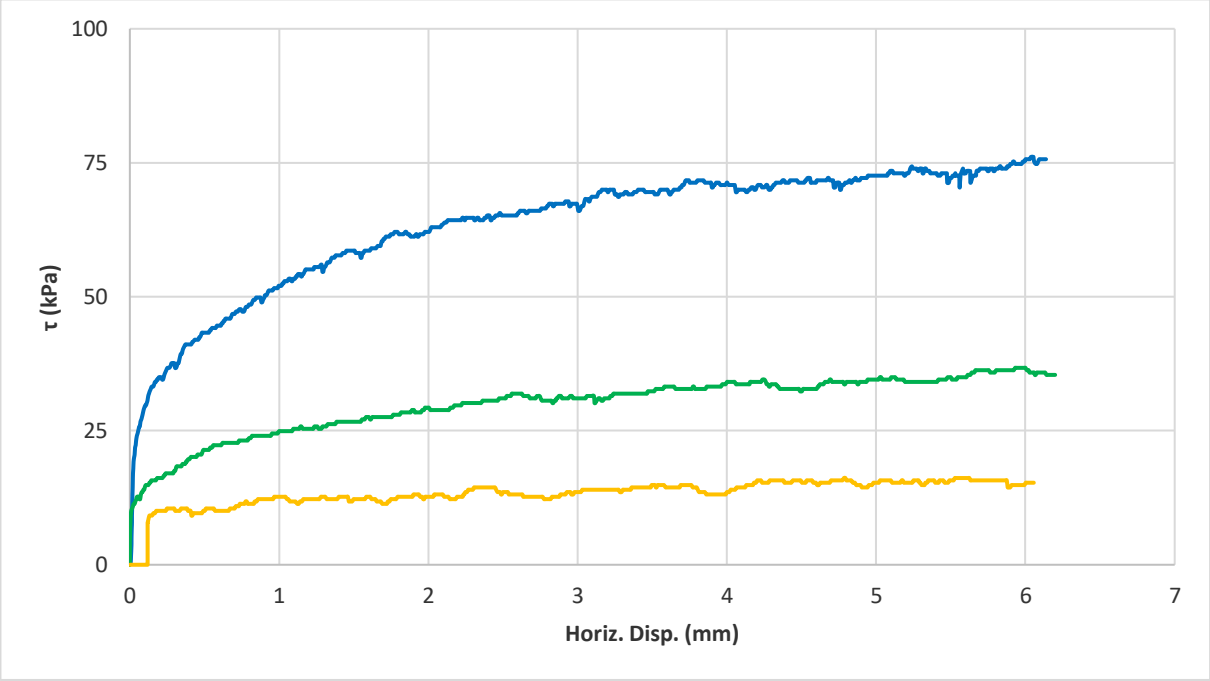

Figure 0.32: Plots from interface shear tests of soil C (foam-conditioned), conducted at normal loads of 50.0, 99.7 and 193.4. Shear resistance is shown function of horizontal displacement.

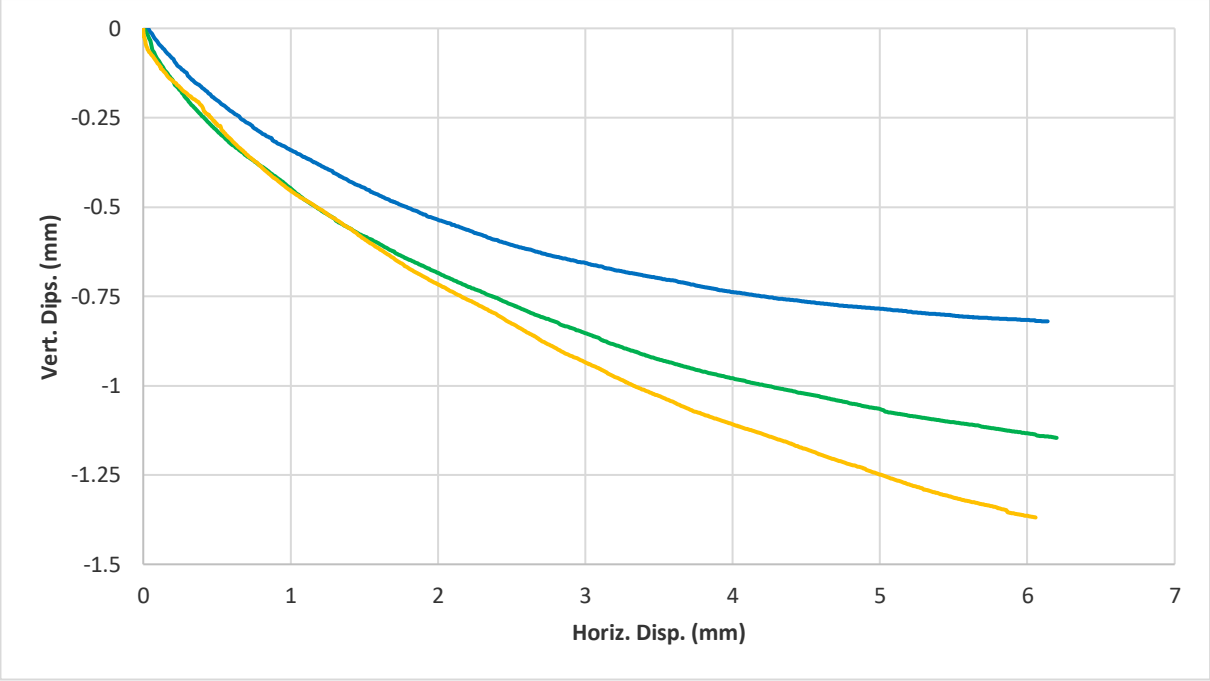

Figure 0.33: Plots from interface shear tests of soil C (foam-conditioned), conducted at normal loads of 50.0, 99.7 and 193.4 kPa. Vertical displacement is shown function of horizontal displacement.

σ [kPa]	$\rho_{dry,0}$; $\rho_{sat,0}$ [g/cm^3]	$\rho_{dry,f}$; $\rho_{sat,f}$ [g/cm^3]	δ [°]; μ [-]	δ_{avg} [°]; μ_{avg} [-]
50.0	1.438; 1.607	1.632; 1.826	16.829; 0.302	
99.7	1.447; 1.639	1.649; 1.846	18.976; 0.344	18.725; 0.339
193.4	1.501; 1.682	1.612; 1.814	20.370; 0.371	